VTT PUBLICATIONS

304

Kari E. J. Lehtinen

Theoretical studies on aerosol agglomeration processes

VTT

TECHNICAL RESEARCH CENTRE OF FINLAND
ESPOO 1997

DISCLAIMER

Portions of this document may be illegible electronic image products. Images are produced from the best available original document.

VTT PUBLICATIONS 304

Theoretical studies on aerosol agglomeration processes

Kari E. J. Lehtinen

VTT Energy

Dissertation for the degree of Doctor of Technology to be presented with due permission for public examination and debate in Auditorium E at Helsinki University of Technology (Espoo, Finland) on the 26th of April, 1997, at 12 o'clock noon.

TECHNICAL RESEARCH CENTRE OF FINLAND
ESPOO 1997

ISBN 951–38–5047–1 (soft back ed.)
ISSN 1235–0621 (soft back ed.)

ISBN 951–38–5048–X (URL: http://www.inf.vtt.fi/pdf/)
ISSN 1455–0849 (URL: http://www.inf.vtt.fi/pdf/)

JULKAISIJA – UTGIVARE – PUBLISHER

Valtion teknillinen tutkimuskeskus (VTT), Vuorimiehentie 5, PL 2000, 02044 VTT
puh. vaihde (09) 4561, faksi 456 4374

Statens tekniska forskningscentral (VTT), Bergsmansvägen 5, PB 2000, 02044 VTT
tel. växel (09) 4561, fax 456 4374

Technical Research Centre of Finland (VTT), Vuorimiehentie 5, P.O.Box 2000, FIN–02044 VTT, Finland
phone internat. + 358 9 4561, fax + 358 9 456 4374

VTT Energia, Energian käyttö, Biologinkuja 7, PL 1401, 02044 VTT
puh. vaihde (09) 4561, faksi (09) 456 7021

VTT Energi, Energiandvändning, Biologgränden 7, PB 1401, 02044 VTT
tel. växel (09) 4561, fax (09) 456 7021

VTT Energy, Energy Use, Biologinkuja 7, P.O.Box 1401, FIN–02044 VTT, Finland
phone internat. + 358 9 4561, fax + 358 9 456 7021

Technical editing Leena Ukskoski

VTT OFFSETPAINO, ESPOO 1997

Lehtinen, Kari E. J. Theoretical studies on aerosol agglomeration processes. Espoo 1997. Technical Research Centre of Finland, VTT Publications 304. 45 p. + app. 89 p.

UDC 541.182.2/.3
Keywords aerosols, aerosol dynamics, electrical agglomeration, agglomerates, particle collisions, coalescence, nanomaterials

ABSTRACT

In this thesis, theoretical modeling of certain aerosol systems has been presented. At first, the aerosol general dynamic equation is introduced, along with a discretization routine for its numerical solution. Of the various possible phenomena affecting aerosol behaviour, this work is mostly focused on aerosol agglomeration. The fundamentals of aerosol agglomeration theory are thus briefly reviewed. The two practical applications of agglomeration studied in this thesis are flue gas cleaning using an electrical agglomerator and nanomaterial synthesis with a free jet reactor.

In an electrical agglomerator the aerosol particles are charged and brought into an alternating electric field. The aim is to remove submicron particles from flue gases by collisions with larger particles before conventional gas cleaning devices that have a clear penetration window in the problematic 0.1 - 1 μm size range. A mathematical model was constructed to find out the effects of the different system parameters on the agglomerator's performance. A crucial part of this task was finding out the collision efficiencies of particles of varying size and charge. The original idea was to use unipolar charging of the particles, and a laboratory scale apparatus was constructed for this purpose. Both theory and experiments clearly show that significant removal of submicron particles can not be achieved by such an arrangement. The theoretical analysis further shows that if the submicron particles and the large collector particles were charged with opposite polarity, significant removal of the submicron particles could be obtained.

The second application of agglomeration considered in this thesis is predicting/controlling nanoparticle size in the gas-to-particle aerosol route to material synthesis. In a typical material reactor, a precursor vapor reacts to form molecules of the desired material. In a cooling environment, a particulate phase forms, the dynamics of which are determined by the rates of collisions and coalescence. In the thesis, it is first theoretically

demonstrated how the onset of dendrite formation and primary particle size can be predicted by studying the characteristic time scales of collision and coalescence. Then it is shown how the linear rate law for coalescence can be approximately applied to agglomerate structures by dividing the agglomerates into sections. The developed models are then applied to a free jet material reactor. From the comparisons between theory and experiment it is obvious that such a model is able to capture the effects of the system parameters (temperature, velocity, volume loading of material and location of collection) on the primary particle size of the produced material.

PREFACE

This thesis is based on studies carried out at the Aerosol Technology Group of VTT Energy and at the Air Quality and Aerosol Technology Laboratory of UCLA Department of Chemical Engineering. I wish to express my gratitude to all reseachers in both groups for a great scientific environment for such work. Especially, I am greatly indebted to the leaders of the groups, Dr. Jorma K. Jokiniemi and Prof. Sheldon K. Friedlander for their continuous and assiduous encouragement and supervision of my work. I am also very grateful to Dr. Esko Kauppinen of VTT Chemical Technology for his guidance and continuous support during my first steps in the field of aerosol science.

I dedicate my warmest thanks to the Laboratory of Computational Dynamics of Helsinki University of Technology, especially Prof. Eero-Matti Salonen and Doc. Juhani von Boehm, for their continuous encouragement and guidance throughout my studies and their useful suggestions regarding the thesis.

I am deeply indebted to the researchers involved in the experimental parts of this thesis, especially Dr. Jukka Hautanen from Tampere University of Technology for conducting the electrical agglomerator experiments and Dr. Robert Windeler from UCLA for our continuous collaboration in nanoparticle synthesis throughout my stay at UCLA.

I am also grateful to Dr. Bertram Schleicher and Mr. Jouni Pyykönen for their helpful suggestions regarding the writing of the thesis.

I am thankful to the Ministry of Trade and Industry's LIEKKI research program for funding the developing of the ABC computer code, the SIHTI research program for funding the electrical agglomeration project and to the VTT Exchange Program, IVO Research Foundation and Leo and Regina Wainstein Foundation for making my stay and work at UCLA possible.

Finally, I wish to thank my friends, my parents and other relatives and especially my beloved fiancee Tarja for their patience and understanding throughout this thesis work.

LIST OF PUBLICATIONS

This dissertation is a review of the author's work in the field of aerosol dynamics modeling. It consists of an overview and the following selection of the author's publications:

A Jokiniemi, J. K., Lazaridis, M., Lehtinen, K. E. J. and Kauppinen, E. I.
Numerical simulation of vapour-aerosol dynamics in combustion processes.
J. Aerosol Sci. 1994. Vol. 25, pp. 429 - 446.

B Hautanen, J., Kilpeläinen, M., Kauppinen, E. I., Jokiniemi, J. K. and Lehtinen, K.
Electrical agglomeration of aerosol particles in an alternating electric field.
Aerosol Sci. Tech. 1995. Vol. 22, pp. 181 - 189.

C Lehtinen, K. E. J., Jokiniemi, J. K., Kauppinen, E. I. and Hautanen, J.
Kinematic coagulation of charged droplets in an alternating electric field.
Aerosol Sci. Tech. 1995. Vol. 23, pp. 422 - 430.

D Lehtinen, K. E. J., Windeler, R. S. and Friedlander, S. K.
Prediction of nanoparticle size and the onset of dendrite formation using the method of characteristic times.
J. Aerosol Sci. 1996. Vol 27, pp. 883 - 896.

E Lehtinen, K. E. J., Windeler, R. S. and Friedlander, S. K.
A note on the growth of primary particles in agglomerate structures by coalescence.
J. Colloid and Interface Sci. 1996. Vol 182, pp. 606 - 608.

F Windeler, R. S., Friedlander, S. K. and Lehtinen, K. E. J.
Production of nanometer-sized metal oxide particles by gas phase reaction in a free jet I: experimental system and results.
Accepted for publication in Aerosol Sci. Tech.

G Windeler, R. S., Lehtinen, K. E. J. and Friedlander, S. K.
Production of nanometer-sized metal oxide particles by gas phase reaction in a free jet II: particle size and neck formation - comparison with theory.
Accepted for publication in Aerosol Sci. Tech.

AUTHOR'S CONTRIBUTION

The research reported in this dissertation has been carried out at the Aerosol Technology Group of VTT Energy in Espoo, Finland (papers A, B and C) and at the UCLA Air Quality and Aerosol Technology Laboratory in Los Angeles, California (papers D, E, F and G), where the author worked as a visiting research scientist from Aug. 1994 to Aug. 1995. Papers B and C were carried out in collaboration with the Physics Dept. of Tampere University of Technology (TUT).

Paper A deals with the ABC computer code and was written mainly by Dr. Jokiniemi. The author's contributions to the paper were programming of the multicomponent gas transport coefficients, coagulation source terms and, jointly with Dr. Jokiniemi, the discrete-nodal grid for the particle size spectrum. The author also wrote the corresponding sections of the paper. The sample calculations of paper A were performed by Dr. Lazaridis.

Electrical agglomeration is discussed in papers B and C. The author's contributions to these papers include participation in the overall planning and analyzing the results of the project, all theoretical modeling of both papers and writing paper C. Dr. Hautanen from TUT performed the experiments and wrote paper B.

Papers D, E, F and G deal with controlled nanoparticle production. The theoretical (not forgetting the guidance of Prof. Friedlander) and computational work of all the papers was done by the author, as was the writing of papers D and E. The comparisons between theoretical and experimental results in paper G were done jointly with Dr. Windeler from UCLA. The author also took part in the statistical analysis of the experimental results of paper F and assisted in writing papers F and G.

TABLE OF CONTENTS

NOMENCLATURE

a	particle surface area
A	cross-sectional area
A	constant in the agglomerate power law
b	proportionality constant in charge distribution
$\bar{c}$, g, l	shortening variables in the Fuchs collision frequency function
C	proportionality function in initial neck growth equation
C_c	slip correction factor
d	particle diameter
$\bar{d}$	mean particle diameter
D	diffusion coefficient
D_0	diffusion coefficient prefactor
D_f	fractal dimension
$\vec{e}_x, \vec{e}_y, \vec{e}_z$	cartesian unit vectors
E_{act}	activation energy for the diffusion coefficient
E_0	amplitude of electric voltage
f	frequency of alternating electric field
F	rate of collisions
k	Boltzmann's constant
m	mass concentration distribution
M	total mass concentration of particles
M	molar mass
n	degree of homogenity of a homogenous function
n	number density function
n	average number of primary particles in an agglomerate
n^m	multicomponent number density function
N	number of primary particles in an agglomerate
p	pressure
q	amount of charge
r	particle radius
r_0	primary particle radius
R	removal term
R	gas constant
R^m	multicomponent removal term
S	source term
S^m	multicomponent source term
t	time
T	temperature
u,v	particle volume
$\bar{v}$	average particle volume
v_0	primary particle volume
v_k	volume of component k in a particle
v_m	molecular volume

$\dot{v}$	condensation rate
$\dot{v}_k$	condensation rate of component k
V	control volume
w	grain boundary width
x	neck radius
$\vec{x}$	position vector
$\dot{\vec{x}}$	velocity vector
x,y,z	coordinates of position vector
α	constant in the self-preserving growth law for average volume
β	collision frequency function
δ	surface thickness
ε	collision efficiency
ε_0	permittivity of vacuum
η	size variable of the self-preserving distribution
ϕ	proportionality constant for deposition
ϕ	volume fraction of particulate matter
Φ	reduction in fine mode concentration
λ	mean free path
μ	viscosity
ρ	density
σ	surface tension
σ	factor that takes into account different charging cases
τ	residence time in agglomerator
τ_c	characteristic collision time
τ_f	characteristic fusion time
ξ	Coulomb correction factor for collision frequency function
ψ	self-preserving distribution function
θ	dimensionless excess surface area
Θ	step function

Subscripts

a	agglomerate
b	grain boundary diffusion
coll	collision
Coul	Coulomb
l	lattice diffusion
p	primary particle
s	surface diffusion
sph	spherical
1	fine particle mode
2	large particle mode

1. INTRODUCTION

Aerosols are suspensions of solid and/or liquid particles in gases. They are formed by the conversion of gases to particulate matter or by the disintegration of liquids or solids. The sizes of aerosol particles range from a few nanometers to roughly hundreds of micrometers. The understanding of the physical properties of aerosols is important in many areas of research and industry, including materials processing, air pollution control, nuclear safety, combustion engineering and cloud and atmospheric sciences.

In combustion processes aerosols may cause severe slagging and fouling problems. Air pollution aerosols can have negative effects on e.g. human health and visibility. On the other hand, aerosol routes provide a convenient way of producing nanomaterials with properties significantly differing from the normal bulk properties. Medicine can also be in the form of aerosols. The basis of the new asthma inhalators lies in knowing the penetration properties of the medicine particles into the human lung.

This overview focuses mainly on methods of modeling aerosol behaviour and covers the author's work on the subject originally reported in papers A-G. A thorough introduction to previous work in this area is omitted in this overview, since it is covered in the introduction of each paper, which are attached. Predicting aerosol behaviour requires knowledge of the particle sizes, concentration, chemical composition and morphology. Chapter 2 introduces the concept of the general dynamic equation (GDE), which is an integro-differential equation describing the time evolution of the particle size distribution. A numerical solution technique for the GDE is also discussed.

Particle collisions play an important role in aerosol dynamics, and thus also in the GDE. Chapter 3 introduces the basics of aerosol agglomeration. Agglomeration is a process, in which particles collide and stick, thus forming larger particles. If the particles coalesce into spherical form, the process is usually termed coagulation. If coalescence does not occur, agglomeration leads to the formation of dendritic structures. These dendritic structures collide with a different rate, compared with spheres of same volume. This is discussed at the end of the chapter.

The remaining chapters deal with two research problems, in which particle collisions are the most important physical process affecting the evolution of the size distribution. The first problem is an example of using aerosol methods in air pollution prevention and is discussed in Chapter 4. It has been found that many particle removal devices have a penetration window in the range 0.1 - 1 μm. One idea for removing the particles in this

problematic range is to use an electrical agglomerator, in which the particles are charged and subsequently brought into an alternating electric field. The purpose of this arrangement is to remove the submicron particles with the larger particles, resulting from collisions caused by the oscillatory motion.

The second aerosol related research problem discussed in this thesis is the possibility to produce nanoparticles in a controlled way by gas-to-particle aerosol methods, which is discussed in Chapter 5. The particles are formed by chemical reactions from the vapor phase and grow by collisions. The size and shape of the formed nanoparticles depend on the relative rates of collision and coalescence. Chapter 5 summarizes the basic theoretical models with which it is possible to predict and control the size and shape of the produced nanoparticle material.

2. THE GENERAL DYNAMIC EQUATION (GDE)

The integro-differential equation that describes the dynamic behaviour of an aerosol is usually termed the general dynamic equation for aerosols (GDE; Friedlander, 1977). In its most general form, it describes the evolution of the size distribution of aerosol particles as functions of particle size and composition, but in many applications and numerical solution routines, only the dependence on size is considered.

The processes that govern the temporal and spatial changes in the size distribution are agglomeration, growth, source and removal processes. Agglomeration is a process in which particles collide and form larger particles. The most common phenomena that cause collisions are Brownian motion, external forces and turbulence. Agglomeration will be studied in more detail in the following chapters. The growth term accounts for the increase or decrease in particle size because of condensation, evaporation or reactions of gases with particle surfaces. Examples of the source and removal processes are nucleation and deposition.

2.1. Continuous GDE for the number density function

The number density function $n = n(\bar{x}, v, t)$, where $\bar{x} = x\bar{e}_x + y\bar{e}_y + z\bar{e}_z$ is the position vector and v the particle volume, is defined in such a way that $n(\bar{x}, v, t)dxdydzdv$ gives the number of particles with volume between v and $v+dv$ at location $\bar{x}$ in the differential box $dxdydz$. It obeys the following partial differential equation (the GDE for aerosol particles; Friedlander, 1977)

$$\frac{\partial n}{\partial t} + \nabla \cdot (\dot{\bar{x}} n) + \frac{\partial}{\partial v}(\dot{v} n) = \left(\frac{\partial n}{\partial t}\right)_{coll} + R + S . \qquad (2.1)$$

The left hand side is comprised of terms describing the temporal and spatial changes in the number density function as well as growth/shrinkage by condensation/evaporation. Here $\dot{\bar{x}} = \dot{\bar{x}}(\bar{x}, v, t)$ is the velocity of a particle of volume v at location $\bar{x}$ and time t. The velocity $\dot{\bar{x}}$ can be set to take into account the migration velocity caused by external forces and the diffusional velocity caused by concentration gradients. Usually in simulating aerosol dynamics, however, it is sufficient to set $\dot{\bar{x}}$ to be equal to the gas velocity. The first term on the right hand side describes the change in the number density function caused by particle collisions or agglomeration. The form of this term will be studied in detail in the next chapter. The last two terms $R(v,n(v),\bar{x},t)$ and $S(v,n(v),\bar{x},t)$ are the removal and source terms,

respectively. The most typical removal and source terms are deposition and nucleation.

The GDE is in its general form an integro-differential equation, since the collision terms are integrals of the size distribution function n. Thus, numerical solutions are practically always necessary. Paper A deals with a computer program ABC, which was written to simulate aerosol behaviour in combustion processes. The computational procedure is sectional, i.e. the size distribution is divided into a number of classes. For each size section the size of the particles is described by the midpoint of the section (for this reason the solution procedure is called a nodal point method in paper A) and there is a differential equation for the number of particles in each section. The numerical procedure is discussed in more detail in Section 2.3.

2.2 Multicomponent GDE

If the aerosol particles contain many chemical components and we wish to keep track of the composition in addition to size, a different type of number distribution is required. If the multicomponent number density function $n^m = n^m(\bar{x}, v_1, v_2, ..., v_m, t)$ is defined in such a way that $n^m(\bar{x}, v_1, v_2, ..., v_m, t)dxdydzdv_1dv_2...dv_m$ gives the number of particles, with the volume of component k between v_k and v_k+dv_k, at location $\bar{x}$ and at time t in the differential box $dxdydz$, the GDE becomes (Gelbard and Seinfeld, 1978):

$$\frac{\partial n^m}{\partial t} + \nabla \cdot \left(\dot{\bar{x}} n^m\right) + \sum_{k=1}^{m} \frac{\partial}{\partial v_k}\left(\dot{v}_k n^m\right) = \left(\frac{\partial n^m}{\partial t}\right)_{coll} + R^m + S^m. \qquad (2.2)$$

The collision term depends on the amounts of all chemical components through its dependence on particle size and density (see Section 3.1). Equation 2.2 can be solved numerically by dividing both the size and composition axes into discrete sections (Kim and Seinfeld, 1992). This is, however, computationally extremely expensive. Another approach is to average the compositions within each size section (Gelbard and Seinfeld, 1980; Sher and Jokiniemi, 1993). The compositions in different size sections may be different and are allowed to vary as functions of time and location, but each section is represented by only one averaged composition. Then, if we have m size classes and n chemical components, we will have mn differential equations to be solved. This is the method used in the ABC computer code (paper A).

2.3. Discretization of the GDE

In the ABC computer code, the flow field is approximated by a plug-flow model. The discretization of the GDE is obtained by a finite volume technique. Many of the calculations of interest are stationary. In the following, the discretization technique in such cases is presented. The discretization routines of RAFT (Im et al., 1987) and NAUA-HYGROS (Jokiniemi and Sher, 1993) have been used as bases for the model.

If the GDE is integrated over a control volume V (Figure 2.1) located at x_i, where the flow is in the positive x-direction in a tube with a cross-sectional area of $A(x)$, the following form of the stationary GDE is obtained:

$$\int_V \nabla\cdot(\dot{x}n)dV + \int_V \frac{\partial}{\partial v}(\dot{v}n)dV = \int_V \left[\left(\frac{\partial n}{\partial t}\right)_{coll} + R + S\right]dV . \tag{2.3}$$

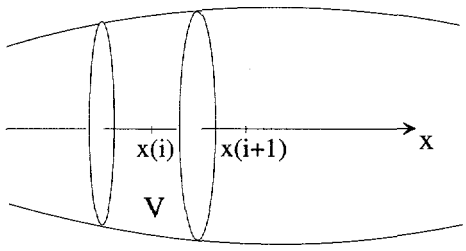

Figure 2.1. Control volume approach to discretizing the GDE.

Here it is also assumed that all the variables are independent of y and z. The first term can be transformed using Gauss's law: $\int_V \nabla\cdot(\dot{x}n)dV = \int_A (\dot{x}n)\cdot d\vec{A}$. The (deposition) removal term R is proportional to the number density function n: $R = -\phi n$. The form of the source (nucleation) term S is discussed in paper A. If, in addition, the volume V is very thin, we can approximate $V(x_i) \approx A(x_i)\cdot\Delta x_i$ and equation 2.3 becomes:

$$\frac{A_{i+1/2}\dot{x}_{i+1/2,j}n_{i+1/2,j} - A_{i-1/2}\dot{x}_{i-1/2,j}n_{i-1/2,j}}{A_i\Delta x_i} + \frac{\dot{v}_{i,j+1/2}n_{i,j+1/2} - \dot{v}_{i,j-1/2}n_{i,j-1/2}}{\Delta v_j} = \left(\frac{\partial n}{\partial t}\right)_{coll,ij} - \phi_{ij}n_{ij} + S_{ij} \tag{2.4}$$

The discretization of the condensation/evaporation term results from similar finite volume thinking as with the convecton term (the index j refers to the radius coordinate).

The cross-sectional areas $A_{i+1/2}$ and $A_{i-1/2}$, the particle velocities $\dot{x}_{i+1/2,j}$ and $\dot{x}_{i-1/2,j}$ as well as the particle growth rates $\dot{v}_{i,j+1/2}$ and $\dot{v}_{i,j-1/2}$ are computed at the cell boundaries using the known geometrical and physicochemical data, but the discretized size distribution is stored only at the midpoints n_{ij}. The discretized size distribution values in the convection and growth terms $n_{i+1/2,j}$, $n_{i-1/2,j}$, $n_{i,j+1/2}$ and $n_{i,j-1/2}$ are approximated by their nearest upwind values, i.e. the first order upwind discretization is used:

$$n_{i+1/2,j} \approx n_{ij} \tag{2.5}$$

$$n_{i,j+1/2} \approx \begin{cases} n_{i,j+1}, & \dot{v}_{i,j+1/2} < 0 \\ n_{ij}, & \dot{v}_{i,j+1/2} > 0 \end{cases} \tag{2.6}$$

By using the first order upwind discretizing technique, the solution method is robust and "reasonable looking" solutions are practically always obtained. However, numerical diffusion decreases the accuracy of the solution.

The terms can now be grouped in such a way that the algebraic nature of the solution procedure can be clearly seen:

$$\begin{aligned} &\left(\phi_{ij} + \frac{A_{i+1/2}\dot{x}_{i+1/2,j}}{A_i \Delta x_i} + \frac{1}{\Delta v_j} \begin{Bmatrix} \dot{v}_{i,j+1/2} & [1] \\ -\dot{v}_{i,j-1/2} & [2] \\ \dot{v}_{i,j+1/2} - \dot{v}_{i,j-1/2} & [3] \end{Bmatrix} \right) n_{ij} \\ &= \frac{1}{\Delta v_j} \begin{Bmatrix} \dot{v}_{i,j-1/2} & [1] \\ 0 & [2] \\ 0 & [3] \end{Bmatrix} n_{i,j-1} + \frac{1}{\Delta v_j} \begin{Bmatrix} 0 & [1] \\ -\dot{v}_{i,j+1/2} & [2] \\ 0 & [3] \end{Bmatrix} n_{i,j+1} \\ &+ \left(S_{i-1,j} + \left(\frac{\partial n}{\partial t} \right)_{coll,i-1,j} + \frac{A_{i-1/2}\dot{x}_{i-1/2,j}}{A_i \Delta x_i} n_{i-1,j} \right) \end{aligned} \tag{2.7}$$

Case [1], [2] or [3] is applied according to the following criteria:

[1] $\dot{v}_{i,j+1/2} \geq 0, \dot{v}_{i,j-1/2} \geq 0$
[2] $\dot{v}_{i,j+1/2} < 0, \dot{v}_{i,j-1/2} < 0$
[3] $\dot{v}_{i,j+1/2} \geq 0, \dot{v}_{i,j-1/2} < 0$

Case [3], where some particles grow and some evaporate, is possible because of the Kelvin effect (Hinds, 1982). If the conditions are such that all particles grow, then we have case [1] for all size classes j. The equation for n_{ij} will then not include $n_{i,j+1}$. The solution of any matrix equations can therefore be avoided, since we can just start by solving the equation for n_{i1}, then n_{i2} and so on. If all particles evaporate and we have case [2] for all size classes, we have a similar situation, except that then we start by solving the equation for $n_{i,max}$. If there exists a size class k such that all particles larger than r_k grow and smaller than r_k evaporate, we start by solving for $n_{i,k}$, after which we proceed to $n_{i,k-1}$ and $n_{i,k+1}$, and so on.

This discretisation scheme, which is taken from RAFT (Im et al.,1987), is semi-implicit in nature. In stationary systems, the solution marches along the x-axis in small increments solving for the size distribution n at every x, at the same time keeping track of the gas phase concentrations. The other terms are treated implicitly, except for the nucleation and collision source terms, in which size distribution values at x_{i-1} are used when calculating term values at x_i.

In the modeling of aerosol dynamics it is convenient to use a sectionalization, in which the sections are evenly spaced on the logarithmic axis (v_{i+1}/v_i = constant). Sometimes, however, a more accurate model for the lower end of the size spectrum is needed and thus a discrete-sectional or discrete-nodal point discretization is more appropriate (Wu and Flagan, 1988, Paper A). This means that the size axis is divided monomer by monomer up to a certain prefixed size, after which the logarithmically even spacing is applied.

3. AGGLOMERATION OF AEROSOL PARTICLES

Agglomeration is a process in which particles collide and form larger particles. Thus, as a consequence of agglomeration the average particle size increases and the total number concentration decreases. If the collided particles coalesce to spherical form, the process is usually called coagulation. If the particles do not coalesce but stick together, dendritic agglomerates tend to form. Here we will use the term agglomeration for all collision processes that result in the particles sticking together, regardless of whether they coalesce or not. Coagulation is regarded as a special case of agglomeration, where there is instantaneous coalescence after collision.

The most common phenomena that cause collisions are Brownian motion, external forces and turbulence. In this chapter Brownian agglomeration and kinematic agglomeration caused by electrical forces are studied in more detail. The theoretical treatment of agglomeration consists of keeping count of the number of particles as a result of the collisions (Schmoluchowski, 1917) and determining the collision frequency function as a function of particle sizes, particle densities and system parameters.

As mentioned in Chapter 2, agglomeration is just one physical phenomenon affecting the time evolution of aerosol systems. Here it is studied in more detail, since it is the dominant particle growth mechanism for both the electrical agglomerator system (papers B and C) and material synthesis (papers D, E and F) processes.

3.1. The continuous agglomeration equation

Let $n(v)$ be the particle size distribution function defined in the previous chapter. Then the rate of collisions per unit volume of gas $F(u,v)$ between particles of size u and v is

$$F(u,v) = \beta(u,v)n(u)n(v)dudv \tag{3.1}$$

Here $\beta(u,v)$ is the collision frequency function. It depends on particle sizes, densities and system variables and will be introduced in more detail in the next two chapters. If particle collisions are the only phenomenon affecting the size distribution, we have the equation (Friedlander, 1977):

$$\left(\frac{\partial n(v)}{\partial t}\right)_{coll} = \frac{1}{2}\int_0^v \beta(u, v-u)n(u)n(v-u)du - \int_0^\infty \beta(u,v)n(u)n(v)du \tag{3.2}$$

The first term is the rate of formation of particles of size v by smaller particles of sizes u and v-u. The factor 1/2 must be introduced since collisions are counted twice in the integral. The second term is the rate of loss of particles of size v by collision with all other particles. The multicomponent collision terms are a simple extension to equation 3.2.

$$\left(\frac{\partial n^m(v_1,\ldots,v_m)}{\partial t}\right)_{coll} = \frac{1}{2}\int_0^{v_1}\ldots\int_0^{v_m}\beta(u_1,\ldots,u_m,v_1-u_1,\ldots,v_m-u_m)$$
$$n^m(u_1,\ldots,u_m)n^m(v_1-u_1,\ldots,v_m-u_m)du_1\ldots du_m \quad (3.3)$$
$$-\int_0^{\infty}\ldots\int_0^{\infty}\beta(u_1,\ldots,u_m,v_1,\ldots,v_m)n^m(u_1,\ldots,u_m)$$
$$n^m(v_1,\ldots,v_m)du_1\ldots du_m.$$

In the ABC model (Paper A), the agglomeration source terms for each source term are computed by the following technique: All the particle size pairs are gone through one by one. If the size of the particle resulting from a collision falls between two nodal points, the resulting particle is divided between those nodal points in such a way that number and volume are conserved (size-splitting).

3.2. Brownian agglomeration

If particles are smaller than about 1 μm in diameter, they collide because of their Brownian motion. The collision frequency function for this mechanism can be expressed as (Fuchs, 1964):

$$\beta(u,v) = \begin{cases} \frac{2kT}{3\mu}\left(\frac{1}{u^{1/3}}+\frac{1}{v^{1/3}}\right)\left(u^{1/3}+v^{1/3}\right); & \text{continuum regime} \\ \left(\frac{3}{4\pi}\right)^{1/6}\left(\frac{6kT}{\rho_p}\right)^{1/2}\left(\frac{1}{u}+\frac{1}{v}\right)^{1/2}\left(u^{1/3}+v^{1/3}\right)^2; & \text{free molec. regime} \end{cases} \quad (3.3)$$

If the particles are large enough that they experience the surrounding gas as a continuum, the particle size is said to be in the continuum regime. Then the particle diameter is larger than the mean free path of the gas ($\approx 0.07\mu$m for air in standard conditions). If the particle diameter is much smaller than the mean free path of the surrounding gas, it is said to be in the free molecular regime. The intermediate region is usually called the transition regime.

The continuum regime expression for the collision frequency function is obtained by solving the diffusion equation of particles of volume v around one particle of volume u that is assumed to be fixed using the relative diffusion coefficient $D(u)+D(v)$ (see Fuchs, 1964). The free molecular collision frequency function is an expression derived by the kinetic theory of gases assuming rigid elastic spheres. There is no simple collision frequency function for the transition regimes that could be derived "from first principles". Fuchs (1964) proposed an interpolation formula for the whole particle diameter range that has been generally accepted:

$$\beta(d_i,d_j)=\frac{2\pi(D_i+D_j)(d_i+d_j)}{\dfrac{d_i+d_j}{d_i+d_j+2\sqrt{g_i^2+g_j^2}}+\dfrac{8(D_i+D_j)}{\sqrt{\bar{c}_i^2+\bar{c}_j^2}(d_i+d_j)}} \tag{3.4}$$

where

$$D_i=\frac{kTC_c(d_i)}{3\pi\mu d_i},\qquad \bar{c}_i=\sqrt{\frac{8kT}{\pi m_i}},\qquad g_i=\frac{(d_i+l_i)^3-(d_i^2+l_i^2)^{3/2}}{3d_il_i}-d_i,$$

$$l_i=\frac{8D_i}{\pi\bar{c}_i},\qquad C_c(d_i)=1+\frac{\lambda}{d_i}\left[2.514+0.800e^{-0.55\frac{d_i}{\lambda}}\right].$$

Here, with some algebra, it can be seen that the nominator of Equation (3.4) is equal to the continuum regime expression in Equation (3.3). Thus the denominator can be thought of as a correction to the continuum collision frequency function. Also it is easily seen that (3.4) reduces to the free molecular collision frequency function in (3.3) when d_i and d_j are both very small. To get a better feeling of how the collision frequency function depends on the particle size, it is plotted in Figure 3.1.

From Figure 3.1. it can be seen that for equally sized particles, the collision efficiency function β has a maximum at about 0.05 μm. For large particles the value of β is low because of their low Brownian diffusivities. Very small particles have high Brownian diffusivities, but the target areas for collisions are very small. Finally, it is seen that β is much larger for a collision of two unequally sized particles than for particles of equal size.

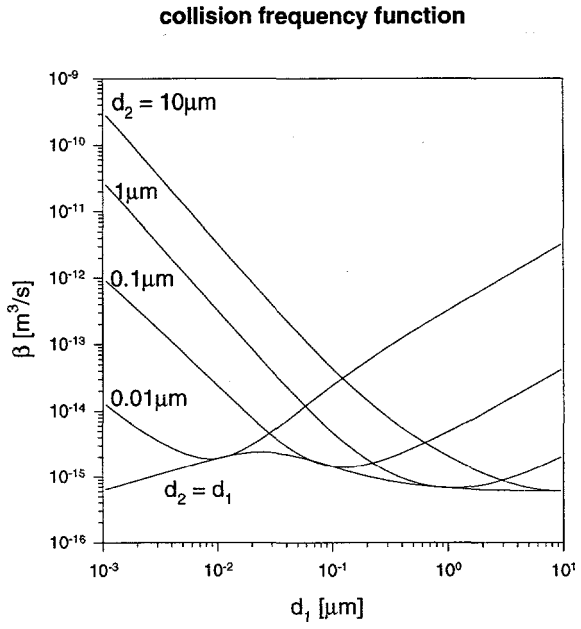

Figure 3.1. Brownian collision frequency function $\beta(d_1,d_2)$ for spherical particles of density 1000 kg/m^3 in air at 293 K and 1 atm using Equation (3.4).

3.3. Kinematic agglomeration

In Brownian agglomeration, particles collide because of their different velocities caused by random Brownian motion. If the velocity difference that is the reason for collisions is caused by external forces (gravitation, electrical forces etc.), the process is called kinematic agglomeration. A common example of kinematic agglomeration is the process of collisions of raindrops with atmospheric aerosol particles. The large raindrops have a larger terminal settling velocity than the much smaller particles. Thus, the falling raindrops sweep the area below them, collecting many of the particles in their way.

The collision frequency function for kinematic agglomeration of particles with diameters d_1 and d_2 is usually written in the following form:

$$\beta(d_1,d_2) = \varepsilon(d_1,d_2)\frac{\pi}{4}(d_1+d_2)^2|v_1 - v_2|, \tag{3.5}$$

where $|v_1 - v_2|$ is the relative velocity between the particles. The meaning of the collision efficiency $\varepsilon(d_1,d_2)$ is evident from Figure 3.2. If the particle moving with greater velocity would sweep all particles that are in its geometrical path, ε would be 1. This is, however, not the case because of the curved streamlines around the particles.

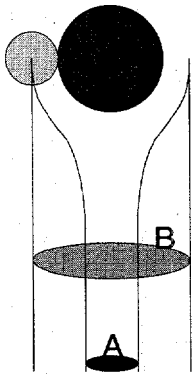

Figure 3.2. The collision efficiency ε is defined as the ratio of the effective collision cross-section to the geometrical collision cross-section $\varepsilon = A/B$.

For gravitational sedimentation it is possible to derive an analytical expression for ε that assumes Stokes flow and negligible inertia of the smaller particle (Pruppacher and Klett, 1978):

$$\varepsilon(d_1,d_2) = \frac{1}{2}\left(\frac{d_1}{d_1+d_2}\right)^2; \quad d_1 << d_2 . \tag{3.6}$$

This means that with significant differences in particle sizes, the collision efficiency will be much lower than unity. If the external force is an electric field and Coulombic forces must be accounted for, the situation becomes more complicated. This problem is discussed in more detail in Chapter 4.

3.4 Agglomeration of non-spherical particles

If the particles that collide are solid and do not have enough time to coalesce before recolliding, fractal-like structures start to form. They are typically built from small almost spherical and equal-sized units, called primary particles. Such structures are conveniently described by a power-law relationship:

$$N = \frac{v}{v_0} = A\left(\frac{r}{r_0}\right)^{D_f} \tag{3.7}$$

where D_f is the fractal dimension. Equation (3.7) gives the average number of primary particles N of radius r_0 in an agglomerate of volume v and characteristic radius r (typically radius of gyration or mobility radius). For a dense structure with spherical shape $D_f = 3$, the factor A is found to be nearly constant and of the order unity (Wu and Friedlander, 1993a). Both experiments and numerical simulations have shown that Brownian movement dominated agglomeration processes tend to produce agglomerates with a fairly low fractal dimension, in the range $1.6 < D_f < 2.2$. It is obvious that such open structures collide and thus grow much more rapidly than spherical particles of the same volume, especially in the free molecular regime.

In the continuum regime, the effects of increased collision cross-section and decreased Brownian mobility approximately cancel each other out and thus there is not much effect on the collision frequencies (Koch and Friedlander, 1990). At present, there is no generally accepted expression available for the collision frequency function of fractal-like agglomerates. However, a first approximation can be obtained by replacing d_i in Equation (3.4) by $2r_0(v_i/v_0)^{1/D_f}$ (assuming A $\approx$ 1). Then we make the very strong assumption that the same characteristic diameter d_i describes both the mobility and capture properties of an agglomerate of any size.

In the free molecular and continuum limits this results in the following collision frequency functions (Matsoukas and Friedlander, 1991):

$$\beta(u,v) = \begin{cases} \dfrac{2kT}{3\mu}\left(\dfrac{1}{u^{1/D_f}} + \dfrac{1}{v^{1/D_f}}\right)\left(u^{1/D_f} + v^{1/D_f}\right); & \text{continuum} \\ & \text{regime} \\ \left(\dfrac{3}{4\pi}\right)^{2/D_f - 1/2} r_0^{\,2-6/D_f}\left(\dfrac{6kT}{\rho_p}\right)^{1/2}\left(\dfrac{1}{u} + \dfrac{1}{v}\right)^{1/2}\left(u^{1/D_f} + v^{1/D_f}\right)^2; & \text{free molecular regime} \end{cases} \tag{3.8}$$

3.5. Self-preserving solution to the agglomeration equation

Friedlander and Wang (1966) pointed out that if the collision frequency function is a homogenous function of degree n, that is if

$$\beta(\lambda u, \lambda v) = \lambda^n \beta(u, v) \tag{3.9}$$

then the transformation

$$\begin{cases} \eta = \dfrac{v}{\bar{v}(t)} \\ \bar{v}(t) n(v,t) = N(t) \psi(\eta) \end{cases} \tag{3.10}$$

reduces the agglomeration equation (3.2) to an ordinary integro-differential equation for ψ of η. This solution is called the self-preserving solution of the agglomeration equation. It is an asymptotic solution $\psi(\eta)$ towards which all systems converge, regardless of the initial distribution. It is easily checked that the collision frequency functions for the free molecular and continuum regimes (3.3) or (3.10) are homogenous functions but the Fuchs equation for the complete size spectrum (3.4) is not. If we wish to have a general solver of the coagulation equation (3.2) for all possible particle size ranges, we must use a discretization of the particle size spectrum and a numerical solution as with the complete GDE, explained in Chapter 2. The form of the self-preserving solution may be obtained by solving the coagulation equation numerically up to the point where the size distribution, expressed in the form $\psi(\eta)$, remains fixed with some preset accuracy.

The free-molecular case will now be analyzed in more detail. By inserting the free-molecular collision frequency function from (3.8) into the agglomeration equation (3.2) and by integrating the equation from 0 to ∞, we get an equation for the total particle concentration $N(t)$. This can be written in terms of the normalized variables (3.10) for the average agglomerate volume $\bar{v}$ to give (Matsoukas and Friedlander,1991; paper E)

$$\frac{d\bar{v}}{dt} = \frac{1}{2} \alpha \sqrt{\frac{6kT}{\rho}} \left(\frac{3\bar{v}}{4\pi} \right)^{1/6} \phi n^{2/D_f - 2/3} \tag{3.11}$$

Here ϕ is the volume fraction of particulate matter (volume of particles/volume of gas), n the average number of primary particles in an agglomerate and α a constant, which depends on D_f approximately by the following equation:

$$\begin{aligned} \alpha &= \int_0^\infty \int_0^\infty \left(\eta_1^{-1} + \eta_2^{-1} \right)^{1/2} \left(\eta_1^{1/D_f} + \eta_2^{1/D_f} \right)^2 \psi(\eta_1) \psi(\eta_2) d\eta_1 d\eta_2 \\ &\approx 6.548 + 112.1 \cdot D_f^{-7.883} \end{aligned} \tag{3.12}$$

Correlation (3.12) was obtained by solving the self-preserving distribution $\psi(\eta)$ numerically for different values of (constant) D_f, then integrating numerically and curve-fitting. Equation (3.11) shows the power of the self-preserving analysis: For systems in the free-molecular regime that have evolved for a sufficiently long time, the complete size distribution is described by a single ordinary differential equation (3.11) for the average agglomerate volume. A similar analysis can be carried out for the continuum regime (Wu and Friedlander, 1993b; Vemury and Pratsinis, 1995).

4. ELECTRICAL AGGLOMERATION

In removing flue gas particles at coal fired power plants, the efficient collection of particles in the diameter range 0.1 to 1.0 μm remains to be solved. The most commonly used flue gas cleaner under these circumstances is the electrostatic precipitator (ESP). According to the studies of Mohr et. al (1996), the total mass collection efficiency with the ESP can be over 99.7 %, while the collection efficiency for the above mentioned range can be only 85 %.

Much research has been done recently to solve this problem of significant submicron penetration by utilizing a particle agglomerator before the ESP in order to shift the particle size distribution in such a way that the resulting particles can be efficiently collected (Eliasson and Egli, 1991, Kobashi, 1979). The possibility of accomplishing this by using particle charging and an alternating electric field was studied in papers B and C and is briefly reviewed here. In the alternating electric field the particles start to oscillate with amplitudes and velocities depending on particle size and charging. The different velocities cause kinematic coagulation between the particles, hopefully removing most of the particles in the problematic size range.

In the experimental part of the project (paper B), unipolar charging was used. In the theoretical treatment (paper C), however, studies were extended to take into account bipolar charging as well. The experimental work was later extended to agglomeration studies of bipolarly charged particles by Laitinen (1994) and Hautanen (1995).

4.1. Parallel plate agglomerator

The basic idea of the agglomerator is simple (Figure 4.1). First, the particles are charged unipolarly with a corona charger, after which they start to oscillate in the alternating electric field of the agglomerator. Larger particles have larger oscillation amplitudes and velocities than the smaller ones, which is supposed to make them collide with each other. The experimental system is presented in detail in paper B.

The Brownian agglomeration mechanism is too weak in this system to remove the submicron particles by collisions with the large supermicron particles, especially since the unipolar charging makes the effect weaker. The aim of this setup is to remove the submicron particles by kinematic coagulation, caused by the oscillating motion. To measure this effect, the particle size distribution is measured after the agglomerator with the alternating electric field on and off. Comparing the results enables us to

separate the effect of the field from all other particle removal mechanisms in the system (Brownian agglomeration, deposition).

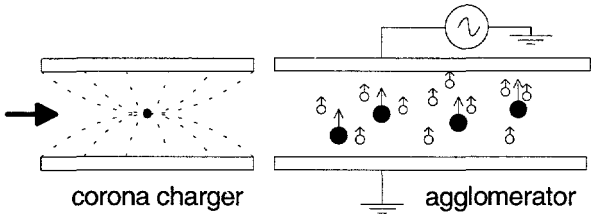

Figure 4.1. Principle of agglomeration (here the case of unipolar charging): Charged particles start to oscillate in the alternating electric field. The amplitude and velocity differences cause collisions.

The laboratory agglomerator (Paper B) had the following characteristics:

- amplitude of electric voltage $E_0 = 710\ 000$ V/m
- frequency of voltage $f = 50$ Hz
- residence time in agglomerator $\tau = 4$ - 6 s
- total mass concentration of particles $M = 1$ - 2 g/m^3
- geometric number mean diameter of fine particle mode $\overline{d}_1 = 0.35$ um
- geometric mass mean diameter of large particle mode $\overline{d}_2 = 3.0$ um
- reduction in fine mode concentration $\Phi = 3$ - 8 %.

In the charger, the particle aquires a charge approximately proportional to its surface area

$$q(d) = bd^2 \tag{4.1}$$

where b is $7.9 \cdot 10^{-6}$ C/m^2. This means that a particle of 0.14 μm will have approximately 1 elementary charge, a particle of 0.45 μm 10 elementary charges, a particle of 1.4 μm 100 elementary charges and so on. The quadratic dependence of particle diameter agrees qualitatively with field charging theory (Hinds, 1982). In the following calculations, Equation 4.1 will be used for all particle sizes even if fractions of elementary charges are impossible.

4.2. Effect of Coulomb forces on Brownian agglomeration

It is possible to derive an expression for the collision frequency function, taking into account Coulomb forces between the particles (Fuchs, 1964). The procedure results in a convenient equation where the effect of the

electric charges can be expressed as a correction factor relative to the neutral case:

$$\beta_{Coul}(d_i, d_j) = \frac{\xi}{e^{\xi} - 1} \beta(d_i, d_j), \tag{4.2}$$

$$\xi = \frac{q_i q_j}{2\pi\varepsilon_0 kT(d_i + d_j)}. \tag{4.3}$$

The term ξ represents the ratio of the electrostatic potential energy at contact to the thermal energy kT. The value of the correction term is plotted in Figure 4.2 for the parameter values mentioned in the last section.

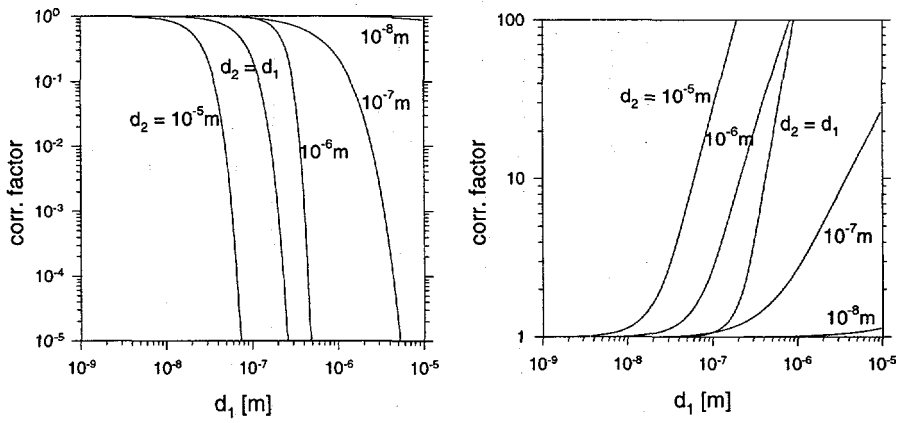

Figure 4.2. Correction factor for the Brownian collision frequency function, caused by Coulomb repulsion (left picture)/attraction (right picture).

4.3. Kinematic agglomeration of particles in an alternating electric field

If the charge of a particle is proportional to its surface area (Equation 4.1), it can easily be seen (Paper C) that the motion of the particle (diameter d) in an alternating electric field (field strength $E_0\cos(2\pi ft)$, frequency f), perpendicular to the gas flow can be described approximately with

$$x = -\frac{bE_0 d}{6\pi^2 \mu f}\sin(2\pi f t), \tag{4.4}$$

$$\dot{x} = -\frac{bE_0 d}{3\pi\mu}\cos(2\pi f t). \tag{4.5}$$

Now we see the cause of collisions. The amplitude of oscillation (and also velocity) is linearly dependent on the particle diameter. Hence the large particles have larger oscillation amplitudes and velocities than the small ones.

In the electrical agglomeration study we are interested in the case where the particles can be clearly divided into large (diameter > 1μm) collector particles and fine particles (diameter < 1 μm). To find out how effective the agglomeration process is, we must find out the volume that the large particles sweep, thus collecting the fine particles that are in their way (Paper C). This can also be conveniently approximated by using the coagulation equation (3.2) with the kinematic collision frequency function (3.5). If the number distribution of the fine particle mode is $n_1(d_1)$ and of the supermicron mode $n_2(d_2)$, the equation

$$\frac{dn_1(d_1)}{dt} = -n_1(d_1)\int_0^\infty \beta(d_1, d_2) n_2(d_2) dd_2, \tag{4.6}$$

is obtained, where the kinematic collision frequency function is

$$\beta(d_1, d_2) = \varepsilon(\sigma, d_1, d_2)\frac{\pi}{4}(d_1 + d_2)^2 \frac{2}{\pi}\frac{bE_0(d_2 - \sigma d_1)}{3\pi\mu}. \tag{4.7}$$

Here we have used the time average velocity difference of the sinusoidal motion for the term $|v_1 - v_2|$ in Equation 3.5. The constant σ takes into account three possible charging cases:

$$\sigma = \begin{cases} 1, & \text{unipolar charging} \\ -1, & \text{bipolar charging} \\ 0, & \text{neutral fine particles} \end{cases} \tag{4.8}$$

In paper B, only unipolar charging is studied. However, the same formalism is easily applied to bipolar charging and the case of neutral, non-oscillating small particles too. Equation (4.6) can now be solved for $n_1(d_1)$, thus the reduction in concentration of particles of diameter d_1 is ($m_2(d_2)$ is the mass concentration of the supermicron mode):

$$\Phi(d_1) \approx 1 - \exp\left(-\frac{bE_0\tau}{\pi^2 \rho \mu} \int_{d_2} \varepsilon(\sigma, d_1, d_2) \cdot m_2(d_2) \frac{(d_2 - \sigma d_1)(d_1 + d_2)^2}{{d_2}^3} \delta d_2 \right). \tag{4.9}$$

An important part of the theoretical study of kinematic coagulation is the determination of the collision efficiency $\varepsilon(\sigma,d_1,d_2)$ of two colliding droplets. The collision efficiency is defined as the ratio of the effective collision cross-section to the geometrical collision cross-section (Figure 3.2). The analytical expressions of Fuchs (1964) and Pruppacher and Klett (1978) for the collision efficiency in the case of gravitational coagulation are no longer valid in the case where interparticle electrical forces are important.

The determination of collision efficiencies between raindrops and aerosol particles in the atmosphere was an active research topic among cloud physicists in the late '60s and early '70s (Pruppacher and Klett, 1978). In most of these studies the equations of motion of the small aerosol particles are integrated into the flow field generated by the falling motion of the larger raindrops. By using a similar technique, the following equations are obtained by curve fitting into numerical results (Paper C):

$$\varepsilon(d_1, d_2) = \begin{cases} 0, & \text{unipolar charging } (\sigma = 1) \\ \dfrac{d_1}{d_2} + \dfrac{3}{2} \dfrac{d_1 {d_2}^2}{(d_1 + d_2)^3} \cdot \dfrac{b}{b_0} \left(1 + \dfrac{b}{10 b_0} \right), & \text{bipolar charging } (\sigma = -1) \\ \dfrac{3}{2} \left(\dfrac{d_1}{d_1 + d_2} \right)^2 & \text{neutral small particles } (\sigma = 0) \end{cases}, \tag{4.10}$$

Here b is a constant for the charge distribution (4.3) and b_0 the "reference value" $b_0 = 7.9 \cdot 10^{-6}$ C/m^2 from the experiments (Paper B).

The curves are plotted in Figure 4.3 for different values of b/b_0. Now, if the collision efficiency $\varepsilon(d_1,d_2)$ from equation (4.10) is inserted into Equation 4.9, the reduction in the submicron mode particle concentration for a given mass distribution $m_2(d_2)$ is readily obtained. Some sample calculations are done in Paper C.

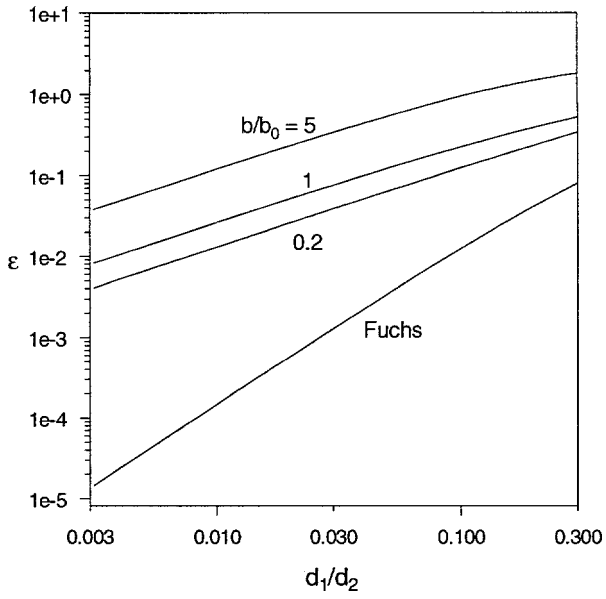

Figure 4.3. Collision efficiencies of bipolarly charged ($|q(d_i)| = bd_i^2$) particles and the Fuchs collision efficiency for the case of neutral fine particles.

4.4 Discussion

Based on the results of the previous section, unipolar kinematic agglomeration in an alternating electric field is negligible, when the fine particles to be collected and the large collector particles are charged with the same polarity. In the experiments, however, (Paper B) some reduction in the fine particle mode number concentration was observed. There are a few possible reasons for this that were not taken into account in the model.

Firstly, a small fraction of the fine particles deposit on the agglomerator walls because of their vibrating motion in the electric field. Secondly, the charge distribution (4.1) is based on an experiment that measures the average charge of the particles. This means that there are particles that have a larger charge than (4.1) and those which are neutral or even of opposite polarity. Thirdly, the electric field induces some polarization within the particles, which increases the rate of Brownian collisions (Fuchs; 1964).

Finally, the sinusoidal motion of the large and small particles is not exactly in the same phase because of the inertia of the large particles (Paper C). This means that in a short time interval, particles of the same polarity move in opposite directions, which increases the collision efficiency dramatically. Since it is already obvious from the simple theoretical analysis of the previous sections and the experimental results that unipolar charging with a subsequent alternating electric field will not be the solution for enhancing available particle removal methods, a more detailed analysis, taking into account all of the above mentioned effects, was not performed in this study.

The case of bipolar charging seems promising in terms of particle removal efficiency. The sample calculations of Paper C show that, if the collector particles and fine particles are of opposite polarity, significant reductions in the fine particle mode concentrations can be obtained. In addition, since this analysis considered only kinematic agglomeration, the fine particle reduction should be even higher because of enhanced Brownian collisions (see Figure 4.2). There is experimental evidence suggesting that actually it is the enhanced Brownian agglomeration that could be used as the fine particle removal mechanism - no electric field is needed. (Eliasson and Egli, 1991; Hautanen, 1995)

5. COALESCENCE OF AEROSOL PARTICLES

As was already briefly mentioned in the introduction to Chapter 3, the rate of coalescence is important in determining the characteristics of the collision processes. By coalescence we mean here the rounding of initially two distinct particles into one spherical particle. If coalescence is fast, only spherical particles are encountered - then the collision-coalescence process is called coagulation. If coalescence is slow, dendritic structures form and the process is called agglomeration.

In the ceramics community, the coalescence process is usually called sintering. In this context coalescence or sintering means the production of a ceramic material by heating a powder. Upon heating, the particles in the powder bond to one another yielding a higher strength. The temperature required for coalescence to become evident is typically above one half of the absolute melting temperature (German, 1996). The industrial interest in sintering results from the change of many physical properties (for example: strength, conductivity and corrosion resistance) accompanying particle bonding.

The first quantitative models of coalescence were presented by Frenkel (1945) and Kuczynski (1949). Most of the work since, reviewed nicely by Kingery et al. (1976), Coblenz et al. (1980) and German (1996), is based on their original formalism. This chapter will first briefly introduce the widely used initial and final stage coalescence models and then summarize the work of papers D, E and F concerning the modeling of simultaneous agglomeration and coalescence. Finally, the gas-to-particle aerosol route to controlled particle production is introduced. The ability to control the particle size in superfine particle production is essential because of the size dependence of many important material properties (Ichinose et al., 1992).

5.1. Initial solid state coalescence models

Here the system of interest consists of two separate spherical particles of radius r, initially touching each other. The reduction in surface free energy is the driving force for coalescence, the result of which being a single spherical particle. The purpose of this chapter is to discuss the modeling of the initial stages of sintering, i.e. the formation and growth of a neck between the particles.

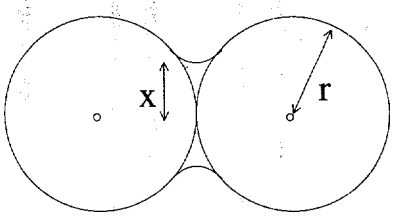

Figure 5.1. Neck formation between two spherical particles during the initial stages of coalescence.

In classical sintering models (Coblenz et al., 1980) the growth of the neck radius x (see Figure 5.1) by a single coalescence mechanism can be described with the equation

$$\left(\frac{x}{r}\right)^n = \frac{C(T)}{r^m} t \tag{5.1}$$

where $C(T)$ is a function that for a specific material and coalescence mechanism depends only on temperature (Table 5.1). The parameters m and n are constants that have different values for different coalescence mechanisms (Table 5.1).

Table 5.1. Initial neck growth model parameters for various coalescence mechanisms.

Coalescence mechanism	C(T)	m	n
viscous flow	$\frac{3\sigma}{2\mu}$	1	2
evaporation-condensation	$\frac{6\sigma p M^{3/2}}{\sqrt{2\pi}\rho^2 (RT)^{3/2}}$	2	3
lattice diffusion	$\frac{64 D_l \sigma M}{\rho RT}$	3	4
surface diffusion	$\frac{225 \delta D_s \sigma M}{\rho RT}$	4	5
grain boundary diffusion	$\frac{192 w D_b \sigma M}{\rho RT}$	4	6

σ = surface energy
μ = viscosity
p = pressure
M = molar mass
R = gas constant
T = temperature
δ = surface layer thickness
w = grain boundary width
ρ = density
D = diffusion coefficient (l = lattice, s = surface, b = grain boundary)

The expression (5.1) for neck growth is based upon simplified geometries for the growing neck that limits its applicability to a neck radius below about $x/r < 0.3$. Even if the whole coalescence process cannot be described in this way, an estimate of the order of the time needed for complete coalescence (characteristic time for coalescence or fusion) can be obtained:

$$\tau_f = \frac{r^m}{C(T)}. \tag{5.2}$$

In addition, Equations 5.1 and 5.2 give us a feeling for how the coalescence process proceeds and depends on particle size. From Equation 5.1 it is clear that the neck grows rapidly at first and then the process slows down. This will be discussed in more detail in the next section. From Equation 5.2 (and Table 5.1) it is also obvious that coalescence takes longer for larger particles. For coalescence by viscous flow the characteristic coalescence time τ_f is proportional to the particle radius, and for the evaporation-condensation and diffusion mechanisms the effect is even stronger.

5.2. Coalescence models for the final stages

In their numerical simulations of coalescence by viscous flow, Hiram and Nir (1983) found that the neck radius x approaches its final value x_{sph} exponentially:

$$\frac{dx}{dt} = -\frac{1}{\tau_f}\left(x - x_{sph}\right). \tag{5.3}$$

This equation was found to hold beyond the very short time interval during which approx. 10% of the neck growth takes place.

Koch and Friedlander (1990) noted that an equation of the same form is then valid for the surface area reduction in the final stages of coalescence:

$$\frac{da}{dt} = -\frac{1}{\tau_f}\left(a - a_{sph}\right) \tag{5.4}$$

where a is the total surface area of the coalescing pair of particles and a_{sph} is the surface area of a spherical particle of the same volume. This result was already theoretically derived by Frenkel (1945) for coalescence by viscous flow and later by Friedlander and Wu (1994) for coalescence by solid state diffusion. Their derivation was based on a solution for the diffusion

equation inside the particle using spherical harmonics, with a boundary condition relating the curvature and difference in pressure across the surface. Their derivation resulted in the following form for the characteristic coalescence time, which is of the same functional form as the time in Table 5.1, differing only by a constant factor of 4:

$$\tau_f = \frac{3kTv}{64\pi D\sigma v_m} \tag{5.5}$$

where T is the absolute temperature, v the particle volume, D the solid state diffusion coefficient, σ the surface energy and v_m the molecular volume. Solid state diffusion is a thermally activated process and its temperature dependence can be represented by an Arrhenius form (Kingery et al., 1976):

$$D(T) = D_0 \exp\left(-\frac{E_{act}}{kT}\right). \tag{5.6}$$

Even if Equation (5.4) is valid only for the final stages of coalescence, it is frequently used to model the complete coalescence process because of its convenient form, which becomes especially evident in studying systems where coalescence is accompanied by simultaneous collisions with other particles. The error of this assumption is discussed in Koch and Friedlander (1990).

5.3. Simultaneous collision and coalescence

A convenient but simple technique to describe nonspherical particle dynamics is to choose the surface area in addition to the volume as particle size and shape variables. Let $n(v,a,t)$ be the particle number concentration per unit mass of gas in a volume range between v and v+dv and an area range between a and a+da at time t. In the absence of condensation and dilution by mixing, the general dynamic equation for the continuous size distribution function becomes (Koch and Friedlander, 1990)

$$\begin{aligned}
&\frac{\partial n}{\partial t} + \frac{\partial}{\partial a}\left(n\frac{\partial a}{\partial t}\right) = \\
&\frac{1}{2}\int_0^v \Theta\left[a > a_{sph}(v') + a_{sph}(v'-v)\right]\int_0^a \beta(v', v-v', a', a-a')n(v', a') \\
&\qquad\qquad n(v-v', a-a')da'dv' \\
&-n(v,a)\int_0^\infty \int_0^\infty \beta(v,v',a,a')n(v',a')da'dv'
\end{aligned} \tag{5.7}$$

The collision frequency function β is assumed to be a function of particle volume and area only. The second term of Equation 5.7 represents the motion in area space due to coalescense. The right hand side is the change due to collision. The step function Θ is required because the surface area of the particle produced by a collision is greater than the sum of the minimum surface areas $a_{\mathrm{sph}}(v)$ of the two original particles.

Using the exponential decay law for the surface area (Equation 5.4), multiplying by a and integrating with respect to a and v (Paper D), the following linear relationship for the total surface area per unit volume A_{sph} of all aerosol particles is obtained:

$$\frac{dA}{dt} = -\frac{1}{\tau_f(\bar{v})}\left(A - A_{sph}\right) \tag{5.8}$$

where A is the total surface area per unit mass of gas, $\bar{v}$ is the average particle volume and A_{sph} is the minimum possible surface area (complete coalescence) per unit mass of gas.

It is convenient to introduce a new variable θ (Paper D), which represents the fractional deviation of the aerosol surface area from the state in which each particle has relaxed to the spherical shape:

$$\theta = \frac{A - A_{sph}}{A_{sph}}. \tag{5.9}$$

Using θ as the surface area variable transforms equation 5.8 into the following form:

$$\frac{d\theta}{dt} + \left[\frac{1}{\tau_f(\bar{v})} - \frac{1}{\tau_c(\bar{v})}\right]\theta = \frac{1}{\tau_c(\bar{v})}, \tag{5.10}$$

where τ_c is the characteristic collision time, defined by

$$\frac{1}{\tau_c} = -\frac{1}{A_{sph}}\frac{dA_{sph}}{dt} = \frac{1}{3\bar{v}}\frac{d\bar{v}}{dt}. \tag{5.11}$$

Studying this form of the equation gives a deeper insight to the problem of simultaneous collisions and coalescence, at least in a cooling system. This is due to the exponential nature of equation 5.10, in which the sign of the

factor before θ determines the nature of the solution (see paper D). At the beginning, when the temperature is high, the characteristic coalescence time τ_f is shorter than the characteristic collision time τ_c. Then θ will stay close to zero. When the temperature falls, the solid state diffusion coefficient decreases very rapidly and at some point τ_f becomes greater than τ_c. Thus, the nature of the solution changes and θ starts to grow rapidly. This is approximately the point at which the primary particle size is determined, and dendritic agglomerate stuctures start to form.

In some applications, much of the primary particle growth may occur within large agglomerates. As the linear coalescence law (equation 5.4) is strictly valid only for the final stages of coalescence, it is not expected to work well for the coalescence of large agglomerates (of n primary particles). In paper E, the applicability of the linear coalescence law is extended by applying it to smaller domains (of m primary particles) of the agglomerate, instead of the complete dendritic structure. By doing so, the following approximate equations are obtained for the growth of the average agglomerate and primary particle sizes:

$$\frac{dv_a}{dt} = \frac{1}{2}\alpha\sqrt{\frac{6kT}{\rho}}\left(\frac{3v_a}{4\pi}\right)^{1/6}\phi n^{2/D_f - 2/3} \tag{5.12}$$

$$\frac{dv_p}{dt} = \begin{cases} \dfrac{64\pi D\sigma v_0}{kT}\left(m^{-1} - m^{-4/3}\right), & n = \dfrac{v_a}{v_p} > m \\ \dfrac{64\pi D\sigma v_0}{kT}\left(n^{-1} - n^{-4/3}\right), & n = \dfrac{v_a}{v_p} \le m \end{cases} \tag{5.13}$$

Equations 5.12 and 5.13 are coupled through $n = v_p/v_a$, the value of which also determines which right-hand-side is used equation 5.13. Although approximate, equation 5.13 is intuitively correct in the sense that it reduces to equation 5.8 if n is small, and does not depend on n if n is large. Equation 5.13 can be actually thought of as an interpolation between the two extreme cases.

5.4 Gas-to-particle aerosol technique for controlled nanoparticle production

The unique properties of matter comprised of superfine structures have raised a lot of attention in recent years (Ichinose et al. 1992, Siegel 1994). Aerosol techniques provide a useful tool to produce high purity materials in a controlled way (Pratsinis and Kodas, 1993). In the gas-to-particle aerosol conversion process, precursor vapors react and form product particles that grow further by collisions. Powders made by such techniques typically have narrow size distributions and they consist of nonporous, spherical primary particles. The gas-to-particle route for material synthesis is used on an industrial scale, for example, in the production of pigmentary titania and fumed silica.

High temperatures are usually required for the reaction of the precursor vapor to produce molecules of the desired material. These molecules grow by condensation or coagulation, retaining a spherical form if the collision rate is slower than the coalescence rate. In the opposite situation, agglomerates of spherical primary particles form. The high temperatures required for the reaction are obtained typically in flame, furnace, plasma or laser reactors.

An example of the gas-to-particle aerosol technique for nanophase material production is the free jet described in paper F (Figure 5.2). The system consists of a precursor vapor introduced as a jet into a methane-air flame, in which the precursor reacts with oxygen to form metal oxide particles. The particles grow by simultaneous collision and coalescence, the rates of which determine the final primary particle size (papers D-G). The particle size is controlled by using temperature, residence time and volume loading as control parameters. The effect of material properties, especially the solid state diffusion coefficient, is studied by performing the experiments with three different materials: Titania, Alumina and Niobium Oxide. Based on comparisons with model calculations it is obvious that even simple models based on characteristic time scales can give valuable information on how the process parameters affect the dynamics of the material synthesis process (Paper G).

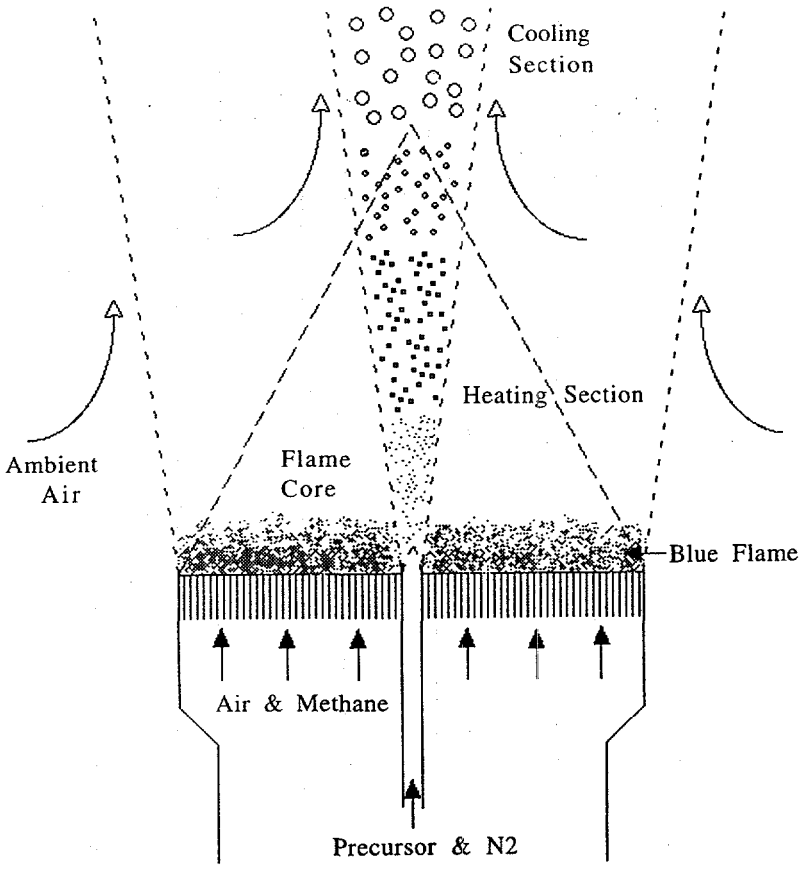

Figure 5.2. The free jet material reactor is comprised of a precursor-nitrogen jet, brought into a methane-air flame. Particles grow along the jet axis until coalescence is quenched by ambient air.

6. CONCLUSIONS

In this thesis, theoretical modeling of certain aerosol systems has been presented. After starting from aspects of a general aerosol dynamics solution routine, the focus of the thesis considers two applications, in which particle collisions are the dominating dynamic mechanism and simple, almost analytical theoretical models are within reach.

The first application is the electrical agglomerator, in which aerosol particles are charged and brought into an alternating electric field. With this arrangement the aim is to remove submicron particles from flue gases by collisions with larger particles before conventional gas cleaning devices that have a clear penetration window in the problematic 0.1-1 μm size range. A model was derived for the removal of the submicron particles in an agglomerator, in which the effect of electric charge on the collision efficiencies was computed numerically.

The theoretical analysis performed clearly demonstrates that bipolar charging is necessary to obtain significant removal of submicron particles by such an arrangement. Optimally, the particles to be collected and the larger collector particles should have opposite charges. The efficiency of bipolar charging comes from two effects: 1) the motion of oppositely charged particles in an alternating electric field is in opposite phase and 2) oppositely charged particles attract each other.

The second application is controlling nanoparticle size in the gas-to-particle aerosol route to material synthesis. In a typical material reactor, a precursor vapor reacts to form molecules of the desired material. In a cooling environment, a particulate phase forms, in which the particles grow by collisions. At first, the collision rate is slower than the coalescence rate - thus the particles remain spherical. The coalescence rate is a strong function of temperature, and at some point the collision rate becomes faster. This is where agglomerate stuctures start to form and approximately the point which determines the primary particle size. These stages were demonstrated using a laboratory scale free jet material reactor.

A theoretical model based on the simultaneous solution of collision and coalescence is presented, which is based on the self-preserving solution to the agglomeration equation and solid state coalescence models. It gives the average agglomerate size and primary particle size as a function of location in a given material reactor. Consequently, the onset of dendrite formation and final primary particle size of the produced material are also predicted.

From the comparisons between theory and experiment it is obvious that such a model is able to capture the effects of the system parameters (temperature, velocity, volume loading of material and location of collection) on the primary particle size of the produced material, and can thus be a valuable tool in producing nanomaterials of desired properties.

REFERENCES

Coblenz, W. S., Dynys, J. M., Cannon, R. M. and Coble, R. L. (1980). Initial solid state sintering models. A critical analysis and assessment. Sintering Processes, Material Science Research 13, pp. 141 - 157.

Eliasson, B. and Egli, W. (1991). Bipolar coagulation - modeling and applications. J. Aerosol Sci. 22, pp. 429 - 440.

Frenkel, J. (1945). Viscous flow of crystalline bodies under the action of surface tension. Journal of Physics 9, pp. 385 - 391.

Friedlander, S. K. (1977). *Smoke, Dust and Haze.* John Wiley and Sons, New York. 317 p.

Friedlander, S. K. and Wang, C. S. (1966). The self-preserving particle size distribution for coagulation by Brownian motion. J. Colloid Interface Sci. 22, pp. 126 - 132.

Friedlander, S. K. and Wu, M. K. (1994). Linear rate law for the decay of the excess surface area of a coalescing solid particle. Phys. Rev. B 49, pp. 3622 - 3624.

Fuchs, N. A. (1964). *The Mechanics of Aerosols.* Dover, New York. 408 p.

Gelbard, F. and Seinfeld, J. H. (1978). Coagulation and growth of a multicomponent aerosol. J. Colloid Interface Sci. 63, pp. 472 - 479.

Gelbard, F. and Seinfeld, J. H. (1980). Simulation of multicomponent aerosol dynamics. J. Colloid Interface Sci. 78, pp. 485 - 501.

German, R. (1996). *Sintering Theory and Practice.* John Wiley and Sons, New York. 550 p.

German, R. M. and Munir, Z. A. (1976). Surface area reduction during isothermal sintering. J. American Ceramic Soc. 59, pp. 379 - 383.

Hautanen, J. (1995). Agglomeration of charged aerosol particles. PhD Thesis, Tampere Univ. of Tech. Publications no. 158. 164 p.

Hinds, W. C. (1982). *Aerosol Technology.* Wiley Interscience, New York. 424 p.

Hiram, Y. and Nir, A. (1983) A simulation of surface tension driven coalescence. J. Colloid Interface Sci. 95, pp. 462 - 470.

Ichinose, N., Ozaki, Y. and Kashu, S. (1992). *Superfine Particle Technology.* Springer-Verlag, Berlin.

Im, K. H., Ahluwalia, R. K. and Lin, H. C. (1987). The RAFT computer code for calculating aerosol formation and transport in severe LWR accidents. EPRI Report NP-5287-CCM.

Kim, Y. P. and Seinfeld, J. H. (1992). Simulation of multicomponent aerosol dynamics. J. Colloid Interface Sci. 149, pp. 425 - 449.

Kingery, W. D., Bowen, H. K. and Uhlmann, D. R. (1976). *Introduction to Ceramics.* John Wiley and Sons, New York. 1032 p.

Kobashi, M. (1979). Particle agglomeration induced by alternating electric fields. PhD Thesis, Stanford University. 212 p.

Koch, W. and Friedlander, S. K. (1990). The effect of particle coalescence on the surface area of a coagulating aerosol. J. Colloid Interface Sci. 140, pp. 419 - 427.

Kuczynski, G. C. (1949). Self-diffusion in sintering of metallic particles. Trans. AIME 185, pp. 169 - 178.

Laitinen, A. (1994). Agglomeration of electrically charged aerosol particles. MSc Thesis, Tampere Univ. of Tech. Dept. Electrical Eng. Report 2-94. 80 p.

Matsoukas, T. and Friedlander, S. K. (1991). Dynamics of aerosol agglomerate formation. J. Colloid Interface Sci. 146, pp. 495 - 506.

Mohr, M., Ylätalo, S., Klippel, N., Kauppinen, E. I., Riccius, O. and Burtscher, H. (1996). Submicron fly ash penetration through electostatic precipitators at two coal power plants. Aerosol Sci. Tech. 24, pp. 191 - 204.

Pratsinis, S. E. and Kodas, T. T. (1993). Manufacturing of materials by aerosol processes, *in Aerosol Measurement: Principles, Techniques and Applications* (ed. Willeke, K. and Baron, P. A.). Van Nostrand Reinhold, New York. pp. 721 - 746.

Pruppacher, H. R. and Klett, J. D. (1978). *Microphysics of Clouds and Precipitation.* D. Reidel Publishing Co., Dordrecht. 714 p.

Sher, R. and Jokiniemi, J. K. (1993). NAUAHYGROS 1.0: A code for calculating the behaviour of aerosols in nuclear plant containments following a severe accident. EPRI Report TR-102775.

Schmoluchowski, M. (1917). Z. Physik. Chem. 92, pp. 129 - 154.

Siegel, R. W. (1994). Nanophase Materials: Synthesis, structure and properties, in *Physics of New Materials* (ed. Fujita, F. E.). Springer-Verlag, Berlin, pp. 65 - 105.

Vemury, S. and Pratsinis, S. E. (1995). Self-preserving size distributions of agglomerates. J. Aerosol Sci. 26, pp. 175 - 185.

Wu, J. J. and Flagan, R. C. (1988). A discrete-sectional solution to the aerosol dynamic equation. J. Colloid and Interface Sci. 123, pp. 339 - 352.

Wu, M. and Friedlander, S. K. (1993a). Note on the power law equation for fractal-like aerosol agglomerates. J. Colloid Interface Sci. 159, 246 - 248.

Wu, M. and Friedlander, S. K. (1993b). Enhanced power law agglomerate growth in the free molecule regime. J. Aerosol Sci. 24, pp. 273 - 282.

Reprinted with permission from the publisher. PAPER A
In: Journal of Aerosol Science 1994. Vol. 25, No. 3, pp. 429 - 446.

NUMERICAL SIMULATION OF VAPOUR–AEROSOL DYNAMICS IN COMBUSTION PROCESSES

JORMA K. JOKINIEMI, MIHALIS LAZARIDIS, KARI E. J. LEHTINEN and ESKO I. KAUPPINEN*

Technical Research Centre of Finland (VTT), Aerosol Technology Group, Nuclear Engineering Laboratory, P.O. Box 208, SF-02151 Espoo, Finland; Laboratory of Heating and Ventilation

(*Received* 4 *May* 1993; *and in final form* 5 *October* 1993)

Abstract—A computer model (ABC-code) has been constructed to describe the steady one-dimensional aerosol dynamics in combustion processes for gas and particle interactions at post-combustion conditions. The aerosol general dynamic equation has been solved numerically using a discrete-nodal point method for describing the particle size distribution. In the present model we consider those mechanisms that will affect the dynamics of alkali species after volatilisation, i.e. nucleation, condensation, coagulation, chemical reactions and deposition. The main features of the ABC code have been explained and an example calculation has been carried out for simulation of aerosol dynamics and alkali vapour behaviour in a real scale pulverised coal fired boiler. The results show that for predicting the gas phase concentrations of alkali species at different temperatures it is important to know the volatilisation of sodium, potassium, chlorine and sulphur and the formation rate of alkali sulphates in the gas phase. The initial ash size distribution determines the distribution of condensed alkalis between sub- and supermicron particle modes. The choice of the homogeneous nucleation model has some importance for the calculated submicron number size distribution. The effect of heterogeneous nucleation to initiate condensation on ash particles was negligible. The predictions of our simulation are in a qualitative agreement with the experimental results. The utilisation of the present code will lead to a better understanding of aerosol behaviour which will be of great importance for the control of toxic flue gas emissions, slagging and fouling in commercial boilers.

1. INTRODUCTION

In solid and liquid fuel combustion processes aerosol particles are formed from volatilised species and from non-volatilised mineral inclusions. The behaviour of inorganic aerosol particles and vapour phase species is of great importance when considering slagging and fouling, effective operation of gas cleaning devices and adverse environmental effects (Sarofim *et al.*, 1977). Behaviour of alkali species is an important factor when corrosion of heat transfer surfaces is considered. The volatilisation and post-combustion behaviour of toxic trace metal species is receiving increased attention when environmental effects of pulverised coal combustion are considered.

Aerosol behaviour has been studied widely in pulverised coal (PC) combustion processes (e.g. Flagan and Friedlander, 1978; Neville and Sarofim, 1982, 1985). Coal contains both organically and inorganically bounded mineral matter. During pulverised coal combustion the mineral matter transforms to vapours and fly ash particles of various sizes and compositions. Experimental and modelling studies have been carried out to understand the aerosol formation in pulverised coal combustion conditions (Neville and Sarofim, 1982; Senior and Flagan, 1982; Joutsensaari *et al.*, 1993). However, there is still a lack of knowledge of the contribution of organically bound inorganic mineral species to the formation of the observed submicron peak and in the volatilisation–condensation mechanisms of alkali species. In the fluidized bed combustion (FBC) systems the suspensions are very concentrated and the peak temperatures of the fuel particles are much lower as compared to the pulverised coal combustion. This affects flow conditions, heat transfer and aerosol behaviour. New particle formation by nucleation of such species as Si, Mg, Ca and Fe is suppressed, but still some amounts of alkali and toxic species are volatilised (Kauppinen *et al.*, 1993b; Lind *et al.*, 1993). In kraft recovery boilers, aerosol dynamics is mainly controlled by the behaviour of sodium, sulphur and chlorine species (Kauppinen *et al.*, 1993a).

Laboratory and field measurements as well as modelling tools are needed to understand the phenomena determining vapour–aerosol dynamics in the above-mentioned processes. This understanding can then be utilised to reduce problems related to these systems and in the development of new fuel conversion techniques for energy production.

In this study we have constructed a general ABC (Aerosol Behaviour in Combustion) computer model to describe the formation, growth and deposition of aerosol particles formed from vapour species and ash components in combustion processes. In the ABC code we use the nodal point method for discretising the particle size distribution, which was first applied for aerosol modelling by Bunz *et al.* (1983). Another widely used method for discretising the particle size spectrum is the sectional method (Gelbard *et al.*, 1980). Both methods "nodal point" and "sectional" conserve mass and are acceptable to discretise the particle size domain. We have chosen the nodal point method, because in our applications the material density and gas composition may change significantly during the simulation. The coagulation and condensation coefficients depend also on gas composition, which is not known *a priori* and is calculated based on the local chemical equilibrium or kinetics and thus coagulation and condensation coefficients must be recalculated after every time step.

So far this model has been applied for alkali species behaviour in pulverised and fluidized bed (Lind *et al.*, 1993) coal combustion processes as well as kraft recovery boilers (Kauppinen *et al.*, 1993a).

In our model the mechanisms that we believe will affect the dynamics of alkali species after volatilisation from fuel into the gas phase are considered. We have also carried out an example calculation for aerosol dynamics in a real scale pulverised coal fired boiler to show the ability of the ABC code to model alkali behaviour in PC combustion conditions during flue gas cooling. In this calculation the local gas phase chemical equilibrium is coupled to aerosol formation by homogeneous nucleation and growth by heterogeneous nucleation, condensation and coagulation.

The most important advantage of the ABC code compared to earlier models is the implementation of several new physico-chemical models, which are applied for coal combustion conditions. This kind of comprehensive model has not been reported in archival journals.

2. MODEL DESCRIPTION

To understand better the behaviour of the gas–vapour–particle system in combustion and gasification, the aerosol dynamics during flue gas cooling have been modelled. The aerosol general dynamic equation (GDE) is solved numerically by combining the solution methods introduced by Im *et al.* (1985) and Bunz *et al.* (1983). Particles are divided into n size classes each of which having different chemical composition. Basic physical interactions, i.e. nucleation, vapour condensation, coagulation and deposition are considered.

In the model the gaseous species balance equation and the aerosol GDE are solved simultaneously as a function of location. It is assumed that the flow is turbulent and that aerosol and vapour concentrations are uniform over the axial volume step ($\Delta V \equiv \Delta x A$). The step size Δx is determined by the characteristic time for nucleation, coagulation and condensation. This 1-D Lagrangian solution marches along the flow direction and solves the aerosol number size distribution, chemical species size distribution, deposition, gaseous species concentration, etc. as a function of location (Im *et al.*, 1985).

Formation of condensible species can be calculated from chemical kinetics or according to local chemical equilibrium. The particle size distribution is discretised according to the discrete-nodal point scheme developed in this work by discretising the particle size distribution monomer-by-monomer up to a particle size which contains user specified number of monomers. For larger particle sizes the number distribution is divided into n_i nodal points distributed evenly according to the logarithm of particle radius r_i. Brownian, turbulent and gravitational coagulation kernels for spherical particles are considered.

2.1. *Numerical solution methods*

Solution of the GDE and gaseous species conservation equations. The discrete and continuous GDEs were originally given by Friedlander (1977). The numerical solution to these equations was first presented by Gelbard and Seinfeld (1978). Several papers dealing with the numerical solution of the GDE have been published during the last two decades. The most common way to solve the continuous part of the GDE has been the sectional method (Gelbard *et al.*, 1980). This method has been later improved to give a more accurate solution for coagulation (Warren and Seinfeld, 1985) and to prevent numerical diffusion during vapour condensation (Gelbard, 1990). Also other methods like the nodal point scheme (Bunz *et al.*, 1983; Bunz and Dlugi, 1991) have been used to solve the continuous part of the GDE. This method has been improved by Sher and Jokiniemi (1993) for multicomponent representation of the size distribution for varying particle density and a moving grid for vapour condensation. Also new physical and chemical phenomena have been implemented in this model (Bunz and Dlugi, 1991). Both of the above-mentioned methods are widely used and they have been shown to give comparable results (e.g. Dunbar and Fermandjian, 1984).

In the ABC code we simulate the combustion process using the elemental volatilisation rates and the initial ash size distribution as input data. The size and chemical composition change in the particle spectrum is due to the mechanisms of chemical reactions, homogeneous nucleation, vapour condensation, coagulation and deposition. The whole process is described by the GDE (Friedlander, 1977). In combustion processes steady-state conditions can be assumed. Thus we solve the aerosol GDE in one-dimensional stationary form along the flow direction:

$$\frac{dn_k}{dx}=\frac{1}{u}J_k\delta(k-k^*)+\left(\frac{dn_k}{dx}\right)_{coag}+\left(\frac{dn_k}{dx}\right)_{grow}-\frac{v_d A_d}{u\Delta V}n_k, \tag{1}$$

where n_k is the particle number concentration for a size class k with particle radius r_k. The first term at the right corresponds to particle formation due to the homogeneous nucleation mechanism (formation of critical size embryo with radius r^*), the second term (coag) describes the coagulation mechanism, the third term (grow) the growth by condensation and chemical reactions and the fourth term the rate of particle removal due to deposition on boundary surfaces, where v_d is the particle deposition velocity, A_d is the deposition area and ΔV is the axial volume step. Time can be related to the location according to particle velocity (u), which is internally calculated by taking into account gas velocity, Stokes drag and gravitation.

Homogeneous nucleation has been evaluated using one of the following models at time: (i) classical model; (ii) a new statistical mechanical approach (Ford *et al.*, 1993); and (iii) stable monomer formation by gas phase chemical reactions (Xiong and Pratsinis, 1991). Condensation is modelled according to the well-known Mason equation for the droplet growth rate (e.g. Mason, 1971; Jokiniemi, 1990). Coagulation has been evaluated using the Smoluchowski equation, where the primary mechanisms considered are relative motion between particles due to Brownian diffusion, turbulence and gravitation. Vapour deposition due to condensation and particle deposition due to diffusion, thermophoresis, impaction and gravitational settling are modelled according to the theory developed by Ahluwalia *et al.* (1986). To describe the vapour deposition we use a model that takes into account mass transport from gas to surface, surface chemical reactions and diffusion through the reacted layer.

Condensible species formation by chemical reactions can be the driving force for nucleation and condensation in combustion processes and thus the chemistry in the gas phase need to be modelled. Behaviour of non-condensible gases is important when the reactions for condensible species are estimated.

We have started the modelling of gas phase reactions by calculating first the chemical equilibrium between all gas phase species. The method of Gibbs free energy minimisation with Lagrange multipliers (Eriksson, 1975) is used to calculate the concentrations of gaseous

species. After this the chemical form of the species in the condensed phase need to be specified to determine correct vapour pressures for condensation and nucleation calculations. In the ABC model any gas phase or condensed phase species can be considered. For this purpose we need to specify the elements, gas phase species, condensed phase species and their appropriate thermochemical data and physical properties. In addition, chemical reactions during condensation need to be specified. If equilibrium is not expected, we can give the reaction kinetic rates. The ABC code can handle reaction rates in the gas phase, gas–particle reactions and gas–surface reactions.

The rate of change of molar concentration of gas phase species is given by the gas phase species conservation equation:

$$\frac{dc_j}{dx}=\left(\frac{dc_j}{dx}\right)_{form}-\left(\frac{dc_j}{dx}\right)_{gtp}-\frac{v_v A_d}{u_g \Delta V}c_j, \tag{2}$$

where c_j is the gas phase molar concentration of the j-species. The first term (form) at the right of the equation represents the formation rate of these species, which can be calculated from local gas phase chemical equilibrium or from reaction kinetics. The second term (gtp) represents the vapour depletion rate due to nucleation, condensation and chemical reactions and the third term represents the depletion due to vapour deposition by condensation and chemical reactions on structures, where v_v is the vapour deposition velocity and A_d is the deposition area. Here time is related to the axial position through the gas velocity (u_g).

The mass size distribution of different species can be calculated by solving the condensed phase species equation:

$$\frac{d(\rho_{ak}Y_{jk})}{dx}=\left[\frac{d(\rho_{ak}Y_{jk})}{dx}\right]_{gtp}+\left[\frac{d(\rho_{ak}Y_{jk})}{dx}\right]_{coag}-\frac{v_d A_d}{u\Delta V}\rho_{ak}Y_{jk}, \tag{3}$$

where ρ_{ak} and Y_{jk} are the average density of particles in the kth grid point and the mass fraction of species j at the kth grid point. In our model the mass size distribution of pre-existing particles is given as input data.

The gas transport coefficients, viscosity, diffusivity, mean free paths and thermal conductivity, are evaluated by the kinetic theory of gases for pure substances. For multicomponent mixtures the properties of pure substances are coupled with semiempirical methods, which give a better accuracy than kinetic theory for mixtures (Reid *et al.*, 1987).

Particle size grid. In the numerical solution of the GDE we have employed a discrete-nodal point scheme, which is explained in the following. We will first consider a system where only one species is nucleating and the formed aerosol particles are chemically homogeneous. In this case the number of grid points in the discrete model is simply the number of molecules in the cluster. Hence the radius of the i-cluster is:

$$r_i=(i+1)^{1/3}r_0; \quad i=0, k, \tag{4}$$

where r_i is the radius of the i-mer and r_0 is the monomer radius.

If we have more than one chemical species and we want to solve the discrete GDE, we need to keep track of all particles which have different size and chemical composition. It can be shown that, in the general case when we have L different chemical species, the number of different i-mers N_i is (spherical particle shape is assumed):

$$N_i=\frac{(i+L-1)!}{i!(L-1)!}. \tag{5}$$

The total number of different combinations is obtained when we take a sum over all i-mers up to k-mer and the corresponding particle radii can then be calculated assuming that mass is conserved (e.g. $m_1+m_2=m_3$). In practice this leads to very large number of combinations (i.e. number of differential equations to be solved) and unreasonable large computing times. Thus for applications where we have more than one species nucleating only the nodal point particle size grid is used.

In the nodal point method the number distribution is divided into $n-1$ nodal points distributed evenly according to the logarithm of particle radius r_i.

$$\ln r_i - \ln r_{i-1} = A; \quad i = k, n \tag{6}$$

and

$$\frac{\ln r_{max} - \ln r_{min}}{A} = n - 1 - k = n_{max}, \tag{7}$$

where A is used to control the number of nodal points n_{max}. The average chemical composition for particles in nodal point i is used, i.e. all particles at a nodal point i have the same chemical composition.

We have combined these two models so that the discrete grid can be used up to the user specified number of coagulated molecules (k-mer) after which the nodal point grid is used.

2.2. *Homogeneous nucleation*

The nucleation process is a first-order phase transition problem, where there is a discontinuous change between two phases. There have been different approaches to the problem, beginning with the classical model of nucleation (Volmer, 1939; Becker and Döring, 1935), statistical (Reiss *et al.*, 1990; Ford *et al.*, 1993) and also with atomistic (Hoare *et al.*, 1980; Abraham, 1974) and computer simulation methods (Binder, 1987). The discussion here is limited to vapour-to-liquid nucleation, and more precisely to homogeneous nucleation. By homogeneous nucleation we mean the formation of droplets from pure vapour.

In the present work we are not interested to resolve the problem of nucleation but mainly to examine the sensitivity of the ABC code based on different nucleation models. The following descriptions of homogeneous nucleation are based on the classical nucleation model, a statistical approach which has been developed recently (Ford *et al.*, 1993) and a monomer coagulation model (Xiong and Pratsinis, 1991). The atomistic models have not been considered since they include many complexities and consume very long computing times, which make them not applicable for practical purposes.

The evolution of the aerosol size distribution depends much on the chemical and physical surroundings where the particles form, grow and deposit. If particles are formed due to condensible vapour cooling or if the production rate of condensible vapours from chemical reactions is slow, classical modelling of aerosol dynamics may be applied. In the classical approach the aerosol dynamics is modelled as critical cluster formation according to the classical nucleation theory based on thermodynamic considerations and their growth by condensation and coagulation.

Classical nucleation model. The classical model for nucleation has been based on the works of Volmer (1939) and Becker and Döring (1935), where they combined the kinetics for cluster formation with the thermodynamics of curved surfaces. As we can see, the classical theory lacks a fundamental microscopic basis and is a simple phenomenological theory. However, it can be expressed in a useful analytical form and it predicts to some extent the experimental data of nucleation (Ford *et al.*, 1993).

In the classical model embryo formation is due to a passage over an energy barrier, which is the energy for embryo formation. The radius, which corresponds to the maximum of the energy barrier is the critical radius for a stable embryo:

$$r^* = \frac{2\sigma}{n_l kT \ln S}. \tag{8}$$

This equation, which describes the critical radius of a stable droplet as a function of the number of liquid molecules (n_l) in a unit volume, saturation ratio (S), temperature (T) and surface tension (σ), represents the energetics of nucleation. When we combine this with nucleation kinetics, which is based on the assumption that clusters grow or shrink via the

gain or loss of single molecules, we get the nucleation rate:

$$J_{\text{class}}=\left(\sqrt{\frac{-1\ \partial^2\Delta G}{2\pi kT\ \partial i^2}}\right)_{i*} c_i^* b_1\ \exp(-\Delta G^*/kT). \tag{9}$$

The first factor in the parentheses is the well-known Zeldovich factor (Z) which takes into account the steady state distribution of clusters. ΔG^* denotes the maximum change in the Gibbs free energy, which is needed for the critical (stable) cluster formation, b_1 is the number concentration of monomers in the system and c_i the impingement rate on the aerosol surface.

Statistical nucleation model. Here we represent an alternative model for the evaluation of the nucleation rate based on statistical mechanical approach. The development of the classical theory is based on continuum thermodynamics and incorporates the use of macroscopic concepts. However, there is a need for the construction of a cluster potential model which will give a more solid foundation of the nucleation model. A first step for the introduction of a new statistical model has been made (Ford *et al.*, 1993; Lazaridis and Ford, 1993) and we will describe it briefly in this section. We must make it clear that we do not attempt here to present a microscopic model for homogeneous nucleation based on molecular interactions but only to give a more solid foundation to the classical model based on a statistical mechanical derivation. Future developments may use Monte Carlo simulations to obtain the potential energy of a cluster. In this case we can say that the above statistical approach includes a microscopic model.

In the present approach we use a cluster potential energy which is independent of monomer position within the constraining volume. However, the way in which the potential energy vanishes for clusters consisting of single monomers is unknown. This has been shown to have an appreciable effect on the nucleation rate (Ford *et al.*, 1993). In these calculations we choose the potential in such a way that the nucleation rate becomes the same as proposed by Girshick and Chiu (1990), which is then a special case of the more general model by Ford *et al.* (1993):

$$J_{\text{stat}}=J_{\text{class}}\left(\frac{\exp(A_1\sigma/kT)\ 5^{3/2}e}{3\pi S}\right), \tag{10}$$

where A_1 is the surface area of a monomer, s is the surface tension, e is the Napier number and S is the saturation ratio.

Monomer coagulation model. If condensible vapours are formed by rapid chemical reactions producing very high supersaturation ratios the critical clusters are of the order of monomer size and the classical approach is not valid. In this case we can model the formation of monomers equal to the nucleation rate. The kinetics of the discrete size spectrum can be considered as a coagulation process (Xiong and Prastinis, 1991). The evaporation flux may now be neglected because of the extremely low saturation vapour pressure at the surface of formed embryos. In our monomer coagulation model the production rate of new monomers, which are allowed to grow by coagulation, is equal the production rate of supersaturated vapour:

$$J_{\text{monomer}}=\frac{1}{\Delta t}(N_j-N_{j,s})=\frac{1}{\Delta t}\left(N_j-\frac{p_{j,s}}{kT}\right), \tag{11}$$

where $p_{j,s}$ is the saturation vapour pressure and N_j the monomer number concentration of j species. The vapour molecule production rate is calculated from local gas phase equilibrium or from reaction kinetics if the reaction rate is known.

2.3. *Vapour condensation on particles*

Heterogeneous nucleation. In the ABC code we have also the possibility to consider the mechanism of heterogeneous nucleation. Heterogeneous nucleation is the process of

nucleation on the surface of pre-existing particles. The formation has been described as the formation of a new phase under the influence of an external potential. This external potential can lead to a lower Gibbs free energy barrier as compared to homogeneous nucleation. As a result, much smaller saturation ratios are necessary for heterogeneous nucleation to take place than in the case of homogeneous nucleation.

The classical heterogeneous nucleation theory has been developed by Volmer (1939) and Becker and Döring (1935). Fletcher (1958) has developed a classical theory of heterogeneous nucleation on aerosol particles including the effect of particle size.

In the ABC code there is a possibility to use the classical theory of heterogeneous nucleation for one component and for binary systems (Lazaridis *et al.*, 1991) before vapour condensation on particle surface begins.

Vapour condensation. When a particle starts to grow due to vapour condensation, after formed by nucleation (homogeneous or heterogeneous), its size may be less than the mean free path of the diffusing substance. For this condition the rate of growth is governed by the rate of random molecular collisions of vapour molecules. The region where the particle is large compared to the mean free path is the so-called continuum regime. In this regime the growth of particles is determined by the rate of diffusion of molecules to the particle surface. Neither of these theories is valid if the particle diameter is of the same order as the diffusing vapour molecules. In this transition regime there does not exist a general solution valid over the full range of Knudsen numbers.

A general way to deal with this problem is to match the continuum and free molecule flux expressions. The general equations for heat and mass transport are usually expressed by the continuum region equations with correction factors for the transition regime. From the first-order phenomenological equations for mass and heat (energy) transport in a binary mixture (diffusing vapour and surrounding gas), steady state solutions for mass and heat transfer to or from a droplet in an infinite fluid can be obtained. These forms for mass and heat transfer toward a single particle also take into account the additional effect of a net flow of gas toward the particle (Stefan flow) (Seinfeld, 1986; Kreidenweis *et al.*, 1987).

The particle growth rate can be solved directly from these heat and mass transfer equations with the use of numerical methods. Unfortunately, in our application, this would need a tremendous amount of computing time. This suggests that we seek approximations to the growth rate equations and check the validity of these simplified equations.

First the Stefan flow term is neglected in the heat transfer equation and secondly, a zeroth-order approximation for the mass transfer equation is used. For evaluating the vapour pressure at the particle surface we can use the Clausius–Clapeyron equation (e.g. Pruppacher and Klett, 1978), which can be approximated by linear expansion and estimating that $T_r T_\infty \approx T_\infty^2$. The error of this approximation is small when the temperature difference $(T_r - T_\infty)$ is small, which is usually the case in our applications.

When we use the above mentioned approximations we get the well-known Mason equation for the mass flux toward the particle (Mason, 1971). In the ABC model a modified Mason equation, where the transitional correction factors are included, is used (Wagner, 1982):

$$\frac{dm}{dt} = \frac{4\pi r (S_\infty - S_r)}{N_M/\beta_M + N_T/\beta_T}, \tag{12}$$

where

$$N_M = \frac{R_g T_\infty}{D_\infty M p_s(T_\infty)} \quad \text{and} \quad N_T = \frac{L}{kT_\infty}\left(\frac{LM}{R_g T_\infty} - 1\right),$$

where β_M and β_T are the transitional correction factors for mass and heat transfer (Smirnov, 1971), D_∞ is the binary diffusion coefficient, M is the molecular weight of the liquid and L is the latent heat of condensation. The saturation ratio of the vapour far from the particle is determined as

$$S_\infty = p_{v,\infty}/p_s(T_\infty).$$

The saturation ratio for vapour at the particle surface S_r can be determined through minimisation of the Gibbs free energy. The inclusion of the surface tension effects leads to (e.g. Wagner, 1982):

$$S_r = \frac{p_{v,r}}{p_{s,r}} = \exp\left(\frac{2\sigma M}{rR_g\rho T_r}\right). \tag{13}$$

Here σ is the surface tension and ρ the density of the liquid film on the droplet, $p_{s,r}$ is the saturation (equilibrium) vapour pressure at the droplet temperature T_r. Equation (17) has been implemented into the ABC code and is used to calculate condensation rates on aerosol particles.

2.4. *The effect of chemistry on aerosol dynamics*

Gas phase reactions. When nucleation, condensation and chemical reactions with surfaces are considered, the speciation in the gas phase is needed. Concentrations of non-condensible gases are important for estimating reactions for condensible species and the chemical forms of condensible elements are needed to determine reactions and the condensation steps taking place. In our model the equilibrium gas phase composition after each axial step is calculated. When kinetic data are available the change of molar concentration of species j can be calculated according to global reaction kinetics.

Chemical affinity. It is also possible that condensible vapours will form solutions with other vapour species in the condensed state or with the liquid phase already existing on aerosol particles. This will change the vapour pressures of nucleating or condensing species.

For homogeneous nucleation, if there are two species nucleating and changing each other's vapour pressures this is called binary nucleation. Vapour condensation on inert particles starts with heterogeneous nucleation and continues with condensation after the particle surface has been wetted by the condensed liquid. In all these cases (condensation, homogeneous and heterogeneous nucleation) the effects of chemical affinity on vapour pressures need to be taken into account.

The change of condensible species vapour pressure over the particle surface can be taken into account by introducing the chemical activity term in the saturation ratio expression:

$$S_{r,j} = A_j \exp\left(\frac{2\sigma_1 M_1}{rR_g\rho_1 T_r}\right). \tag{14}$$

The chemical activity of species j (A_j) can be expressed as a function of the mole fraction of condensing species in the liquid (x_j) solution and the molal activity coefficient (γ_j):

$$A_j = x_j\gamma_j. \tag{15}$$

Several semiempirical formulas are available for calculating the activity coefficients for different systems in consideration (Ball *et al.*, 1985; Jokiniemi, 1990; Reid *et al.*, 1987). If the activity data are not available an ideal solution approximation ($\gamma_j \equiv 1$) can be used to estimate the importance of this effect. In the ABC code the user may choose the expression to be used in the calculations.

Binary nucleation. Although homomolecular nucleation occurs in supersaturated systems, binary nucleation can occur when a mixture of vapours is unsaturated with respect to the pure substances. Consequently, binary nucleation is a favourable mechanism in combustion conditions. The Gibbs free energy in the case of a binary system is expressed in the classical theory with the help of the species activities (Lazaridis *et al.*, 1991).

In order to calculate the nucleation rate, the free energy change at the saddle point has to be determined. In a manner analogous to the one adopted by the revised classical theory (Wilemski, 1984) we calculate the critical value of the free energy barrier by using the equation $\nu_b\Delta\mu_a = \nu_a\Delta\mu_b$ at the critical particle size, which determines the composition of the embryo.

Chemical reactions with surfaces. The modelling of possible chemical reactions of vapour species with aerosol particles has been done with the use of the shrinking core model (Levenspiel, 1972). The model incorporates together diffusion through the boundary gas film, diffusion through the reacted ash layer and chemical reactions. The change of mass of a gaseous species j due to chemical reactions with a spherical aerosol particle of radius r can be written as:

$$\frac{dm_j}{dt}=\frac{-C_j A\pi}{\frac{1}{k_g r^2}+\frac{1}{k_s r_c^2}+\frac{r-r_c}{D_c r r_c}}, \tag{16}$$

where C_j is the mass concentration of species j in the gas phase, r_c is the radius of the unreacted core of the aerosol particle, k_g is the mass transfer coefficient through the boundary gas layer around the particle, D_c is the diffusion coefficient through the reacted ash layer and k_s is the first order rate constant for surface reaction. A similar flat surface model is used for vapour deposition on boundary surfaces by chemisorption.

2.5. *Coagulation*

As a result of coagulation between particles, particles are both removed from and added to size bins. If two particles of masses m_1 and m_2 coagulate, the mass of the particle thus formed is $m_3=m_1+m_2$. If $K_{12}n_1n_2$ is the coagulation rate between particles of masses m_1 and m_2, then: $dn_1/dt=-K_{12}n_1n_2$, $dn_2/dt=-K_{12}n_1n_2$ and $dn_3/dt=+K_{12}n_1n_2$.

Note that there is a net loss of one particle per coagulation; the total mass, however, is conserved. Generalising the above equations one obtains:

$$\frac{dn_k}{dt}=\frac{1}{2}\sum_{i+j=k}K(m_i, m_j)n_in_j-n_k\sum_{i=1}^{\infty}K(m_i, m_k)n_i, \tag{17}$$

where $i+j=k$ means that the summation is taken over those grid points for which

$$m_i+m_j=m_k.$$

Here m_k includes all particles which are in bin k. The first term on the right-hand side represents the gain in bin k due to coagulations between smaller particles; the second term in equation (21) represents the loss out of size bin k due to coagulation with all other bins (including coagulation events between particles both of which are in bin k).

If a coagulated particle has a radius r that falls between bins m and n ($n=m+1$) the number of particles in bin m is increased by $(r_n^3-r^3)/(r_n^3-r_m^3)$, and the number in bin n is increased by $(r^3-r_m^3)/(r_n^3-r_m^3)$. The mass in bin m is increased by $4\pi\rho_p r^3(r_n^3-r^3)/(3(r_n^3-r_m^3))$, while the mass in bin n is increased by $4\pi\rho_p r^3(r^3-r_m^3)/(3(r_n^3-r_m^3))$. This procedure correctly conserves the total number of particles (one) and the total mass $4\pi\rho_p r^3/3$. Same procedure is applied for condensation.

In ABC the following coagulation kernels are modelled: Brownian coagulation (Wagner and Kerker, 1977), turbulent coagulation (Saffman and Turner, 1956) and differential sedimentation (Pruppacher and Klett, 1978).

The total coagulation rate is obtained by combining the different coagulation kernels in the following way:

$$K_T=K_B+(K_G^2+K_S^2+K_I^2)^{1/2}. \tag{18}$$

According to Saffman and Turner (1956) the turbulence contributions need to be added quadratically and in addition Dunbar and Fermandjian (1984) have pointed out that the reasoning used by Saffman and Turner also applies to the gravitational kernel.

3. SAMPLE CALCULATIONS

3.1. *Boiler geometry and input data description*

As a sample calculation a typical PC boiler was modelled. Here we have concentrated on the behaviour of volatilised sodium (Na) and potassium (K) during the flue gas cooling. These elements are of great interest because of their contribution to fouling and slagging.

The geometry and gas temperatures of the boiler are described in Fig. 1. The initial fly ash size distribution was taken as input for the ABC code. This particle size distribution was given as a bi-modal lognormal distribution. For the submicron mode a number median radius (NMR) of 0.018 μm and a geometric standard deviation (GSD) of 1.4 were used. For the supermicron mode NMR of 1.5 μm and GSD of 1.8 were used, respectively. The mass fraction of the submicron mode was assumed to be 0.15% of the assumed 6 g N^{-1} m^{-3} total mass concentration. The experimental low pressure impactor and DMA results analysed with data inversion methods (Kauppinen *et al.*, 1993c) indicate that there might be more than two peaks in the aerosol size distribution in PC boilers before the electrostatic precipitator (ESP). However, in this sample calculation only the above-mentioned bi-modal size distribution for pre-existing ash particles was used.

The following elemental gas and particle input rates were used [kg s^{-1}]: C 11.9, Cl 0.08, S 0.254, H 0.762, O 46.0, N 119.69, Na 2.5E-4, K 5.0E-4 and Particles 1.18. This corresponds to typical PC boiler conditions where 0.6–3% of the total fuel Na and K content has been volatilised (Joutsensaari *et al.*, 1993; Kauppinen and Pakkanen, 1990). The corresponding calculated gas velocity, gas temperature and Reynolds number at different locations of the boiler are shown in Fig. 2a, b and c. The surface temperatures of heat exchangers were set equal to gas temperatures, because deposition was not our primary interest.

In this calculation only base case options; classical nucleation, nodal point size grid, vapour condensation without chemical effects, Brownian, turbulent and gravitational coagulation were employed. In the size distribution 59 nodal points were used and the corresponding minimum and maximum particle radii were 5 Å and 30 μm.

Following elements, gas phase chemical species and condensible species were included in the calculation.

Elements:

C, Cl, S, H, O, N, Na, K.

Gaseous species

C, CO_2, CO, Cl, Cl_2, HCl, S, SO_2, SO_3, H_2S, H_2SO_4, H, H_2, OH, H_2O, O, O_2, N_2, Na, NaCl, Na_2Cl_2, NaOH, Na_2SO_4, K, KCl, K_2Cl_2, KOH, K_2SO_4

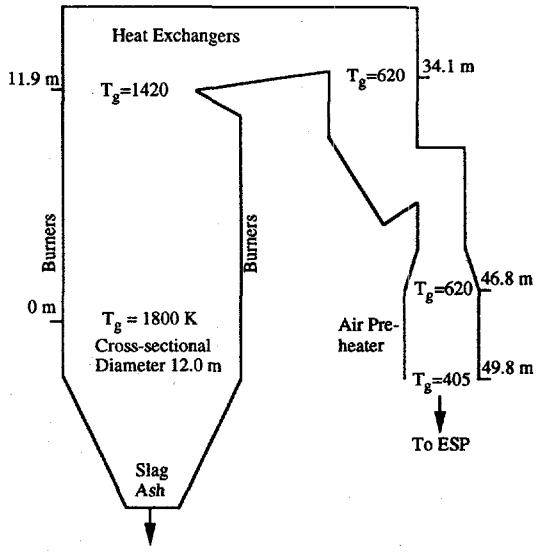

Fig. 1. Schematic figure of the PC boiler geometry and gas temperatures used in the sample calculation.

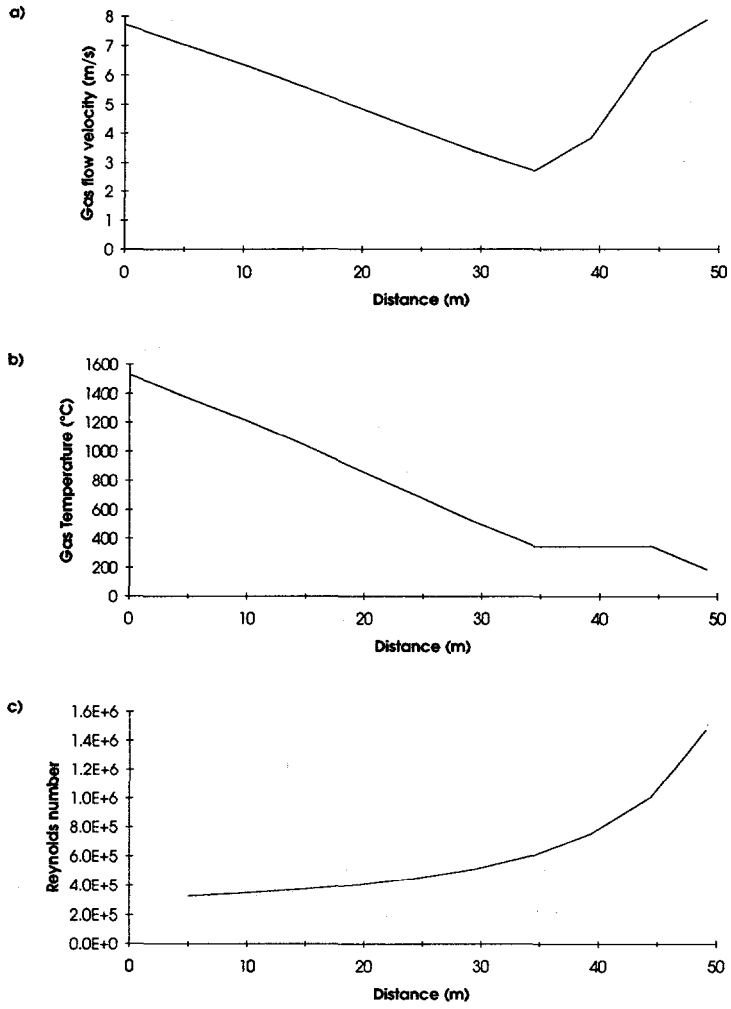

Fig. 2. Flow conditions for the simulated PC boiler: (a) gas velocity, (b) gas temperature and (c) Reynolds number.

Condensible species:

NaCl, Na_2SO_4, NaOH, KCl, K_2SO_4, KOH and inert ash particles.

3.2. *Results and discussion*

We have calculated two cases where in the first case sodium and potassium sulphates are allowed to form in the gas phase (case 1). The global gas phase reactions describing this case are (similar for K):

$$\begin{aligned} 2NaOH + SO_2 + \tfrac{1}{2}O_2 &\leftrightarrow Na_2SO_4 + H_2O \\ 2NaCl + SO_2 + \tfrac{1}{2}O_2 + H_2O &\leftrightarrow Na_2SO_4 + 2HCl. \end{aligned} \tag{19}$$

In the second case this is not allowed (case 2) and thus Na and K condenses mainly as chlorides. The total mass size distributions at the end of the calculations (just before the ESP) for the two cases are shown in Fig. 3. To obtain full convergence 159 nodal points were needed in case 1. In case 2 full convergence was reached with 59 nodal points. We used 59 nodal points in both cases, because increasing points from 59 to 159 caused only very minor change in the size distribution for case 1.

If the equilibrium in the gas phase is assumed, then the main components of Na and K at flame temperatures are NaCl and KCl (Fig. 4). Detailed kinetic calculations show that equilibrium concentrations of sodium chlorides and hydroxides are achieved readily (Srinivasachar *et al.*, 1990). As the gas temperature decreases the chlorides are converted to sulphates in the gas phase (case 1), when the equilibrium assumption is used (Fig. 4). The saturation ratios for alkali metals in the presence of sulphates in the gas phase are the gas phase partial pressures of Na_2SO_4 and K_2SO_4 divided by their saturation pressures at gas

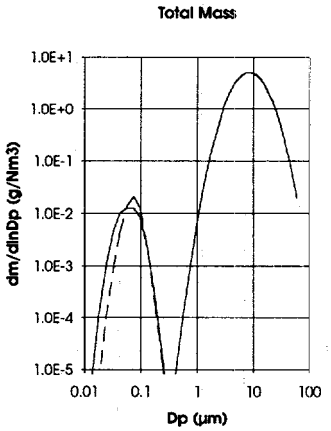

Fig. 3. Total mass size distribution before ESP in the cases where sodium and potassium sulphates are allowed to form in the gas phase according to local chemical equilibrium —— (case 1) and in the case where these species are not allowed to form ----- (case 2).

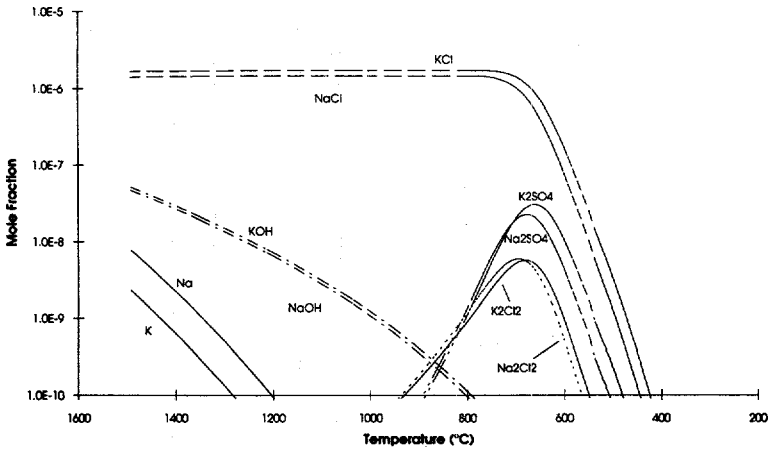

Fig. 4. The chemical composition of Na and K species as a function of gas temperature (case 1).

temperature T_g

$$Na_2SO_4(g) \rightarrow Na_2SO_4(c)$$

$$K_2SO_4(g) \rightarrow K_2SO_4(c).$$

Gaseous alkali sulphates have very low vapour pressures and thus due to high supersaturations (Fig. 5) extremely high numbers of new particles are formed by homogeneous nucleation (Fig. 6). Later these tiny particles grow by coagulation and condensation. Some vapour is also condensing on pre-existing ash particles. The evolution of the number size distribution is presented in Fig. 7a–d. The size distribution does not change in the first 5 m (Fig. 7a). At the point where nucleation and condensation have started at 29.5 m (Fig. 7b) a minor increase of the submicron particles as compared to the initial size distribution can be observed. Notable is the additional mode on the left-hand side of the original submicron mode in case 1. Later this additional mode almost disappears due to coagulation (Fig. 7c and d). The new mode is initially formed by rapid nucleation of gaseous alkali sulphates. The final mass size distribution of condensed sulphates is shown in Fig. 8.

However, it is unlikely that the formation of alkali sulphates in the gas phase follows equilibrium (reliable kinetic data are not available). According to gas phase kinetic

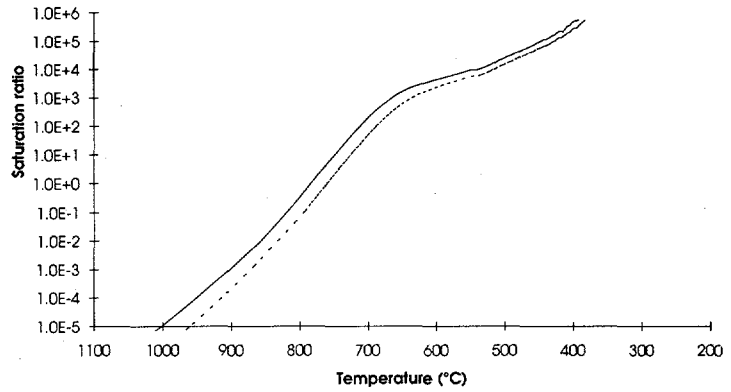

Fig. 5. The saturation of Na_2SO_4 (——) and K_2SO_4 (- - - -) as a function of temperature (case 1).

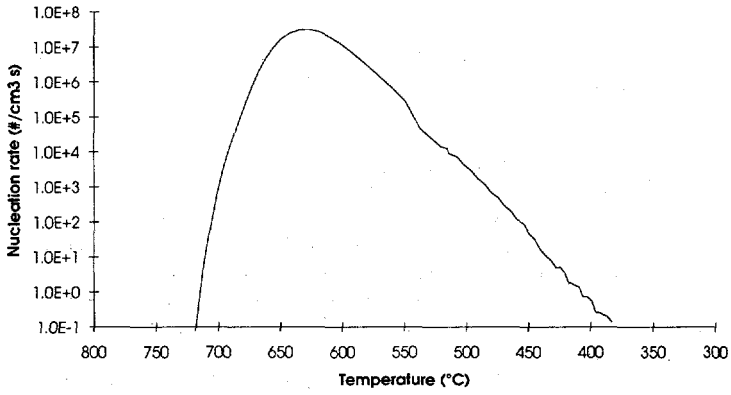

Fig. 6. Nucleation rate as a function of temperature (case 1).

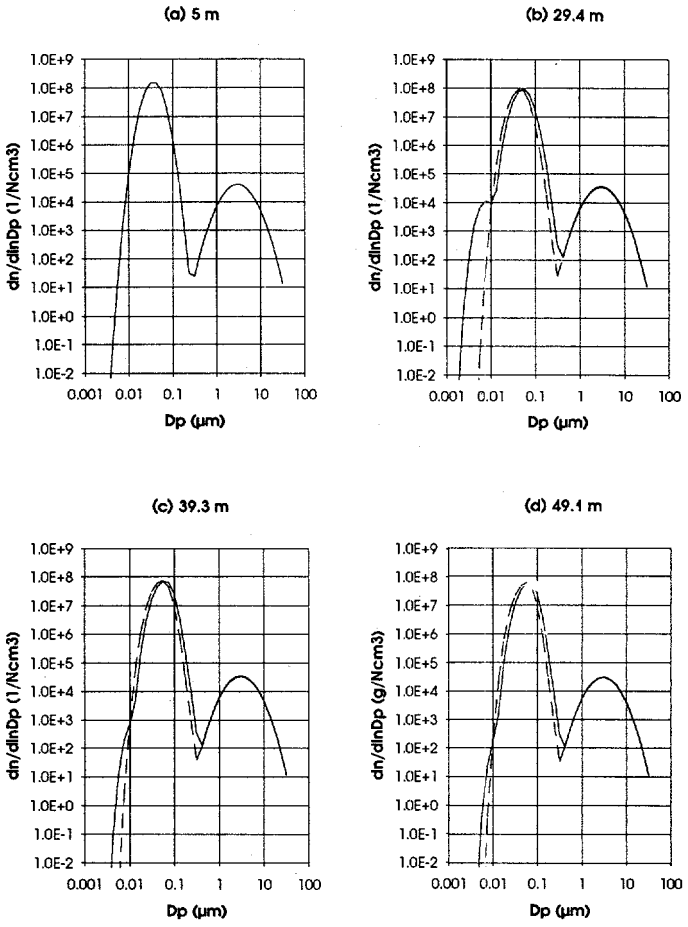

Fig. 7. The evolution of number size distribution as a function of location in the calculated cases 1 (——) and 2 (- - - -); (a) 5.0 m, (b) 29.4 m, (c) 39.3 m and (d) 49.1 m.

considerations (Steinberg and Schofield, 1990) only a small fraction of the equilibrium value for gas phase alkali sulphates is expected to form. If sulphates are not allowed to form in the gas phase (Fig. 9), Na and K will condense as chlorides. These condensed chlorides will then convert to sulphates in the condensed (particle) phase. In this case the submicron peak formed by $Na_2SO_4(g)$ and $K_2SO_4(g)$ nucleation is not formed, but instead all NaCl and KCl are condensed on pre-existing ash particles. The evolution of the number size distribution is presented in Fig. 7 and the final mass size distribution of chlorides in Fig. 10.

The importance of sulphate formation in the gas phase is shown in Figs 11a and b, where the total gas phase K and Na is compared in the two cases, when sulphates are allowed to form and condense (case 1) and when they are not allowed to form in the gas phase (case 2). To condense 80% of the gaseous alkalis about 100°C lower temperature is needed in case 2 as compared to case 1.

Direct comparison of calculated results with experimental results is difficult, because no data are available for the amount of volatilised alkalis, gas phase compositions and elemental particle size distributions at different temperatures. However, in contrast to the

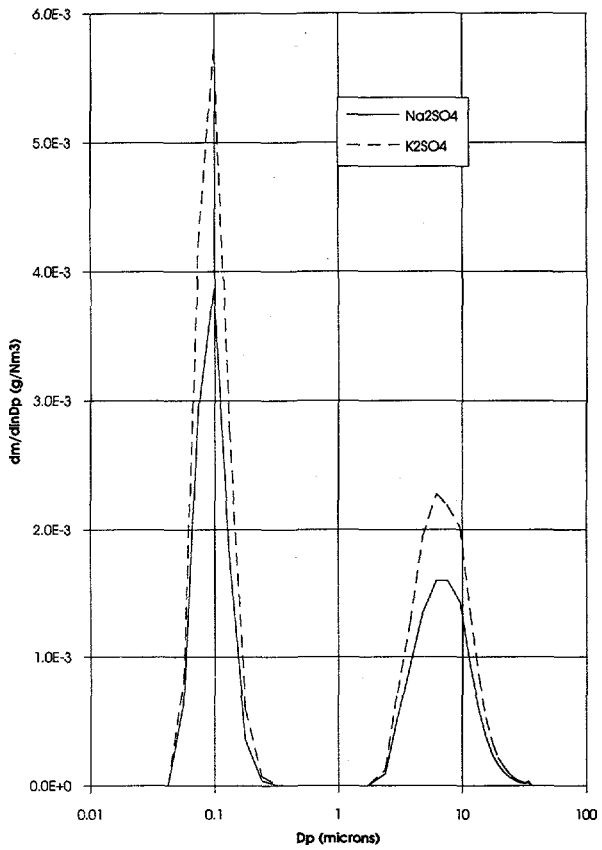

Fig. 8. The final mass size distributions of Na_2SO_4 (——) and K_2SO_4 (- - - -) (case 1).

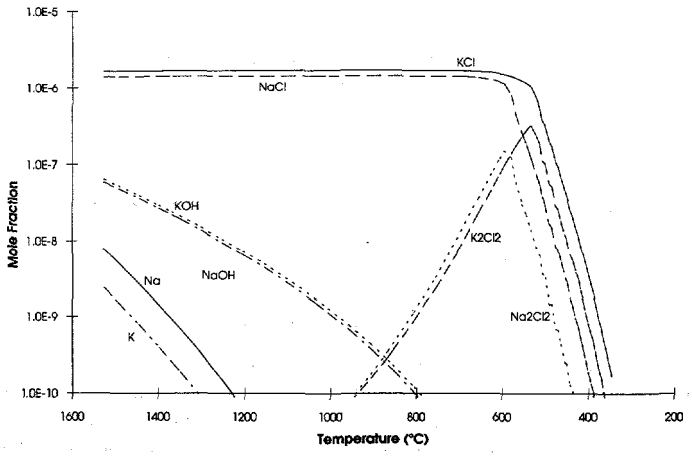

Fig. 9. The chemical composition of Na and K species as a function of gas temperature (case 2).

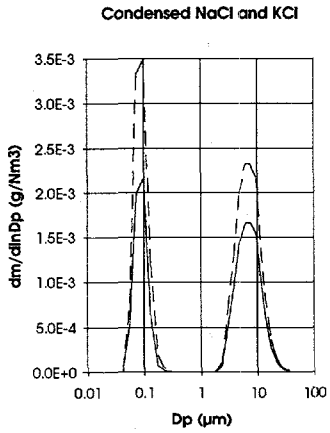

Fig. 10. The final mass size distributions of NaCl (——) and KCl (- - - -) (case 2).

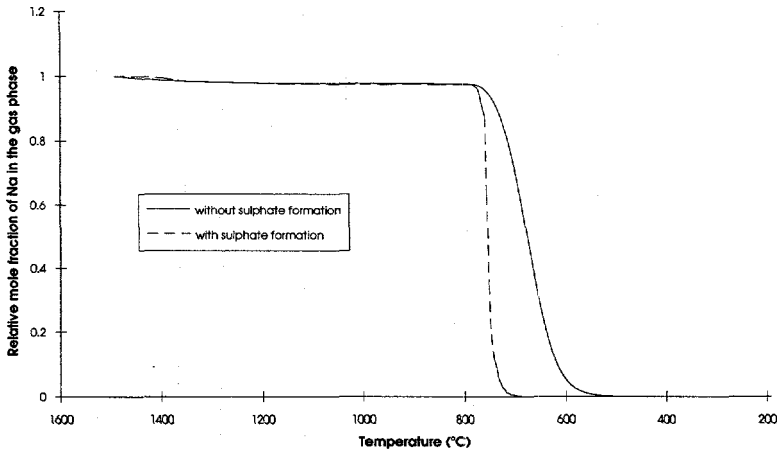

Fig. 11. The relative mole fraction of Na species in the gas phase as a function of temperature in cases 1 (- - - -) and 2 (——).

earlier laboratory studies where the measured alkali mass in the submicron mode has been related to the volatilised amount (Neville and Sarofim, 1985) our calculations indicate that a greater fraction than the amount in the submicron mode has been in the gas phase prior to condensation (Figs 8 and 10).

4. CONCLUSIONS

A new model for numerical simulation of volatilised condensible species behaviour in combustion conditions has been developed. The importance of different mechanisms for combustion processes can be determined by incorporating them into a same model. Our model incorporates gas phase chemistry, gas–surface chemistry, aerosol particle formation by nucleation and growth by heterogeneous nucleation, condensation and coagulation. Also deposition by diffusion, impaction, thermophoresis, sedimentation, vapour condensation

and chemisorption are modelled. The model is flexible to chemical speciation, pre-existing particle size distribution, temperature, pressure and geometry for deposition calculations. These parameters are specified with the user input data.

A sample calculation for a pulverised coal combustion boiler showed the importance of sodium and potassium sulphates formation in the gas phase when alkali gas phase concentrations are of interest (Fig. 11). When sulphates were not allowed to form in the gas phase, alkali vapours condensed as chlorides at considerable lower temperatures, i.e. the differences in the temperature for 80% condensation were about 100°C for Na in the two calculated cases. The behaviour of potassium was similar to that of sodium. Also the sub and supermicron fractions of condensed alkalis depend on if sulphates are formed or not, i.e. more chlorides condensed on supermicron fly ash particles than sulphates.

The initial size distribution of the pre-existing ash particles is playing an important role in determining the distribution of condensed species between sub- and supermicron size particles. Downstream gas phase concentrations of Na and K depend strongly on their concentration in the gas phase prior to condensation. Furthermore this dependence seems to be a non-linear process as a function of gas phase concentration.

The choice of the homogeneous nucleation model has some importance for the calculated submicron number size distribution. The effect of heterogeneous nucleation to initiate condensation on ash particles was negligible at the considered high temperature gradient and consequently rapid condensation process. Thus we can conclude that at the simulated conditions the modelling for the formation of the first monolayer before condensation is not needed. Other parameters like particle shape and porosity may affect the condensation behaviour, but were beyond the scope of this study.

Thorough sensitivity studies are needed to find out the most important mechanisms affecting the dynamics of condensible alkali and toxic vapours in different combustion processes. This would require the on-going experimental and theoretical research to concentrate on the primary factors determining the dynamics of vapour phase species in combustion conditions. To validate the numerical model developed in this work carefully designed laboratory scale experiments are needed.

Acknowledgements—This study is part of the Finnish combustion research program LIEKKI and is funded by the Finnish Ministry of Trade and Industry, Ahlström Corporation, IVO and Tampella Power.

REFERENCES

Abraham, F. F. (1974) Homogeneous nucleation theory. In *Advances in Theoretical Chemistry*. Academic Press, New York.

Ahluwalia, R. K., Im, K. H., Chuang, C. F. and Hajduk, J.-C. (1986) 31st *Int'l Gas Turbine Conference*. Düsseldorf, West Germany, 86-GT-239.

Ball, F. X., Furst, W. and Renon, H. (1985) *AIChE J.* **31,** 392.

Becker, R. and Döring W. (1935) *Ann. Phys.* **24,** 719.

Binder, K. (1987) *Rep. Prog. Phys.* **50,** 783.

Bunz, H. and Dlugi, R. (1991) *J. Aerosol Sci.* **22,** 441.

Bunz, H., Koyro, M. and Schöck, W. (1983) NAUA Mod4: Code description and users manual, KfK report 3554. Karlsruhe, West Germany.

Dunbar, I. H. and Fermandjian, J. (1984) Comparison of sodium aerosol codes. EUR 9172 en.

Eriksson, G. (1975) *Chemica Scripta* **8,** 100.

Flagan, R. C. and Friedlander, S. K. (1978) In *Recent Developments in Aerosol Science* (Edited by Shaw, D. T.), p. 25. Wiley, New York.

Fletcher, N. (1958) *J. Chem. Phys.* **29,** 572.

Ford, I. J., Barrett, J. C. and Lazaridis, M. (1993) *J. Aerosol Sci.* **24,** 581.

Friedlander, S. K. (1977) *Smoke, Dust and Haze*. John Wiley, New York.

Gelbard, F. (1990) *Aerosol Sci. Technol.* **12,** 399.

Gelbard, F. and Seinfeld, J. H. (1978) *J. Comp. Phys.* **28,** 357.

Gelbard, F., Tambour, Y. and Seinfeld, J. H. (1980) *J. Colloid Interface Sci.* **76,** 541.

Girshick, S. L. and Chiu, C. P. (1990) *J. Chem. Phys.* **93,** 1273.

Hoare, M. R., Pal, P. and Wegener, P. P. (1980) *J. Colloid Interface Sci.* **75,** 126.

Im, K. H., Ahluwalia, R. K. and Chuang, C. F. (1985) *Aerosol Sci. Technol.* **4,** 125.

Jokiniemi, J. (1990) *Aerosol Sci. Technol.* **12,** 891.

Joutsensaari, J., Kauppinen, E. I. and Jokiniemi, J. K. (1993) Studies on ash vaporization in real scale pulverized coal combustion. *Proceedings of Engineering Foundation Conference on The Impact of Ash Deposition on Coal Fired Plants*. Birmingham, U.K., 20–25 June 1993, to be published.

Kauppinen, E. I., Jokiniemi, J. K., Mikkanen, P. and Lazaridis, M. (1993a) Aerosols in black liquor combustion. In *LIEKKI Combustion Research Program, Technical Review* 1988–1992, Report L93-1 (Edited by Hupa, M. and Matinlinna, J.), p. 619. Turku, Finland.

Kauppinen, E. I., Lind, T., Jokiniemi, J. K. and Lehtinen, K. E. J. (1993b) Aerosol Formation in Fluidized Bed Solid Fuel Conversion Processes. In *LIEKKI Combustion Research Program, Technical Review* 1988–1992, Report L93-1 (Edited by Hupa, M. and Matinlinna, J.), p. 417. Turku, Finland.

Kauppinen, E. I. and Pakkanen, T. A. (1990) *Envir. Sci. Technol.* **24,** 1811.

Kauppinen, E. I., Lind, T., Joutsensaari, J., Jokiniemi, J. K., Maenhaut, W., Royset, O. and Vadset, M. (1993c) Characteristics of fly ash particles formed in circulating fluidized bed and pulverized coal fired boilers. 10th *Particulate Control Symposium and* 5th *Int. Conf. on Electrostatic Precipitation.* Washington, D.C. 5–8 April 1993.

Kreidenweis, S. M., Flagan, R. C. and Seinfeld, J. H. (1987) *Aerosol Sci. Technol.* **6,** 1.

Lazaridis, M. and Ford, I. J. (1993) *J. Chem. Phys.* submitted.

Lazaridis, M., Kulmala, M. and Laaksonen, A. (1991) *J. Aerosol Sci.* **22,** 823.

Lind, T., Kauppinen, E. I., Jokiniemi, J. K., Maenhaut, W. and Pakkanen, T. (1993) Alkali metal behaviour in atmospheric circulating fluidized bed coal combustion. *Engineering Foundation Conference on The Impact of Ash Deposition on Coal Fired Plants.* Birmingham, U.K., 20–25 June 1993.

Levenspiel, O. (1972) *Chemical Reaction Engineering,* 2nd edition. John Wiley, New York.

Mason, B. J. (1971) *The Physics of Clouds,* 2nd edition. Clarendon Press, Oxford.

Neville, M. and Sarofim, A. F. (1982) 19th *Symp. (Int'l) on Combustion,* pp. 1441–1449.

Neville, M. and Sarofim, A. F. (1985) *FUEL* **64,** 384.

Pruppacher, H. R. and Klett, J. D. (1978) *Microphysics of Clouds and Precipitation.* Reidel, Dordrecht.

Reid, R. C., Prausnitz, J. M. and Poling, B. E. (1987) *The Properties of Gases & Liquids,* 4th edition. McGraw-Hill, New York.

Reiss, H., Tabazadeh, A. and Talbot, J. (1990) *J. Chem. Phys.* **92,** 1266.

Saffman, P. G. and Turner, J. S. (1956) *J. Fluid Mech.* **1,** 16.

Sarofim, A. F., Howard, J. B. and Padia, A. S. (1977) *Combustion Sci. Technol.* **16,** 187–204.

Seinfeld, J. H. (1986) *Atmospheric Chemistry and Physics of Air Pollution.* Wiley, New York.

Senior, C. E. and Flagan, R. C. (1982) *Aerosol Sci. Technol.* **1,** 371.

Sher, R. and Jokiniemi, J. (1993) NAUAHYGROS 1.0: A code for calculating the behavior of aerosols in nuclear plant containments following a severe accident, EPRI TR-102775. Palo Alto, CA.

Smirnov, V. I. (1971) *Pure appl. Geophys.* **86,** 184.

Srinivasachar, S., Helble, J. J., Ham, D. O. and Domazetis, G. (1990) *Prog. Energy Combust. Sci.* **16,** 303.

Steinberg, M. and Schofield, K. (1990) *Prog. Energy Combust. Sci.* **16,** 311.

Volmer, M. (1939) *Kinetik der Phasenbildung.* Verlag Theodor Steinkopff, Dresden.

Wagner, P. E. (1982) In *Topics in Current Physics, Aerosol Microphysics* II (Edited by Marlow, W. H.), p. 129. Springer-Verlag, Berlin.

Wagner, P. E. and Kerker, M. (1977) *J. Chem. Phys.* **66,** 638.

Warren, D. and Seinfeld, J. H., (1985) *Aerosol Sci. Technol.* **4,** 31.

Wilemski, G. (1984) *J. Chem. Phys.* **80,** 1370.

Xiong, Y. and Pratsinis, S. E. (1991) *J. Aerosol Sci.* **22,** 637.

Reprinted with permission from the publisher.
In: Aerosol Science and Technology 1995. Vol. 22, pp. 181 - 189.

PAPER B

Electrical Agglomeration of Aerosol Particles in an Alternating Electric Field

Jukka Hautanen,* and Markku Kilpeläinen
Tampere University of Technology,
Department of Physics,
P.O. Box 692, FIN-33101 Tampere, Finland

Esko I. Kauppinen, Jorma Jokiniemi, and Kari Lehtinen
Technical Research Center of Finland (VTT),
VTT Energy (J. J.; K. L.),
VTT Chemical Technology,
Aerosol Technology Group,
P.O. Box 204, FIN-02151 Espoo, Finland

A laboratory scale test system has been designed and constructed to study the electrical agglomeration of charged aerosol particles as a method to increase the fine particle collection efficiency of electrostatic precipitators. The system consists of test aerosol generator, aerosol charger, agglomerator chambers, and aerosol measurement equipment. Air atomizing nozzles and the TSI six-jet atomizer have been used as the test particle generators. The test particles have been charged by a corona discharge. Two types of agglomerator chambers have been investigated. In one agglomerator the gas flows between two parallel plates, across which the alternating high voltage is applied. The other agglomerator is a quadrupole structure with cylindrical electrodes positioned between the grounded plates. Particle concentration and size distribution measurements have been carried out downstream of the agglomerator with agglomerator voltage on and off. Particle concentrations and size distributions have been measured with differential mobility analyzer (DMA) and a Berner low pressure impactor. These measurements show that agglomeration causes about a 4%–8% decrease in the fine particle concentration when the total mass concentration is between 1 and 2 g/m^3. There was no difference between the results measured with the parallel plate and the quadrupole agglomerator.

INTRODUCTION

The electrostatic precipitator is a commonly used flue gas particle collector at coal fired power plants. The total mass collection efficiency can exceed 99.7% (penetration 0.3%) but the collection efficiency for the fine particles (0.1–1 μm) may be as low as 85% (penetration 15%) (Ylätalo et al., 1992).

The fine fly ash particles are the most detrimental to the environment since they travel long distances in the atmosphere and they can easily penetrate into the respiratory tract of human beings. Also, the heavy metals and other toxic volatile and condensing species are concentrated on the fine particles (Flagan and Seinfeld, 1988; Kauppinen and Pakkanen, 1990).

Because of the hazard posed by the small fly ash particles, future emission regulations will take account not only the total mass emissions but also the emission of the fine particles. The upper particle size limit of 10 μm, has been proposed, but laws will likely be more strict in the

* Corresponding author.

Aerosol Science and Technology 22:181–189 (1995)

Published by Elsevier Science Inc.

0278–6826/95/$9.50
SSDI 0278-6826(94)00032-W

future, i.e., separate limits for submicron particle emission may be realized.

The concern about the fly ash particle emissions increases the need to improve electrostatic precipitator efficiency. The collection efficiency of the precipitator can be enhanced by increasing the size of the precipitator, increasing the plate-to-plate distance or utilizing pulse voltage or flue gas conditioning (Oglesby and Nichols, 1978). All of these methods are utilized commercially but new more economical methods should also be developed.

Electrical agglomeration is one method to overcome the problem caused by the poor collection efficiency for the fine particles. The principle of the electrical agglomeration is presented in Figure 1. Particles are first charged by a corona discharge like in a conventional electrostatic precipitator. The particles then enter an alternating electric field where they oscillate. The oscillation velocity and the amplitude depend on the particle size, so that the larger the particle size the larger are the velocity and the amplitude. The velocity and the amplitude difference of the particles causes collisions between the fine and the large particles. If the particles remain attached to each other after the collisions, the concentration of the fine particles will decrease, and the remaining large particles are easily removed by conventional particle collection equipment.

Electrical agglomeration has been studied previously by several authors. Kobashi (1979) and Mitchner and Self (1983) have used so-called parallel plate agglomerator, in which the gas flows between parallel plates at high voltage. The test particles were produced by dispersing fly ash into the air flow, and the particles were charged bipolarly by triboelectric effects resulting in a charge to mass ratio ± 8 μC/g. Measurements were carried out in the size range 0.3–10 μm with impactor and optical particle counter. The agglomeration

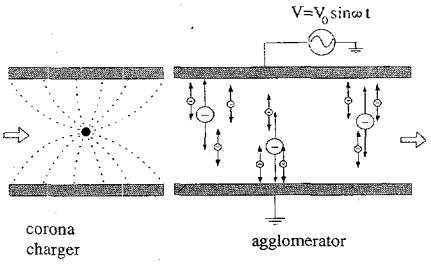

FIGURE 1. Principle of electrical agglomeration. Air containing aerosol particles is introduced from the left. Particles are charged by a corona charger. Then the aerosol flows into an alternating electric field. Large particles oscillate with larger amplitude and velocity than the small particles (0.1 ~ 1.0 μm). The difference in particle velocities and amplitudes causes particle collisions.

caused a concentration reduction of about 30% in the particle size range of 0.3–2 μm. The particle mass concentration was 8 g/m^3, the charge/mass ratio ± 8 μC/g and residence time in the agglomerator was 1 s.

Watanabe (1988) and Watanabe and Suda (1990) had used a so-called quadrupole agglomerator, which is based on the idea that the electrical quadrupole field focuses charged particles into the middle of the quadrupole (Masuda and Fujibayashi 1970). The bimodal test aerosol (0.06 and 4 μm) was produced by re-dispersing fly ash particles and burning incense sticks. The particle measurements were carried out with low pressure impactors. The particle mass concentration was under 500 mg/m^3, the charge/mass ratio 1 μC/g and the residence time in the agglomerator 1 s. The results of these measurements suggested that the agglomeration causes 20% concentration reduction for the particles under 1 μm.

Hughes and Richardson (1987) have used bipolar charging and turbulent mixing of aerosol particles to enhance the

agglomeration. The test aerosol consisted of fly ash and polyester particles. Agglomerate formation was observed by microscope, but no quantitative measurements of agglomeration were presented.

Ohkubo et al. (1987) conducted experiments with bipolarly charged aerosol in DC-electric fields. The test aerosol with the mean diameter of 0.4 μm was produced by burning incense sticks and the particle concentrations were measured with an optical particle counter in the size range 0.3–5 μm. The electric field was 2 kV/cm and the residence time in the agglomerator was 0.25 s.

However, no results have been reported for the agglomeration efficiency of particles smaller than 0.3 μm in diameter. Also, the results published so far have been measured with aerosol size spectrometers having limited size resolution, especially in the submicron size range. Detailed agglomeration efficiency of particles below 1 μm is important due to rather narrow penetration function (penetration as a function of the particle size) of the electrostatic precipitator. (Ylätalo et al., 1992; Joutsensaari et al., 1992; Kauppinen, 1991). In addition, the effect of wall losses within the agglomerator on the agglomeration efficiency has not been clarified in the work reported so far.

In this work, both the parallel plate and the electric quadrupole agglomerator have been studied using liquid, vegetable oil aerosols generated with air atomizing nozzles, in order to find out the effect of agglomerator geometry on the efficiency. Particle number size distributions were measured with high resolution using the differential mobility analyzer (DMA). Mass size distributions with Berner-type low pressure impactor (Berner and Lurzer, 1980; Hillamo and Kauppinen, 1991). The effect of agglomerator wall losses was studied separately by introducing submicron vegetable oil aerosols as generated with collision type atomizers into the agglomerator. The effects of particle mass concentration and residence time was studied.

EXPERIMENTAL SYSTEM

Principle

The experimental system is presented in Figure 2. The system includes a test particle generation chamber, particle generator, particle charger, agglomerator chamber, and measurement equipment. The air flow is controlled by a fan and the air flow rate can be adjusted in the range 0–1.5 m^3/min. Vegetable oil test particles are generated by air atomizing nozzles in the generation chamber. Particles are charged by a corona discharge. The aerosol then flows into the alternating electric field of the agglomeration chamber. The effect of

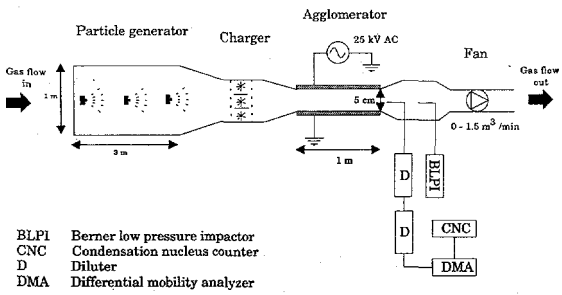

FIGURE 2. An experimental set-up to study the electrical agglomeration of charged aerosol particles. Vegetable oil test particles are generated by air atomizing nozzles and charged by a corona charger. In this picture only the parallel plate agglomerator is presented, but the quadrupole agglomerator was also studied.

the electrical agglomeration on the particle size distribution is measured after the agglomerator. The measurements are carried out in turns with and without the agglomerator voltage, so the measured change in the particle size distribution is caused by the agglomerator electric field and not by the space charge effects and turbulent losses.

Test Particle Generation

Test particles were generated from vegetable oil by air atomizing nozzles produced by Spraying Systems Inc. The liquid flow rate and particle size distribution depends on the pressures of the liquid and the atomizing air. In this research the air pressure was 3 bar, the liquid pressure 0.25 bar and the liquid flow rate through one nozzle was about 10 mL/min.

The test particle generation chamber was a cylindrical tube whose length and diameter were 3 and 1 m. The reason for the large dimensions of the chamber was the large size of the liquid spray coming out of the nozzle. If the generation chamber were smaller, the spray would hit the walls of the chamber and the particle losses would be very high.

The optimum number and position of the nozzles were investigated by trial and error. Nine nozzles were required to maximize the particle concentration in the agglomeration chamber and to minimize the liquid consumption. Three of them were situated on the rear end of the chamber and six nozzles were situated at 1 m distance from the rear. Increasing the number of the nozzles from nine did not increase the particle concentration significantly because of the kinematic coagulation between the particles originating from different nozzles and the turbulent losses to the walls of the generation chamber.

Corona Charger

The aerosol particles were charged by corona charger consisting of a thin corona wire (diameter 50 μm) between two metal plates. The height, length, and width of the charger were 40 cm, 3 cm, and 3.5 cm respectively. The electric power to the charger was supplied by an ignition transformer and a rectifier. The input voltage of the ignition transformer was controlled by a variable transformer. The maximum output voltage of this ignition transformer was 10 kV and the short circuit current 25 mA. The inexpensive ignition transformer tolerates sparks and short circuits without damage, making it ideal for the present study. The voltage and current used in this research were 7 kV and 15 μA. The polarity of the corona was positive, but negative corona could be used as well.

Agglomerators

The measurements were carried out using two different agglomerator chambers. One type of agglomerator was the simple parallel plate agglomerator (Mitchner and Self, 1983) and the other a quadrupole agglomerator (Watanabe and Suda, 1990).

The parallel plate agglomerator is presented in Figure 3a. The electric power was produced by a high-voltage transformer controlled by a variable transformer. The maximum voltage of the high voltage was 25 kV, thus the maximum electric field in the agglomerator was 5 kV/cm. The frequency was 50 Hz.

The electrical quadrupole agglomerator is illustrated in Figure 3b. It consists of two parallel plates and four cylindrical electrodes between the plates. The electric field is produced by a combination of AC and DC voltages. The maximum AC voltage was 25 kV and maximum DC voltage 10 kV.

Measurement Equipment

The total particle mass concentration was determined from samples collected on 25-

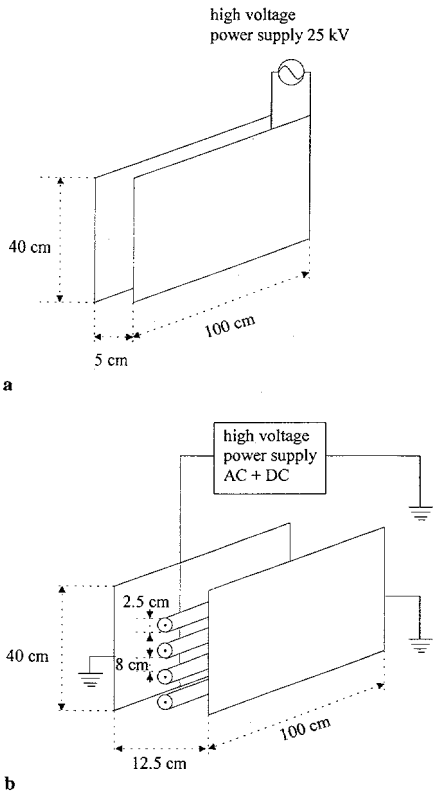

FIGURE 3. (a) Parallel plate agglomerator. Length 1 m, height 40 cm, separation between the plates 5 cm, electric field 5 kV/cm. (b) Quadrupole agglomerator. Length 1 m, height 40 cm, separation between plates 12.5 cm, diameter of the cylindrical electrodes 2.5 cm. Maximum AC-voltage 25 kV, maximum DC-voltage 10 kV.

mm glass fiber filters at a gas flow rate 0.77 L/min. The flow was controlled by critical orifice and monitored with a rotameter. Particle size distributions were measured with a TSI DMA system and a Berner low-pressure impactor; similar sampling heads were used with both. The sampling head was an electrically grounded metal tube, with the inner diameter 2 cm and a radioactive source (Am-241) was attached inside the tube to neutralize the charged particles. The impactor was connected directly to the sampling head. Collection substrates were aluminium foils. No grease was needed since the test particle material was sticky.

The DMA measurement system is presented in Figure 4. Because of the high particle concentration, dilution was needed with the DMA measurements. Two diluters were used and the total dilution ratio was about 1/100. The diluters operated on the ejector principle described by Koch et al. (1988), and the sample flow rate into the diluter was 5 L/min. The dilution air flow was controlled by a critical orifice.

Particle charge was monitored using a Faraday cell method. An insulated metallic filter holder is positioned in an electrically grounded metal tube. When air is drawn through the filter, aerosol particles are collected on it and the current coming from the particles is detected by an electrometer. When the mass collected on the filter is weighed the charge/mass ratio can be calculated.

RESULTS AND DISCUSSION

The particle concentration and size distribution were measured after the agglomerator with agglomerator voltage turned off and on several times. The particle charger was on all the time. Because the measurements were carried out after the agglomerator the losses caused by gas turbulence and space charge effects did not affect the measured concentration reduction. The voltage between the plate electrodes was 25 kV thus the electric field was 5 kV/cm. Two particle concentrations (1 and 2 g/m^3) and two residence times (4 and 6 s) were used.

Parallel Plate Agglomerator

The results for the impactor measurement on the effect of agglomerator voltage to

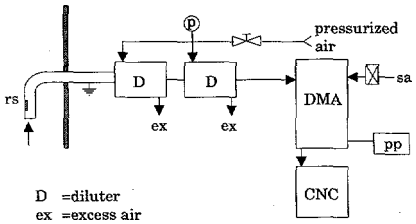

FIGURE 4. Principle of size distribution measurement with DMA system. The radioactive source was Am-241. The sample flow into the diluter 5 L/min. Dilution air flow into one diluter 50 l/min. Total dilution ratio 1:100. DMA sample flow rate 0.3 l/min and sheath air flow rate 3 L/min.

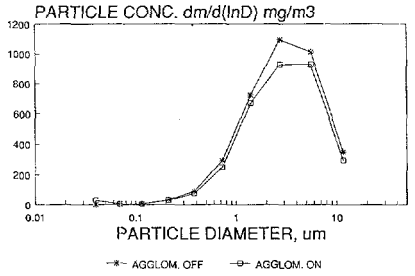

FIGURE 5. Parallel plate agglomerator measurement. The effect of the agglomerator on the particle size distribution as measured by the Berner low pressure impactor. Charging voltage 7 kV, charging current 15 μA, charge/mass 6 μC/g. Electric field in the agglomerator 5 kV/cm, residence time in the agglomerator 4 s, gas velocity 25 cm/s.

the mass size distribution are presented in Figure 5. Here particle concentration was 2 g/m^3 and the residence time in the agglomerator 4 s. It can be seen, that the particle concentration is reduced when agglomerator voltage is connected and the larger the particle size the larger the concentration reduction. However, the concentration reduction is caused by the wall losses within the agglomerator. This was verified by measuring total mass concentrations using a filter sampler. When the agglomerator voltage was on, the total mass concentration was reduced 10%–20%. Because of the low mass concentration and limited sensitivity of the gravimetric analyses, no effect could be seen with BLPI in the submicron particle size range.

Fine particle concentration reduction due to agglomeration was studied by measuring the number concentration of particles with CNC in the mobility channel separated by the DMA when the agglomerator voltage was turned on or off. The singly charged particle diameter corresponding to the channel midpoint mobility was 0.33 μm. In addition to the test aerosol generated by the air atomizing nozzles, test aerosol consisting of only fine particles (< 1 μm) were generated by six-jet atomizer (TSI six-jet) with a small cyclone attached to its outlet to remove the particles larger than about 1 μm. When agglomerator voltage was turned on, a reduction of about 5% was observed when supermicron particles were simultaneously introduced into the agglomerator. No concentration reduction was observed when only aerosols below 1 μm were present in the agglomerator. This confirms that the submicron particle number concentration reduction is caused by the electrical agglomeration rather than by wall losses within the agglomerator.

The effect of agglomerator voltage on the particle number distributions as determined with DMA for the aerosol generated with air atomizing nozzles is shown in Figure 6. The concentration reduction is shown as the function of particle size in Figure 7, as determined from the size distributions shown in Figure 6. The sig-

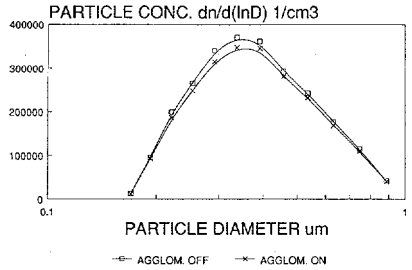

FIGURE 6. Parallel plate agglomerator measurement. The effect of the agglomerator on the particle size distribution as measured by the DMA. Average of five measurements. Charging voltage 7 kV, charging current 15 μA, charge/mass 6μC/g. Particle mass concentration 2 g/m^3, electric field in the agglomerator 5 kV/cm, residence time in the agglomerator 4 s, gas velocity 25 cm/s.

nificant scatter in the results is due to slight variation of the generator output with respect to particle size distribution and also due to variations in the charger operating conditions.

The effect of the total mass concentration and the residence time on the agglomeration efficiency is shown in Table 1. The increase of both the supermicron particle mass concentration and the residence time increases the agglomeration efficiency.

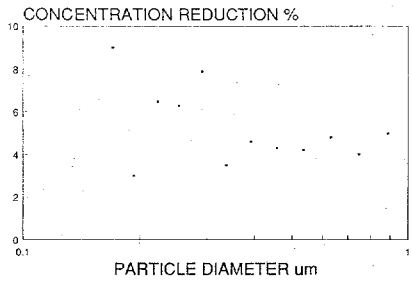

FIGURE 7. Particle reduction caused by the parallel plate agglomerator. The reduction is calculated from the results presented in Figure 6. The average reduction is 5%.

TABLE 1. The Effect of the Total Mass Concentration and the Residence Time on the Agglomeration Efficiency[a]

Total mass (g/m^3)	time (s)	Agglomeration Efficiency (%)
2	4	5
2	6	8
1	6	4

[a] The agglomerator efficiency is defined as the submicron particle concentration reduction.

Quadrupole Agglomerator

Similar experiments with the air atomizing nozzle generated test aerosols were carried out with the quadrupole agglomerator as with the parallel plate agglomerator. The AC voltage was 25 kV, the frequency was 50 Hz and the value of DC voltage was varied in the range 0-10 kV. When the mass concentration was 2 g/m^3 and the residence time in the agglomerator was 4 seconds, the average agglomeration efficiency was 5%, being relatively independent of the DC voltage value. This indicates, that within the experimental conditions used in this study, the focusing effect of the quadrupole geometry as proposed by Watanabe and Suda (1990) does not significantly affect the agglomeration.

Error Estimation

The aerosol generation, charging, and dilution were reasonably stabile. The short-term (1-min) time average of the measured aerosol concentration varied less than $\pm$2% and the long term (30 min) time average varied less than $\pm$1%. Thus, the worst case error in the calculated removal efficiency is $\pm$2%.

Comparison with Theory

Lehtinen et al. (1994) have proposed a model for the agglomeration efficiency of charged aerosol particles in external electric fields. The agglomeration efficiency can be calculated using the formula

$$\Phi = 1 - \left\{ 1 - \frac{\epsilon(d, D) b E_0 M_D}{4\pi^2 \eta \rho f} \times \frac{(D-d)(D+d)^2}{D^3} \right\}^{4Tf} \quad (1)$$

where

Φ = reduction of the submicron particles,
D = diameter of the supermicron particles,
d = diameter of the submicron particles,
ϵ = collision efficiency,
E_0 = electric field strength,
M_D = total mass concentration of the supermicron particles,
ρ = density of the particles,
η = viscosity of the gas,
T = residence time,
b = constant, $7.9 \cdot 10^{-6}$, and
f = frequency of the electric field.

The collision efficiency can be calculated by solving the equation of the motion of the particles and taking into account the inertial, electrical and drag forces. To perform this calculation, the flow field around the large particle must be solved. When we compare the observed agglomeration efficiency to the one calculated from Eq. 1, we find that the collision efficiency required is 0.3 for the calculated and experimental results to be in agreement. However, the calculations presented by Lehtinen et al. (1994) show that the collision efficiency of unipolarly charged aerosol particles is negligible. This means that the aerosol studied in this research has contained in addition to positive particles also negative or neutral particles. Aerosol particles can be charged negatively even in the presence of a positive corona discharge if a back corona exists on the passive electrode (Kobashi, 1979). The back corona can also neutralize the positively charged aerosol particles.

CONCLUSIONS

The electrical agglomeration of the unipolarly charged aerosol particles in the alternating electric field has been observed. The agglomeration decreases the submicron particle concentration from 4% to 8%, when the total mass concentration is 1–2 g/m^3, particle mass mean diameter 4 μm, geometric standard deviation about 2.8, particle charge/mass ratio 6 μC/g, residence time in the agglomerator 4–6 s and average electric field 5 kV/cm. The agglomeration efficiency increases when increasing the total mass concentration and the residence time in the agglomerator.

The total mass and large particle concentration were decreased about 15%–25% because of the wall losses caused by the agglomerator electric field. When the gas contained only fine particles, no particle concentration reduction could be seen. This proves that the small particle concentration reduction was caused by the electrical agglomeration and not by the particle collection on the agglomerator walls.

The comparison with theory indicates that unipolar electrical agglomeration alone could not cause this agglomeration effect. So, the aerosol studied has contained not only positive aerosol particles but also negative or neutral particles.

Measurement shows that the large particle concentration is important for the electrical agglomeration in alternating electric fields. The reason for this is that the large particles have large oscillation amplitude and velocity compared with fine particles. The larger the oscillation amplitude and the velocity, the larger volume

the particles sweep and the larger is the amount of collected fine particles. If the gas contains only fine particles and the concentration is about 10^6 cm^{-3}, no agglomeration would occur. The reason is the small oscillation amplitude of the fine particles.

This research did not show any differences between the parallel plate and the quadrupole agglomerator. At this moment one cannot say whether there is a focusing effect in the quadrupole field, so particle behavior in an alternating electric quadrupole field needs more theoretical and experimental research.

This research shows that electrical agglomeration could be one possible method to decrease the fine particle concentration in gases. These measurements resulted in a quite small concentration reduction effect, but it must be remarked that the particle concentration in real flue gas is more favorable for agglomeration than in this investigation. In real flue gases particle concentration is very high, for example, at pulverized coal combustion it is about 10 g/m^3 and at circulating fluidized bed combustion 20–30 g/m^3.

Lossless high-efficiency particle chargers that deliver ten times greater electric charge levels to aerosol particles than the charger used in this paper have also been developed (Tassicker and Schwab 1977).

The experimental and theoretical research must be continued to receive more information about the parameters affecting the agglomeration. One of the important basic issues is the collision efficiency of two charged particles. Test particle generation and charging must also be developed so that higher particle concentration and charge/mass ratio can be achieved. Since the theory shows that the bipolar agglomeration is much more efficient than the unipolar agglomeration (Lehtinen et al., 1994) the research looking for practical applications must concentrate on the bipolar agglomeration.

This study has been funded by the Finnish Ministry of Trade and Industry, IVO and Tampella Power via environmental engineering research program SIHTI. We thank prof. T. Watanabe, Dr. J. Keskinen, Dr. K. Janka, and Mr. M. Hahkala for useful discussions and suggestions. We also thank Dr. M. Lehtimäki for helping us with the instrumentation.

REFERENCES

Berner, A., and Lurzer, C. (1980). *J. Phys. Chem* 84:2079–2083.

Flagan, R. C., and Seinfeld, J. H. (1988). *Fundamentals of Air Pollution Engineering.* Prentice Hall, Englewood Cliffs, NJ.

Fuchs, N. A. (1964). *The Mechanics of Aerosols.* Pergamon Press.

Hillamo, R. E., and Kauppinen, E. I. (1991). *Aerosol Sci. Technol.* 14:33–47.

Hughes, J. F., and Richardson, R. B. (1987). *Proceedings of Precipitation,* Massimo Rea. pp. 337–432.

Joutsensaari, J., Kauppinen, E. I., Ahonen, P., Lind, T., Ylätalo, S., Jokiniemi J., Hautanen, J., and Kilpeläinen, M. (1992). *J. Aerosol Sci.* 23:S241–S244.

Kauppinen, E. I. (1991). *J. Aerosol Sci.* 22:S451–S454.

Kauppinen, E. I., and Pakkanen, T. A. (1990). *Environ. Sci. Technol.* 24:1811–1818.

Kobashi, M. (1979). Ph.D. thesis, Stanford University.

Koch, W., Lödding, H., Mölter, W., and Munzinger, F. (1988). *Staub Reinhaltung Luft* 48:341–344.

Lehtinen, K., Jokiniemi J., Kauppinen, E., and Hautanen, J. (1994). Submitted.

Masuda, S., and Fujibayashi, K. (1970). *J.I.E.E. Jpan.* 90:861–869.

Mitchner, M., and Self, S. (1983). EPRI Report CS-3226.

Oglesby, S., and Nichols, G. (1978). *Electrostatic Precipitation.* Marcel Dekker, New York.

Ohkubo, T., Kanazawa, S., Nomoto, Y., Adachi, T., and Hughes, J. F. (1990). *Proceedings of the Fourth International Conference on Electrostatic Precipitation.* (Ruinian Li, Ed.). International Academic Publisher.

Tassicker, O., and Schwab, J. (1977). *EPRI J.* June/July:56–61.

Watanabe, T. (1988). Criepi report ET 880.

Watanabe, T., and Suda, T. (1990). *Proceedings of the Third International Aerosol Conference,* (S. Masuda and K. Takahashi, Eds.). Vol. 2, pp. 749–752.

Ylätalo, S., Kauppinen, E., Hautanen, J., Joutsesaari, J., Ahonen, P., Lind, T., Jokiniemi J., and Kilpeläinen, M. (1992). *J. Aerosol Sci.* 23 (suppl. 1):795–798.

Received April 1, 1993; revised May 16, 1994

Reprinted with permission from the publisher.
In: Aerosol Science and Technology 1995. Vol. 23, No. 3, pp. 422 - 430.

PAPER C

Kinematic Coagulation of Charged Droplets in an Alternating Electric Field

Kari E. J. Lehtinen,* Jorma K. Jokiniemi and Esko I. Kauppinen
Technical Research Centre of Finland (VTT), Aerosol Technology Group, P.O. Box 1401, SF-02044 VTT, Finland. VTT Energy, (K. E. J. L.; J. K. J.) VTT Chemical Technology (E. I. K.)

Jukka Hautanen
Tampere University of Technology, P.O. Box 692, SF-33101 Tampere, Finland.

An analytic-numerical model has been developed to study kinematic coagulation caused by the vibrational motion of charged particles in an alternating electric field. The primary aim of this study was to find out the reduction in the number concentration of fine particles of diameter 0.1 μm-1.0 μm caused by collisions with larger, supermicron particles. Three cases are considered: (1) unipolar charging, (2) fine particles are neutral, and (3) fine particles and large particles have opposite polarity. We find out that in cases 1 and 2 the rate of kinematic coagulation in negligible and in case 3 significant. The results are demonstrated with two sample calculations with total mass loadings of 2 and 20 g/m³. In the former, where the mass median diameter is 3.0 μm, we discover a 20%–50% reduction in number concentration of particles in the range 0.5–1.0 μm and less significant reduction in smaller particles. The latter (MMD = 6.0 μm) represents power plant conditions. In this case the reduction varies from 10% (0.1 μm) to 95% (1.0 μm).

INTRODUCTION

In removing flue gas particles at coal fired power plants, the efficient collecting of particles in the diameter range 0.1–1.0 μm remains to be solved. The most commonly used flue gas cleaner in these circumstances is the electrostatic precipitator (ESP). According to the studies of Ylätalo et al. (1992), the total mass collection efficiency with the ESP can be over 99.7%, while the collection efficiency for the above mentioned range can be only 85%.

To reduce air pollution and thus negative human health effects, it is of great importance to reduce the penetration of these fine fly ash particles. Because of their small inertia they travel long distances in the atmosphere and can easily get into the human respiratory system. Also the heavy metals and other toxic volatile and condensing species are concentrated on the fine particles (Seinfeld 1986). In addition to the already existing restrictions on toxic trace metal emissions, it is thus probable that the environmental laws in the future will not only make restrictions on the total mass emissions but take into account also the particle size aspects.

Much research has been made recently to solve this problem of significant submicron penetration by utilizing a particle agglomerator before the ESP in order to shift the particle size distribution in such a way that the resulting particles can be

*Corresponding author: Kari Lehtinen, current address (8/1/94–8/31/95): UCLA Department Chemical Engineering, 5531 Boelter Hall, Los Angeles, CA 90024.

0278-6826/95/$9.50
SSDI 0278-6826(95)00062-K

efficiently collected (for example, Eliasson and Egli 1991, Löffler and Gutsch 1993; Magill, et al. 1992). Here we study theoretically, if this could be accomplished by using particle charging and an alternating electric field. In the alternating electric field the particles start to oscillate with amplitudes and velocities depending on particle size and charging. The different velocities cause kinematic coagulation between the particles hopefully removing some of the particles in the problematic size range.

This study was much inspired by the work of Kobashi (1979) and Eliasson and Egli (1991). Kobashi investigated both theoretically and experimentally, how particles of diameter 1–10 μm are removed by collisions with larger particles of diameter 10–100 μm. His agglomerator consisted of two parallel plates in high voltage, between which the alternating field was applied. This is also the basis of this theoretical study (Fig. 1) and we are carrying out experimental work with a similar arrangement. However, the particle size ranges are different: In this study the small particles are in the problematic range 0.1–1 μm and the large particles under 20 μm. This means that inertial effects are here much less important than in Kobashi's study. Eliasson and Egli use a different approach: Their agglomerator is based on the increased rate of thermal coagulation because of attractive forces caused by bipolar particle charging. In this study we consider only kinematic coagulation thus neglecting thermal coagulation altogether, but have adopted much of the terminology of their paper, especially the concept asymmetric bipolar coagulation. Asymmetric bipolar coagulation refers to the situation where the density distribution of positive particles is different from the distribution of negative particles. In this study, when considering bipolar coagulation, we have an ideal case of asymmetric bipolar coagulation: The fine particles to be removed and the large collector particles have opposite sign (see Fig. 3).

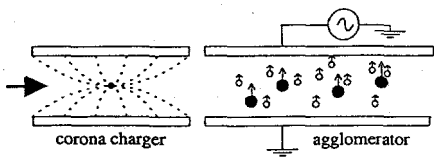

FIGURE 1. Principle of agglomeration (here the case of unipolar charging): Charged particles start to oscillate in the alternating electric field. The amplitude and velocity differences cause collisions.

An important part of the theoretical study of kinematic coagulation is the determination of the collision efficiency of two colliding droplets. The collision efficiency is defined as the ratio of the effective collision cross section to the geometrical collision cross section (Fig. 2). The analytical expressions of Fuchs and Pruppacher and Klett (Pruppacher and Klett, 1977) for the collision efficiency in the case of gravitational coagulation are no longer valid in this case where interparticle electrical forces are important. The determination of collision efficiencies between raindrops and aerosol particles in the atmosphere was an active research topic among cloud physicists in the late 1960s and early 1970s (Pruppacher and Klett 1977). In most of these studies the equations of motion of the small aerosol particles are integrated in the flow field generated by the falling motion of the larger raindrops. A similar technique is used here.

MODEL ARRANGEMENT

The model is based on an assumption that the particles can be clearly divided into large collector particles (diameter > 1 μm) and fine particles (diameter < 1.0 μm) to be removed (Fig. 3). We will first

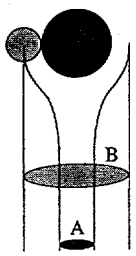

FIGURE 2. The collision efficiency ε is defined as the ratio of the effective collision cross section to the geometrical collision cross section: $\varepsilon = A/B$.

solve the equation of motion of oscillation for the charged spherical particles in the alternating electric field. Thus we find out the volume that the large particles sweep during one oscillation in the small particle space. This brings us then to the reduction in number concentration of the fine particle mode.

Reduction of Submicron Particles

The equation of motion of a particle with mass m and charge q in an alternating electric field with amplitude $\vec{E}_0$ and frequency f is

$$m\ddot{\vec{r}} = q\vec{E}_0 \cos(2\pi ft) - \vec{F}_{\text{drag}} + \vec{F}_g. \quad (1)$$

Here $\vec{r}$ is the position vector of the particle, $\vec{F}_{\text{drag}}$ the drag force and $\vec{F}_g$ the gravitational force. If the particle is spherical ($m = \frac{1}{6}\pi\rho D^3$) and Stokesian drag ($\vec{F}_{\text{drag}} = 3\pi\mu D\dot{\vec{r}}$, μ = viscosity) is applicable, we get in the direction of oscillation (x):

$$\tfrac{1}{6}\pi\rho D^3\ddot{x} = qE_0 \cos(2\pi ft) - 3\pi\mu D\dot{x}. \quad (2)$$

This has the analytical solution

$$x = -\frac{1}{\sqrt{1+\tan^2\varphi}}\frac{qE_0}{6\pi^2\mu Df}\sin(2\pi ft - \varphi) + C_1 e^{-t/\tau} + C_2, \quad (3)$$

with characteristic time

$$\tau = \frac{\rho D^2}{18\mu}. \quad (4)$$

and phase difference φ:

$$\tan\varphi = 2\pi f\tau = \frac{\pi\rho D^2 f}{9\mu}. \quad (5)$$

The unknown constants C_1 and C_2 are determined by the initial place and velocity.

In the following sample calculations we will use the parameter values from our experiments: $\rho = 900$ kg/m^3, $\mu = 1.8\cdot 10^{-5}$ kg/m·s, $E_0 = 7.1\cdot 10^5$ V/m and $f = 50$ Hz. Then φ and the second term on the right-hand side of Eq. 3 are negligible, and a very good approximation of solution 3 for particles with diameter $D <$ 20 μm is

$$x = -\frac{qE_0}{6\pi^2\mu Df}\sin(2\pi ft). \quad (6)$$

In the experiments the particle charge was measured to be proportional to its surface area i.e.,

$$q(D) = bD^2. \quad (7)$$

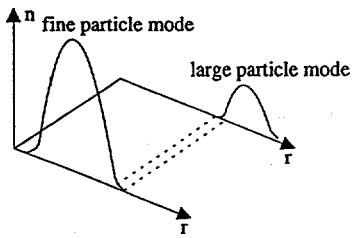

FIGURE 3. We assume that the fine particles to be removed and the collector particles have distinguishable size distributions. Asymmetric bipolar coagulation refers to the case where the fine particles and the large particles have opposite sign.

In the example calculations we use the measured value $b = 7.9 \cdot 10^{-6}$ C/m^2 for the proportionality constant. If we combine Eqs. 7 and 6, we get

$$x = -\frac{bE_0 D}{6\pi^2 \mu f} \sin(2\pi f t). \tag{8}$$

Now we see the cause of collisions. The amplitude of oscillation (and also velocity) is approximately linearly dependent of the particle diameter. Hence the large particles have larger oscillation amplitudes and velocities than the small ones. With the earlier mentioned values of the parameters we get for the oscillation amplitude X:

$$X = \frac{bE_0 D}{6\pi^2 \mu f} \approx 100 \cdot D \tag{9}$$

and for the velocity amplitude $\dot{X}$:

$$\dot{X} = 2\pi f \cdot X \approx 3.1 \cdot 10^4 \tfrac{1}{s} \cdot D. \tag{10}$$

With this magnitude of the velocity amplitude, it is easily noticed that the Reynolds number is small enough for particles with diameter smaller than 20 μm that the Stokesian drag can be used with reasonable accuracy.

Let the number concentration of the aerosol be $n(D)$ and the mass concentration $m(D)$. The volume fraction of the fine particle space that the large particles sweep during oscillation of one amplitude distance is

$$V = \int_D \varepsilon \cdot \frac{1}{4}\pi (D+d)^2 \cdot [X(D) - \sigma X(d)] \cdot n(D)\,\delta D. \tag{11}$$

Here the term fine particle space accounts for the volume where the fine particle center must be in the symmetry point of oscillation for a collision to occur. This is why the term $X(d)$ is included. $(1/4)\pi(D+d)^2$ is the cross-sectional area of the swept volume assuming that the small particles move in straight lines by the larger ones. The collision efficiency ε is the correction to this false assumption (see Fig. 2) and is dealt with later. In this study, we include three different charging cases:

1. Unipolar charging ($\sigma = 1$), where all the particles are charged unipolarly according to Eq. 7.
2. Bipolar charging ($\sigma = -1$), where the magnitude of charge is calculated according to Eq. 7, but the large and fine particles are of opposite charge.
3. Neutral small particles ($\sigma = 0$), where the magnitude of charge of the large particle mode is calculated according to Eq. 7 and the small particles are neutral.

If the initial number concentration of the small particles is $n(d)$, then the number concentration after one such 1/4 oscillation decreases to $(1 - V) \cdot n(d)$. If the residence time in the agglomerator is T, there are $4Tf$ such 1/4 oscillations and the concentration decreases to $(1 - V)^{4Tf} \cdot n(d)$. The total relative decrease in number concentration, taking Eq. 9 into account, is thus

$$\Phi(d) = 1 - \left\{1 - \frac{bE_0}{4\pi^2 \rho \mu f} \int_D \varepsilon(d, D) \cdot m(D) \frac{(D - \sigma d)(D+d)^2}{D^3}\,\delta D\right\}^{4Tf}. \tag{12}$$

Here we have taken into account the relationship between mass and number distributions $m(D) = (1/6)\pi \rho D^3 n(D)$. We have also assumed that the aerosol is homogeneous and that collisions do not disturb this homogenity (the volume that large particles sweep is instantaneously filled with small particles) or the size distribution of the large particle mode.

A very useful (and accurate) approximation for Eq. 12 can be obtained by

using the exponential function:

$$\Phi(d) \approx 1 - e^{-\frac{bE_0T}{\pi^2\rho\mu}I(d)}, \tag{13}$$

where $I(d)$ is the integral

$$I(d) = \int_D \varepsilon(d, D)\cdot m(D) \times \frac{(D-\sigma d)(D+d)^2}{D^3}\delta D. \tag{14}$$

Collision Efficiency

Now we turn to the calculation of the collision efficiency ε. An accurate solution of the problem would require a simultaneous numerical solution to the equations of motion of both particles and the surrounding fluid. However, when the fine particle is much smaller than the larger one, it is reasonable to assume that it doesn't disturb the flow field around the larger one. Thus we fix the coordinate system into the center of the large particle and integrate the equation of motion of the smaller one in the flow field around the large particle (Fig. 4).

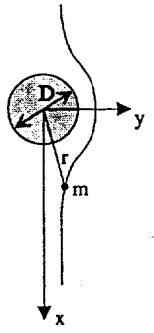

FIGURE 4. The coordinate system is fixed to the center of the large particle and the flow field is calculated in these coordinates. The equation of motion of the smaller particle is integrated numerically in the flow field.

The equation of motion of the fine particle (mass = m) is

$$m\ddot{\vec{r}} = \vec{F}_C + \vec{F}_E + \vec{F}_A, \tag{15}$$

where $\vec{F}_C = \sigma k(bD^2\cdot bd^2/r^2)(\vec{r}/r)$ is the Coulombic force, $\vec{F}_E = \sigma bd^2E_c\vec{e}_x$ the electric field induced force, $\vec{F}_A = 3\pi\mu d(\vec{v}_{\text{flow}} - \dot{\vec{r}})$ the aerodynamic force, $k = 8.988\times10^9$ Nm^2/C^2, $E_C = 2E_0/p$ (the average absolute value of E), $\vec{e}_x$ = unit vector in the x-direction and $\vec{v}_{\text{flow}}$ = velocity of the fluid. Here it must be noted that we have neglected the corrections (image forces) to the electric forces caused by polarization.

For the fluid velocity, we use here the Stokes solution to viscous flow around a sphere:

$$\begin{aligned}\vec{v}_{\text{flow}} &= \frac{bE_cD}{3\pi\mu}\vec{e}_{\text{flow}} \\ &= \frac{bE_cD}{3\pi\mu}\left[\frac{3}{4}\frac{Dx^2}{2r^3}\left(\frac{D^2}{4r^2}-1\right)\right. \\ &\quad \left. -\frac{1}{4}\frac{D}{2r}\left(3+\frac{D^2}{4r^2}\right)+1\right]\vec{e}_x \\ &\quad + \frac{bE_cD}{3\pi\mu}\left[\frac{3}{4}\frac{Dxy}{2r^3}\left(\frac{D^2}{4r^2}-1\right)\right]\vec{e}_y\end{aligned} \tag{16}$$

For the sake of numerical computations, we make the following changes of variables:

$$t = \frac{3\pi\mu}{2bE_c}\tau, \quad \vec{r} = \frac{D}{2}\vec{s}, \quad d = \hat{d}\cdot10^{-6}\ \mu\text{m}$$

$$\text{and} \quad D = \hat{D}\cdot10^{-6}\ \mu\text{m}.$$

Then the equation of motion becomes:

$$\ddot{\vec{s}} = \frac{\sigma\beta\alpha}{s^3}\frac{\hat{d}}{\hat{D}}\vec{s} + \sigma\alpha\frac{\hat{d}}{\hat{D}} + \alpha\left(\vec{e}_{\text{flow}} - \dot{\vec{s}}\right), \tag{17}$$

where

$$\alpha = \frac{27\pi\mu^2}{\rho b E_c (10^{-6}\ \mu\mathrm{m})^2}\frac{1}{\hat{d}^2} \quad \text{and} \quad \beta = \frac{4kb}{E_c}.$$

If we write $\vec{s} = s_x\vec{e}_x + s_y\vec{e}_y$, Eq. 17 can be transformed into component form:

$$\ddot{s}_x = \frac{\sigma\beta\alpha}{s^3}\frac{\hat{d}}{\hat{D}}s_x + \sigma\alpha\frac{\hat{d}}{\hat{D}} + \alpha(e_{\mathrm{flow},x} - \dot{s}_x), \tag{18}$$

$$\ddot{s}_y = \frac{\sigma\beta\alpha}{s^3}\frac{\hat{d}}{\hat{D}}s_y + \alpha(e_{\mathrm{flow},y} - \dot{s}_y). \tag{19}$$

Now we can find out the collision efficiency ε by solving the equations of motion 18 and 19 with different initial conditions. Thus we find out the critical $s_{y0c}(y_{0c})$ so that the collision barely occurs. ε will then be:

$$\varepsilon = \frac{y_{0c}^2}{(d/2 + D/2)^2} = \frac{s_{y0c}^2}{\left(1 + \hat{d}/\hat{D}\right)^2}. \tag{20}$$

The other initial conditions are chosen in the following way: Firstly, x_0 must be large enough that the streamlines are, at that distance, straight: here we have chosen $x_0 = 25 \cdot D$ ($s_{x0} = 50$). Secondly, we must also give initial values to the dimensionless velocities s_x and s_y. Those we get from Eqs. 18 and 19 by setting $\ddot{s}_x = 0$ and $\ddot{s}_y = 0$:

$$\dot{s}_{x0} = \frac{\sigma\beta}{s_0^3}\frac{\hat{d}}{\hat{D}}s_{x0} + \sigma\frac{\hat{d}}{\hat{D}} + e_{\mathrm{flow},x} \tag{21}$$

and

$$\dot{s}_{y0} = \frac{\sigma\beta}{s_0^3}\frac{\hat{d}}{\hat{D}}s_{y0} + e_{\mathrm{flow},y}. \tag{22}$$

The equations of motion 18 and 19 were solved numerically using the Gear fourth order predictor-corrector method. The collision efficiency was calculated with different values of charge coefficient $b(b_0 = 7.9 \cdot 10^{-6}\ \mathrm{C/m^2})$, electric field strength E_c and particle diameters d and D. We observed that electric field strength had negligible effect in all charging cases. Also the particle diameters affected the results only via the ratio d/D. In all calculated cases, where the particles had charge of same sign, no collisions occurred. Thus the collision efficiency is

$$\varepsilon_U = 0. \tag{23}$$

The collision efficiency of Fuchs

$$\varepsilon_N = \frac{3}{2}\left(\frac{d}{d+D}\right)^2 \tag{24}$$

seemed to describe very accurately the numerical results for the case of neutral small particles, which was of course to be expected. In the bipolar case the dependence on charging is strong. In Fig. 5 the numerically calculated bipolar collision efficiency is presented as a function of the ratio d/D calculated with different values of b/b_0. The numerical data are quite

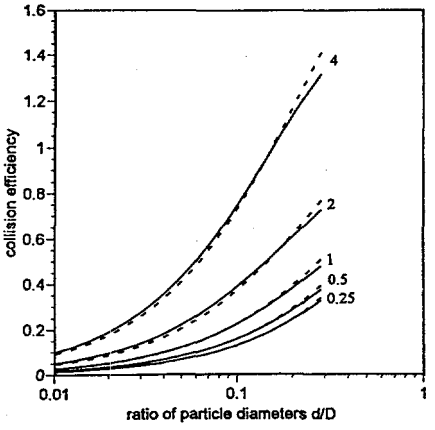

FIGURE 5. Bipolar collision efficiencies: The numerical results are represented with solid lines and the corresponding approximating functions (formula 25) with dotted lines. The calculations are done with the values 4, 2, 1, 0.5, and 0.25 for the charge coefficient b/b_0.

well approximated by the analytical expression

$$\varepsilon_B = \frac{d}{D} + \frac{3}{2}\frac{dD^2}{(d+D)^3}\cdot\frac{b}{b_0}\left(1+\frac{b}{10b_0}\right), \quad (25)$$

which is also presented in Fig. 5. These analytical expressions are very useful, because now we can insert them directly into Eqs. 13 and 14 and thus get an analytical approximation for the reduction in number concentration of small particles in the agglomerator.

CALCULATED RESULTS

In the following, we will calculate the decrease in number concentration of an initially lognormal number concentration distribution of small particles

$$\delta N = \frac{N}{\sqrt{2\pi}\ln\sigma_g^d}\exp\left[-\frac{1}{2}\left(\frac{\ln d - \ln\bar{d}}{\ln\sigma_g^d}\right)^2\right] \times\delta(\log d), \quad (26)$$

where N = total number concentration of small particles (here $4.7\cdot10^6$ cm^{-3}), σ_g^d = geometric standard deviation (here 1.6) and $\bar{d}$ = number median diameter (here 0.35 μm). This distribution represents well the number distribution of the small particle mode in our experiments.

The reason of the decrease in the number concentration of the fine particle mode is a lognormal mass distribution of larger particles:

$$\delta M = \frac{M_i}{\sqrt{2\pi}\ln\sigma_{gi}} \times\exp\left[-\frac{1}{2}\left(\frac{\ln D-\ln\bar{D}_i}{\ln\sigma_{gi}}\right)^2\right]\delta(\log D). \quad (27)$$

The calculations are made with two sets of parameter values of the lognormal mass distribution:

1.

$M_1 = 2\frac{g}{m^3}$, $\sigma_{g1} = 1.7$ *ja* $\bar{D}_1 = 3$ μm and

2.

$M_2 = 20\frac{g}{m^3}$, $\sigma_{g2} = 2.2$ *ja* $\bar{D}_2 = 6$ μm

Here case 1 approximates the large particle mass distribution in our experiments and case 2 a mass distribution measured at a power plant by Joutsensaari et al. (1993). Inserting Eq. 27 together with Eqs. 23–25 into Eq. 14, and integrating with respect to D in the range $[D_{\min},\infty]$, we get

$$I^U(b,d) = 0, \quad (28)$$

$$I^B(b,d) = I_1 + \frac{3B(10+B)}{20}I_2 \quad \text{and} \quad (29)$$

$$I^N(b,d) = \frac{3}{2}I_2, \quad (30)$$

where

$$I_1 = \frac{M}{2}\sum_{k=1}^{4}\binom{3}{k-1}\left(\frac{d}{\bar{D}}\right)^k \exp\left(\frac{1}{2}k^2\ln^2\sigma_g\right) \times\operatorname{erfc}\left[\frac{\ln(D_{\min}/\bar{D}) + k\ln^2\sigma_g}{\sqrt{2}\ln\sigma_g}\right] \quad (31)$$

$$I_2 = \frac{M}{2}\left(\frac{d}{\bar{D}}\right)^2 \exp\left(2\ln^2\sigma_g\right) \times\operatorname{erfc}\left[\frac{\ln(D_{\min}/\bar{D}) + 2\ln^2\sigma_g}{\sqrt{2}\ln\sigma_g}\right]. \quad (32)$$

The choice of $D_{\min}$ still remains. The problem is that the upper end tail of the fine particle size distribution might overlap with the lower end tail of the large particle size distribution (Fig. 3) together with the fact that in the collision efficiency calculations it was assumed that the large particle is 'sufficiently' larger than the fine particle. To get a feeling of how much the choice of $D_{\min}$ effects the

results, we made the calculations with two choices: (a) $D_{min} = 0$ and (b) $D_{min} = \bar{d}(\sigma_g^d)^2$. The b-choice is made in such a way that there is only little overlapping of the distributions: For the fine particle log-normal distribution, only approx. 2% of the particles are greater than $\bar{d}(\sigma_g^d)^2$. In the following, these cases are referred to subscripts a and b.

Completing the calculations with the earlier mentioned parameter values, we get the reduction in the number concentration of small particles as a function of $\hat{d}$, where $d = \hat{d} \cdot 1\ \mu$m, as a result of coagulation with the large particle modes (1) and (2) described by Eq. 27.

Reduction of small particles with large particle distribution 1:

$$\Phi_a^B = 1 - \exp[-0.162\hat{d} - 0.382\hat{d}^2 - 0.147\hat{d}^3 - 0.0493\hat{d}^4], \quad (33)$$

$$\Phi_b^B = 1 - \exp[-0.155\hat{d} - 0.340\hat{d}^2 - 0.125\hat{d}^3 + 0.0277\hat{d}^4], \quad (34)$$

$$\Phi_a^N = 1 - \exp[-0.082\hat{d}^2], \quad (35)$$

$$\Phi_b^N = 1 - \exp[-0.073\hat{d}^2]. \quad (36)$$

Reduction of small particles with large particle distribution 2:

$$\Phi_a^B = 1 - \exp[-0.960\hat{d} - 1.89\hat{d}^2 - 0.960\hat{d}^3 - 0.467\hat{d}^4], \quad (37)$$

$$\Phi_b^B = 1 - \exp[-0.909\hat{d} - 1.51\hat{d}^2 - 0.459\hat{d}^3 - 0.107\hat{d}^4], \quad (38)$$

$$\Phi_a^N = 1 - \exp(-0.405\hat{d}^2), \quad (39)$$

$$\Phi_b^N = 1 - \exp(-0.324\hat{d}^2). \quad (40)$$

The bipolar (B) cases are plotted in Fig. 6 and the cases with neutral small particles in Fig. 7. Here we notice that there is not much difference between cases a and b, which means that the choice of D_{min} did not crucially affect the results in this example calculation. A much more concrete picture of the result can be obtained if we study the effect of the concentration reduction on some distribution: Eqs. 34, 36, 38, and 40 are applied for the small particle size distribution (Eq. 26) and the result is presented in Fig. 8.

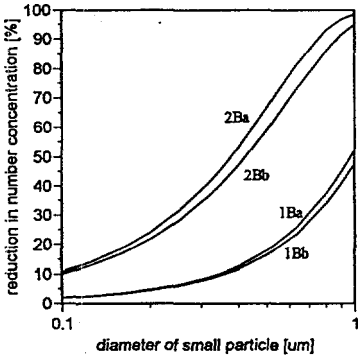

FIGURE 6. Bipolar charging: Reduction in number concentration of fine particles because of kinematic coagulation with large particles described by distributions 1 and 2 and choices a and b of D_{min}.

It is obvious from these results that kinematic coagulation alone caused by the vibrating particle motion in the alternat-

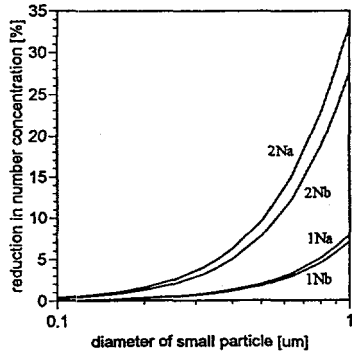

FIGURE 7. Neutral small particles: Reduction in number concentration of fine particles because of kinematic coagulation with large particles described by distributions 1 and 2 and choices a and b of D_{min}.

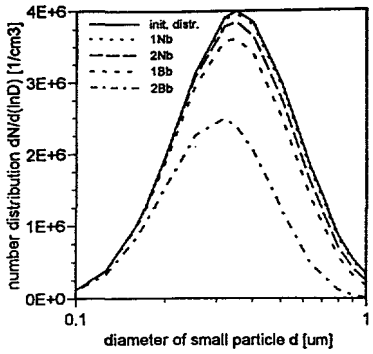

FIGURE 8. Change of fine particle number distribution (Eq. 26) because of kinematic coagulation with large particles described by distributions 1 and 2 and choice b of D_{min}. Calculations are done for the cases B = bipolar charging and N = neutral fine particles.

ing electric field is not a solution to increase the collection efficiency of flue gas cleaning systems in the diameter range near 0.1 μm. However, here we have neglected Brownian unipolar coagulation between the particles of the fine particle mode, which shifts the size distribution to larger particles thus increasing the kinematic coagulation rate also.

In the fine particle range near 1.0 μm the kinematic coagulation effect for the bipolar case seems to be significant. Even in the laboratory conditions we see a reduction of 20%–50% for particles of diameter 0.5 μm–1.0 μm. Such an ideally bipolar situation is difficult to obtain and in the experiments there are actually fine particles and large particles of both polarities. Modeling such a situation is much more difficult because then the charge distribution deviates significantly from its d^2-shape because of the increased amount of intermodal collisions. This, the effect of nonsphericality of the particles and the incorporation of Brownian coagulation into the model are the subjects of our future studies concerning electrical coagulation.

CONCLUSIONS

We have shown in an approximative theoretical study of electrically induced coagulation that kinematic coagulation caused by the vibrating motion of charged droplets in an alternating electric field is

1. negligible, when the fine particles to be collected and the large collector particles are charged with same polarity (unipolar charging) or when the fine particles are neutral; and
2. significant, when bipolar charging is ideally asymmetric, i.e., fine particles and large particles have charges of opposite sign.

With asymmetric bipolar coagulation between the fine particles that would normally penetrate through the ESP and the larger collector particles one can shift the size distribution towards larger sizes. Such a shifted particle distribution can then be collected with better efficiency in an ESP.

This research was financed by the Ministry of Trade and Industry and IVO.

REFERENCES

Eliasson, B., and Egli, W. (1991). *J. Aerosol Sci.* 22:429–440.

Joutsensaari, J., Kauppinen, E. I., Jokiniemi, J. K., and Helble, J. J. (1993). Studies on Ash Vaporization in Power Plant Scale Pulverized Coal Combustion. Engineering Foundation Conference, Birmingham, UK.

Kobashi, M. (1979). Ph. D. thesis, Stanford.

Löffler, F., and Gutsch, A. (1993). *J. Aerosol Sci.* 24:S505–S506.

Magill, J. et al. (1992). *J. Aerosol Sci.* 23:S803–S806.

Pruppacher, H. R., and Klett, J. D. (1978). *Microphysics of Clouds and Precipitation.* D. Reidel, Dordrecht.

Seinfeld, J. H. (1986). *Atmospheric Chemistry and Physics of Air Pollution.* Wiley, New York.

Ylätalo, S. et al. (1992). *J. Aerosol Sci.* 23:S795–S798.

Received May 3, 1994; revised April 13, 1995.

Reprinted with permission from the publisher.
In: Journal of Aerosol Science 1996. Vol. 27, No. 6, pp. 883 - 896.

PAPER D

PREDICTION OF NANOPARTICLE SIZE AND THE ONSET OF DENDRITE FORMATION USING THE METHOD OF CHARACTERISTIC TIMES

Kari E. J. Lehtinen,* Robert S. Windeler and Sheldon K. Friedlander

Air Quality and Aerosol Technology Laboratory, Chemical Engineering Department, University of California, Los Angeles, CA 90024, U.S.A.

Abstract—The behaviour of an aerosol, in which particles are simultaneously growing by collisions and coalescing, is determined by the difference between the local collision and coalescence times. An equation is written for the dimensionless excess surface area of the agglomerates which shows the sharp change in the behaviour of the system when the characteristic times become equal. This sharp change and the growth of primary particles are illustrated by example calculations. The resulting primary particle size depends on the time–temperature history, volume loading and material properties of the system. Increasing initial temperature or volume loading increases primary particle size, while an increase in velocity decreases primary particle size. Copyright © 1996 Elsevier Science Ltd

NOMENCLATURE

a	particle surface area
a_{sph}	surface area of a spherical particle of the same volume
b	grain boundary width
d_0	jet orifice diameter or pipe diameter
d_p	primary particle diameter
k	Boltzmann's constant
n	particle number concentration distribution per unit mass of gas
p	fraction of doublets
r_p	primary particle radius
t	time
u	velocity
u_0	initial velocity
$\hat{u}$	dimensionless velocity
v	particle volume
v^*	intermediate particle volume between v_0 and $\bar{v}$
$\bar{v}$	average particle volume
$\bar{v}_T$	an average particle volume
$\hat{v}$	dimensionless average particle volume
v_0	initial particle volume
v_m	molecular volume
x	spatial coordinate
$\hat{x}$	dimensionless spatial coordinate
A_m	total surface area of particles per unit mass of gas
$A_{m,sph}$	total surface area of spherical particles of the same volume per unit mass of gas
A_v	surface area of particles per unit mass of gas in volume range $[v, v + dv]$
$A_{v,sph}$	surface area of spherical particles of the same volume per unit mass of gas in volume range $[v, v + dv]$
D	solid state diffusion coefficient
$D_{0,gb}$	prefactor in the Arrhenius form of the solid state diffusion coefficient for grain boundary diffusion
$D_{0,v}$	prefactor in the Arrhenius form of the solid state diffusion coefficient for volume diffusion
$E_{act,gb}$	activation energy in the Arrhenius form of the solid state diffusion coefficient for grain boundary diffusion
L	latent heat of fusion
N	average number of primary particles in an agglomerate
N_m	number of particles per unit mass of gas
Pr	Prandtl number
Re	Reynolds number
St	Stanton number
T	temperature

*Present address: VTT Energy, P.O. Box 1401, 02044 VTT, Finland.

T_a temperature at infinity or wall temperature
T_b bulk melting temperature
T_0 initial temperature
T_p particle melting temperature
$\hat{T}$ dimensionless temperature

Greek letters

α constant from self-preserving theory, $\alpha = 6.6$ for spherical particles
Δ_{coll} rate of change of particle surface area concentration in volume range $[v, v + dv]$ resulting from collisions
θ dimensionless excess (compared to spherical particles) surface area
ρ_g density of gas
ρ_l density of liquid particles
ρ_p density of particles
ρ_s density of solid particles
σ surface tension
τ_c characteristic collision time
$\hat{\tau}_c$ dimensionless characteristic collision time
τ_f characteristic coalescence time
$\hat{\tau}_f$ dimensionless characteristic coalescence time
σ_l surface tension of liquid
σ_s surface tension of solid
ϕ_0 initial volume fraction of particles
$\hat{\phi}$ dimensionless volume fraction of particles
ϕ volume fraction of particles
ϕ_m volume of particles per unit mass of gas

1. INTRODUCTION

In the initial stages of particle formation in many industrial aerosol processes, a high concentration of very small particles undergoes rapid coagulation. This may lead to the formation of fractal-like agglomerates consisting of a large number of spheroidal primary particles of approximately uniform diameter (Megaridis and Dobbins, 1990). The size of the primary particles depends on the time–temperature history of the system, dilution rate and material properties. At high temperatures, coalescence occurs almost on contact resulting in agglomerates of large primary particles and hence small surface area. At low temperatures, the collision rate is faster than the rate of coalescence leading to fractal-like agglomerates consisting of very small primary particles and thus large surface area. The ability to predict and control primary particle and agglomerate growth is important in the production of powdered materials, because the properties of materials formed from nanosized particles depend strongly on particle size, polydispersity, morphology, crystal structure and chemical composition (Siegel, 1994). A key to control is the strong dependence of the solid state diffusion coefficient on the temperature. It may also be possible to suppress dendrite formation (necking) by charging, dilution or addition of surface active agents at the proper time.

Ulrich and Subramanian (1977) described simultaneous collision and coalescence (by the viscous flow mechanism) of agglomerates in flames assuming that agglomerates consist of a large number of primary particles and thus treating collision and coalescence separately. Koch and Friedlander (1990) realized that coalescence depends also on the overall size of the agglomerates and assumed that the coalescence rate of an agglomerate is directly proportional to its excess surface area (actual surface area − equivalent spherical area). Friedlander and Wu (1994) later showed that this assumption is exact for the final stages of decay to sphericity by solid state diffusion of an originally (slightly) non-spherical particle. Xiong and Pratsinis (1993) included a similar coalescence term in the aerosol general dynamic equation (GDE) and solved two-dimensionally for both the agglomerate volume distribution and surface area distribution. If the main goal is to predict average primary particle size, a much simpler approach is applicable. Koch and Friedlander (1991) derived a model for particle dynamics at a constant cooling rate, assuming a self-preserving distribution of free-molecular agglomerates (Friedlander, 1977) and a monodisperse primary particle size distribution. This permitted an analytical solution to the average agglomerate volume and a simple differential equation for primary particle size. Later, Wu

et al. (1993) applied this simple model to simulate formation of alumina particles in a turbulent free jet, and Kruis *et al.* (1993) and Fotou *et al.* (1994) assuming a monodisperse agglomerate distribution, the primary particle size of dendritic silica particles in aerosol reactors.

It may be desirable to minimize dendrite formation, for example, if the particles form undesirable "hard" aggregates, that is strong particle bonds. In this case a criterion for dendrite formation would be useful. Also, the transition from spherical particles to dendrites causes a dramatic change in the optical properties. In the region of fast coalescence, the particles remain spherical and the light scattering intensity is proportional to the average particle volume (Friedlander, 1977). When coalescence rates fall and dendritic structures with a fractal dimension below two have formed, the light scattering intensity is almost unaffected by additional collisions (Colbeck *et al.*, 1989). Light scattering measurements can thus help determine the onset of dendrite formation.

The goal of this paper is to calculate the primary particle size up to the onset of dendrite formation in a new way with enhanced physical significance. From a theoretical point-of-view, the approach simplifies the collision–sintering theory of agglomerate (assumed to have a self-preserving size distribution) and primary particle (monodisperse) growth, using a set of equations that clearly show the effect of characteristic collision and coalescence times on the evolution of the primary particle size, following the approach of Windeler (1994). In addition, the equations are formulated in such a way that they can easily be applied in situations including mixing and dilution. The results of this analysis are then illustrated by sample calculations representing idealizations of commercial TiO_2 reactors (Willcox, 1957; Kruse, 1966), where vaporized $TiCl_4$ is injected into an oxygen stream, resulting in quick mixing and reaction. The TiO_2 particles then grow by collisions and, up to the onset of dendrite formation, coalesce to form spheres. In some applications, there is also significant primary particle growth thereafter. This is however beyond the scope of this paper.

2. THEORY

2.1. *Basic equations for surface area and volume*

Let $n(v, a, t)$ be the particle number concentration per unit mass of gas in a volume range between v and $v + dv$ and an area range between a and $a + da$ at time t. In the absence of condensation, and dilution by mixing, the general dynamic equation for the continuous size distribution function becomes (Koch and Friedlander, 1990)

$$\frac{\partial n}{\partial t} + \frac{\partial}{\partial a}\left(n\frac{\partial a}{\partial t}\right) = \frac{1}{2}\int_0^v \theta\left[a > a_{\mathrm{sph}}(v') + a_{\mathrm{sph}}(v' - v)\right]\int_0^a \beta(v', v - v', a', a - a') \times n(v - v', a - a')\,da'\,dv' - n(v, a)\int_0^\infty\int_0^\infty \beta(v, v', a, a')n(v', a')\,da'\,dv'. \quad (1)$$

The collision frequency function β is assumed to be a function of particle volume and area only. The second term of equation (1) represents the motion in area space due to coalescence. The right-hand side is the change due to collision. The step function is required because the surface area of a particle produced by collision is greater than the sum of the minimum surface areas $a_{\mathrm{sph}}(v)$ of the two original particles. The diffusion terms which should appear in a formulation where dilution is important are not included. This is however accounted for in the analysis that follows. Multiplying equation (1) by a and integrating with respect to a, the following equation is obtained:

$$\frac{dA_v}{dt} - \int_a n(v, a', t)\frac{da'}{dt}\,da' = \Delta_{\mathrm{coll}}, \quad (2)$$

where A_v is the surface area per unit mass of gas contained within the volume range v to $v + dv$. The second term of equation (2) represents the rate of change of the surface area in

the volume range v to $v + \mathrm{d}v$ resulting from coalescence and Δ_{coll} is the net rate of change in surface area in the volume range $\mathrm{d}v$ resulting from collisions.

For the coalescence rate $\mathrm{d}a/\mathrm{d}t$, the following linear relationship (Koch and Friedlander, 1990) is assumed to hold:

$$\frac{\mathrm{d}a}{\mathrm{d}t} = -\frac{1}{\tau_{\mathrm{f}}}(a - a_{\mathrm{sph}}), \tag{3}$$

where the coefficient τ_{f} is the characteristic coalescence time, a the surface area of a particle of volume v, and a_{sph} the surface area of a spherical particle of the same volume. The value of τ_{f} has been derived by Friedlander and Wu (1994) for the case of solid state diffusion based on a solution to the diffusion equation inside the particle, with a boundary condition relating the curvature and difference in pressure across the surface:

$$\tau_{\mathrm{f}} = \frac{3kTv}{64\pi D\sigma v_{\mathrm{m}}}, \tag{4}$$

where T is the absolute temperature, v the particle volume, D the solid state diffusion coefficient, σ the surface and v_{m} the molecular volume. Solid state diffusion is a thermally activated process and its temperature dependence can be represented by an Arrhenius form (Kingery *et al.*, 1976):

$$D(T) = \begin{cases} D_{0,v}\exp\left(-\dfrac{E_{\mathrm{act},v}}{kT}\right), & \text{for volume diffusion,} \\ D_{0,\mathrm{gb}}\dfrac{b}{d_{\mathrm{p}}}\exp\left(-\dfrac{E_{\mathrm{act,gb}}}{kT}\right), & \text{grain boundary diffusion.} \end{cases} \tag{5}$$

Here b is the grain boundary width and d_{p} the particle diameter. Substituting equation (3) into equation (2) gives

$$\frac{\mathrm{d}A_v}{\mathrm{d}t} + \frac{A_v - A_{v,\mathrm{sph}}}{\tau_{\mathrm{f}}} = \Delta_{\mathrm{coll}}, \tag{6}$$

where $A_{v,\mathrm{sph}}$ is the minimum possible surface area in the size range v to $v + \mathrm{d}v$ corresponding to a spherical form in each volume range. By integrating with respect to v, the collision term vanishes because there is no net change in surface area by collision processes (but only by coalescence):

$$\frac{\mathrm{d}A_m}{\mathrm{d}t} = -\frac{1}{\tau_{\mathrm{f}}(\bar{v}_T)}(A_{\mathrm{m}} - A_{\mathrm{sph}}), \tag{7}$$

where $A_{\mathrm{m}} = \int_0^\infty A_v\,\mathrm{d}v$ is the total surface area per unit mass of gas, $\bar{v}_T$ is an average particle volume defined by the relation

$$\int_0^\infty \frac{A_v}{\tau_{\mathrm{f}}(v)}\,\mathrm{d}v = \frac{1}{\tau_{\mathrm{f}}(\bar{v}_T)}A_{\mathrm{m}} \tag{8}$$

and A_{sph} is defined by

$$A_{\mathrm{sph}} = \tau_{\mathrm{f}}(\bar{v}_T)\int_0^\infty \frac{A_{v,\mathrm{sph}}}{\tau_{\mathrm{f}}(v)}\,\mathrm{d}v. \tag{9}$$

Equation (7) is the basic starting point of the calculation of primary particle size. Furthermore, the average particle volume, defined as

$$\bar{v} = \frac{\phi_{\mathrm{m}}}{N_{\mathrm{m}}} = \frac{\int_0^\infty\int_0^\infty vn(v,a)\,\mathrm{d}v\,\mathrm{d}a}{\int_0^\infty\int_0^\infty n(v,a)\,\mathrm{d}v\,\mathrm{d}a}, \tag{10}$$

will be used as an approximation for $\bar{v}_T$ and the minimum surface area, in which each particle has relaxed to the spherical shape, as an approximation for A_{sph}. (This would be

exact if the aerosol were monodisperse.) Here ϕ_m is the total volume and N_m the total number of the aerosol particles per unit mass of gas.

It is convenient to introduce a new variable, which represents the fractional deviation of the aerosol surface area from the state in which each particle has relaxed to the spherical shape:

$$\theta = \frac{A_m - A_{sph}}{A_{sph}} \tag{11}$$

with which equation (7) becomes

$$\frac{d\theta}{dt} + \left[\frac{1}{\tau_f(\bar{v})} - \frac{1}{\tau_c(\bar{v})}\right]\theta = \frac{1}{\tau_c(\bar{v})}, \tag{12}$$

where τ_c is the characteristic collision time, defined by

$$\frac{1}{\tau_c} = -\frac{1}{A_{sph}}\frac{dA_{sph}}{dt} = \frac{1}{3\bar{v}}\frac{d\bar{v}}{dt}. \tag{13}$$

The term τ_c can be interpreted as a characteristic collision time since it is equal to three times the time needed for a particle to grow to double in size, if the growth rate would remain at a constant value. It is easy to see that equation (13) holds for monodisperse and self-preserving distributions, although it is not generally valid. The value of $\bar{v}$ can be estimated as follows: If the size distribution remains (nearly) self-preserving throughout the time of interest, the rate of decrease in the number of particles per unit mass of gas is given by (Flagan and Friedlander, 1978):

$$\left(\frac{dN_m}{dt}\right)_{coll} = -\frac{1}{2}\alpha\left(\frac{6kT}{\rho_p}\right)^{1/2}\left(\frac{3}{4\pi}\right)^{1/6}\rho_g\phi_m^{1/6}N_m^{11/6}, \tag{14}$$

where ρ_p is the density of the particles, ρ_g the density of the gas and α a constant, which has the value 6.6 for spherical particles (Lai *et al.*, 1972). This expression takes into account charges in N_m because of possible density variations, but not dilution by mixing. A convenient equation for the average particle volume, $\bar{v} = \phi_m/N_m$, which also accounts for dilution, can be obtained in the following way:

$$\begin{aligned}\frac{d\bar{v}}{dt} &= -\frac{\phi_m}{N_m^2}\frac{dN_m}{dt} + \frac{1}{N_m}\frac{d\phi_m}{dt}\\ &= -\frac{\phi_m}{N_m^2}\left[\left(\frac{dN_m}{dt}\right)_{coll} + \left(\frac{dN_m}{dt}\right)_{dil}\right] + \frac{1}{N}\left(\frac{d\phi_m}{dt}\right)_{dil}\\ &= \frac{1}{2}\alpha\left(\frac{6kT}{\rho_p}\right)^{1/2}\left(\frac{3}{4\pi}\right)^{1/6}\rho_g\phi_m\bar{v}^{1/6} - \frac{\phi_m}{N_m}\left[\frac{1}{N_m}\left(\frac{dN_m}{dt}\right)_{dil} - \frac{1}{\phi_m}\left(\frac{d\phi_m}{dt}\right)_{dil}\right].\end{aligned}$$

The last term in the brackets is zero, if it is assumed that dilution is homogeneous (affects all particle sizes in the same way). By introducing the aerosol particle volume fraction $\phi = \rho_g\phi_m$, the following equation is obtained:

$$\frac{d\bar{v}}{dt} = \frac{1}{2}\alpha\left(\frac{6kT}{\rho_p}\right)^{1/2}\left(\frac{3}{4\pi}\right)^{1/6}\phi\bar{v}^{1/6}. \tag{15}$$

Thus dilution does not affect the differential equation for the average particle volume. For initially spherical particles with average size v_0, the following initial conditions for equations (12) and (15) apply:

$$\theta(0) = 0, \tag{16}$$

$$\bar{v}(0) = v_0. \tag{17}$$

2.2. *Nature of the solution, onset of dendrite formation*

Before going into details of the numerical solution of equations (12) and (15), the nature of the solution can be studied qualitatively. To see the effect of the characteristic times more clearly, by using equation (13), a change in variable is made in equation (12) from t to $\bar{v}$:

$$3\bar{v}\frac{\mathrm{d}\theta}{\mathrm{d}v}+\left[\frac{\tau_c(\bar{v})}{\tau_f(\bar{v})}-1\right]\theta=1 \tag{18}$$

with the initial condition

$$\theta(v_0)=0. \tag{19}$$

The solution to equation (18) with initial condition (19) can be expressed formally as

$$\theta(\bar{v})=\frac{\bar{v}-v_0}{3v^*}\exp\left[-\int_{v^*}^{\bar{v}}\frac{1}{3\xi}\left(\frac{\tau_c(\xi)}{\tau_f(\xi)}-1\right)\mathrm{d}\xi\right], \tag{20}$$

where v^* is an intermediate volume between the initial particle volume v_0 and $\bar{v}$ defined by

$$\frac{\bar{v}-v_0}{3v^*}\exp\left[\int_{v_0}^{v^*}\frac{1}{3\xi}\left(\frac{\tau_c(\xi)}{\tau_f(\xi)}-1\right)\mathrm{d}\xi\right]=\int_{v_0}^{\bar{v}}\frac{1}{3\eta}\exp\left[\int_{v_0}^{\eta}\frac{1}{3\xi}\left(\frac{\tau_c(\xi)}{\tau_f(\xi)}-1\right)\mathrm{d}\xi\right]\mathrm{d}\eta. \tag{21}$$

In the beginning, when the temperature is high, the characteristic coalescence time τ_f is shorter than the characteristic collision time τ_c. Then the argument of the exponential in equation (18) is a large negative number and θ will stay close to zero. When the temperature decreases, the solid state diffusion coefficient decreases very rapidly and at some point τ_f becomes greater than τ_c. Thus the exponent in equation (20) turns positive and θ starts to grow more rapidly. This is approximately the point where the primary particle size is determined, and dendritic agglomerate structures start to form. If the intention is to collect or modify particles before they agglomerate, the crossing point of the characteristic times is a good first estimate. The term θ has also, by definition, a close relationship to the structure of the particles. If it is assumed that in the initial stages of growth all particles are either single spheres or doublets consisting of two primary particles, θ and the fraction of doublets p are related as follows:

$$\theta=\frac{2-2^{2/3}}{1/p+2^{2/3}-1}. \tag{22}$$

For example, if 70% of the particles are to be single spheres, particles should be collected at a point where $\theta=\theta(0.3)\approx 0.11$.

For agglomerates consisting of distinct spheres of equal size, there is a simple relationship between the primary particle diameter d_p, θ and average agglomerate volume $\bar{v}$, namely

$$d_p=\left(\frac{6\bar{v}}{\pi}\right)^{1/3}\frac{1}{\theta+1} \tag{23}$$

which comes directly from the definition of θ, equation (11) and $\bar{v}=n\pi d_p^3/6$, where n is the average number of primary particles in an agglomerate. Thus, solving for $\bar{v}$ and θ as functions of time, gives the primary particle diameter d_p.

An important advantage of this formulation is that it is not affected by dilution or diffusion, because they do not cause explicit changes in $\bar{v}$ or θ. That is, new terms are not needed in differential equations (12) and (15). These effects are taken into account through the volume fraction ϕ in equation (15). The distribution of ϕ can usually be estimated through the appropriate equation of conservation of species.

3. RESULTS AND DISCUSSION

3.1. *Range of system variables*

Sample calculations were made for a one-dimensional gas flow with TiO_2 particles and (a) in the absence of dilution having the following velocity, volume loading and temperature profiles:

$$\frac{u}{u_0} = 1, \tag{24}$$

$$\frac{\phi}{\phi_0} = 1, \tag{25}$$

$$\frac{T - T_a}{T_0 - T_a} \approx 1 - 0.092\,\mathrm{Re}^{-0.2}\mathrm{Pr}^{-0.7}\frac{x}{d_0}. \tag{26}$$

and (b) dilution by mixing and the following velocity, volume loading and temperature profiles:

$$\frac{u}{u_0} = \frac{6.85}{x/d_0 + 6.85}, \tag{27}$$

$$\frac{\phi}{\phi_0} = \frac{5}{x/d_0 + 5}, \tag{28}$$

$$\frac{T - T_a}{T_0 - T_a} = \frac{5}{x/d_0 + 5}. \tag{29}$$

Case (a) is an approximation of a steady turbulent gas flow in a pipe (diameter d_0) with initial gas temperature T_0, volume loading ϕ_0, velocity u_0 and constant wall temperature T_a (Welty *et al.*, 1984). Re is the Reynolds number and Pr the Prandtl number. The temperature profile (26) is a linear approximation valid over most of the range of interest. Case (b) is an approximation of the gas flow along the centerline of a steady turbulent round free jet, with initial gas temperature T_0, injected into a cooler gas of temperature T_a (Abramovich, 1963). In equations (27)–(29), the distance x is measured along the centerline from the end of the potential core. These flow regimes were chosen because of their practical importance and because their comparison illustrates the effect of mixing on particle characteristics. From this point onward, Case (a) is referred to as pipe and Case (b) as jet.

The following ranges of the system variables were studied: $d_0 = 1$ cm, $T_0 = 1500$–2500 K, $T_a = 500$–1500 K, $u_0 = 25$–$250\ \mathrm{m\,s^{-1}}$ and $\phi_0 = 10^{-6}$–10^{-4}. The residence time up to the onset of dendrite formation with these parameter values used is roughly 1–10 ms. The temperature and volume loading ranges were extended beyond those of industrial TiO_2 reactors to show the effect of these variables on the particle growth dynamics. The velocities were chosen to cover the Reynolds number range of about 10^3–10^4. The lower end extends to the laminar or transitional region, where the turbulent flow assumption becomes incorrect.

First one set of parameter values, $T_0 = 2000$ K, $T_a = 1000$ K, $u_0 = 100\ \mathrm{m\,s^{-1}}$ and $\phi_0 = 10^{-5}$ (Reynolds number ≈ 3000, Mach number ≈ 0.1) is used, to show in detail, how the characteristic times, θ and primary particle diameter evolve as a function of distance. Later, the effect of each of the process variables on the final primary particle size is studied, by varying them one at a time, in the above mentioned ranges, while keeping the others constant.

For these flows, it is convenient to transform to the spatial coordinate by setting $(\mathrm{d}/\mathrm{d}t) = u(x)(\mathrm{d}/\mathrm{d}x)$ in equations (12) and (15). Here $u(x)$ is the velocity in the pipe or along

the jet axis. In addition, for numerical convenience, equations (12) and (15) are nondimensionalized by introducing dimensionless distance $\hat{x} = x/d_0$, velocity $\hat{u} = u/u_0$, temperature $\hat{T} = T/T_0$, volume loading $\hat{\phi} = \phi/\phi_0$ and average agglomerate volume $\hat{v} = v/v_0$:

$$\frac{d\theta}{d\hat{x}} = -\left[\frac{1}{\hat{\tau}_f} - \frac{1}{\hat{\tau}_c}\right]\theta + \frac{1}{\hat{\tau}_c}, \tag{30}$$

$$\frac{d\hat{v}}{d\hat{x}} = \frac{3\hat{v}}{\hat{\tau}_c}. \tag{31}$$

Here $\hat{\tau}_f$ and $\hat{\tau}_c$ can be interpreted as dimensionless characteristic times:

$$\hat{\tau}_f = \frac{\tau_f u}{d_0}, \tag{32}$$

$$\hat{\tau}_c = \frac{\tau_c u}{d_0}. \tag{33}$$

For the solid state diffusion coefficient of TiO_2, the semiempirical correlation for grain boundary diffusion of Kobata *et al.* (1991) is used (assuming the grain boundary width b remains, in the absence of a more complex theoretical treatment, constant during the collision–coalescence process):

$$bD_{0,gb} = 1.6 \times 10^{-14} \exp\left(\frac{-258{,}000}{RT}\right) \tag{34}$$

(in $m^3 s^{-1}$) which results in the following coalescence time:

$$\tau_f = 7.44 \times 10^{16} T d_p^4 \exp\left[\frac{258{,}000}{RT}\right]. \tag{35}$$

3.2. *Effect of characteristic collision and coalescence times*

Equations (30) and (31) were then solved numerically with the classical fourth-order Runge–Kutta method using the following parameter values: $T_0 = 2000$ K, $T_a = 1000$ K, $u_0 = 100\ m\,s^{-1}$, $\phi_0 = 10^{-5}$, $d_0 = 1$ cm, $\rho = 3840\ kg\,m^{-3}$ and $v_0 = 3.46 \times 10^{-29}\ m^3$ ($d_{p0} = 0.40$ nm). The values for the process parameters were chosen such that the change in θ at the onset of dendrite formation is clearly illustrated. The initial particle size, chosen here to be the size of a molecule, has practically no effect on the results.

Figure 1 shows the dimensionless characteristic coalescence time $\hat{\tau}_f$ and collision time $\hat{\tau}_c$ as a function of dimensionless distance $\hat{x}$ for the pipe and the jet. The collision time $\hat{\tau}_c$ increases rapidly at first because of the high particle concentrations. At about $\hat{x} = 10$, the curve starts to flatten. The Arrhenius form of the diffusion coefficient causes the rapid increase in coalescence time $\hat{\tau}_f$ when x increases and temperature T decreases. The location of intersection is about $\hat{x} = 3.1$ for the jet and $\hat{x} = 11$ for the pipe. Figure 2 shows θ as a function of dimensionless average agglomerate volume $\hat{v}$. The locations of intersection of $\hat{\tau}_f$ and $\hat{\tau}_c$ are indicated arrows. At first, when $\hat{\tau}_f$ is much less than $\hat{\tau}_c$, the value of θ is close to zero. However, near $\hat{x} = 3.1$ for the jet and $\hat{x} = 11$ for the pipe flow, where $\hat{\tau}_f = \hat{\tau}_c$, there occurs a sharp increase in θ as expected. In Fig. 3, which shows the primary particle size as a function of $\hat{x}$, the change in the solution, where $\hat{\tau}_f = \hat{\tau}_c$, is even more evident. The primary particle diameter increases rapidly in the high temperature region, where $\hat{\tau}_f < \hat{\tau}_c$. When the temperature decreases, the primary particle size d_p approaches a constant value of about 26 nm for the pipe and 16 nm for the jet. The points of intersection of the characteristic times ($\hat{\tau}_f = \hat{\tau}_c$) are good indicators of the start of the region in which d_p approaches a constant value. The smaller particle size in the case of the jet results from the dilution compared with the plug-flow. Figure 4, which shows the fraction of doublets as a function of distance, can be used to select a location for particle collection.

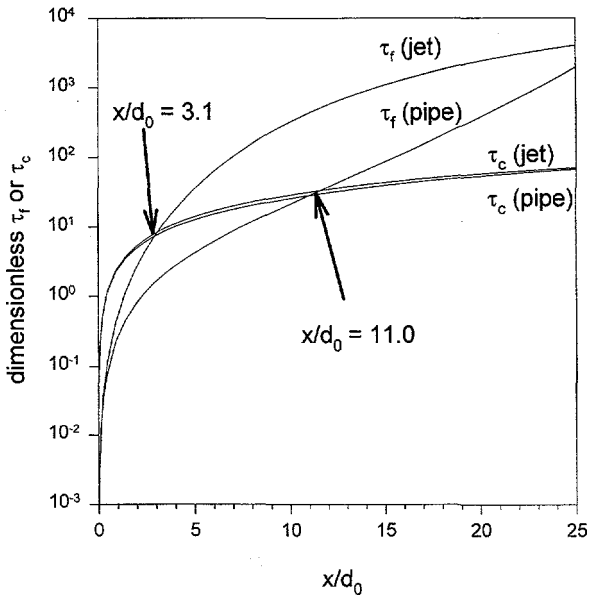

Fig. 1. Dimensionless coalescence time τ_f and collision time τ_c as a function of dimensionless axial distance x/d_0 for jet and pipe for the following conditions: $d_0 = 1$ cm, $T_0 = 2000$ K, $T_a = 1000$ K, $u_0 = 100\,\mathrm{m\,s^{-1}}$ and $\phi_0 = 10^{-5}$. The points where τ_f and τ_c are equal, $x = 3.1d_0$ for the jet and $x = 11d_0$ for the pipe, are indicated with arrows.

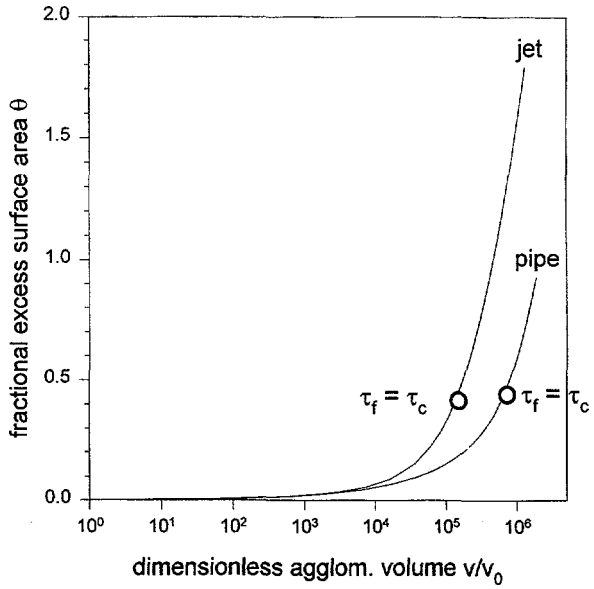

Fig. 2. The fractional excess surface area θ as a function of dimensionless average agglomerate volume v/v_0 with the following conditions: $d_0 = 1$ cm, $T_0 = 2000$ K, $T_a = 1000$ K, $u_0 = 100\,\mathrm{m\,s^{-1}}$ and $\phi_0 = 10^{-5}$. The points where the characteristic times τ_f and τ_c are equal, $x = 3.1d_0$ for the jet and $x = 11d_0$ for the pipe, are indicated with circles.

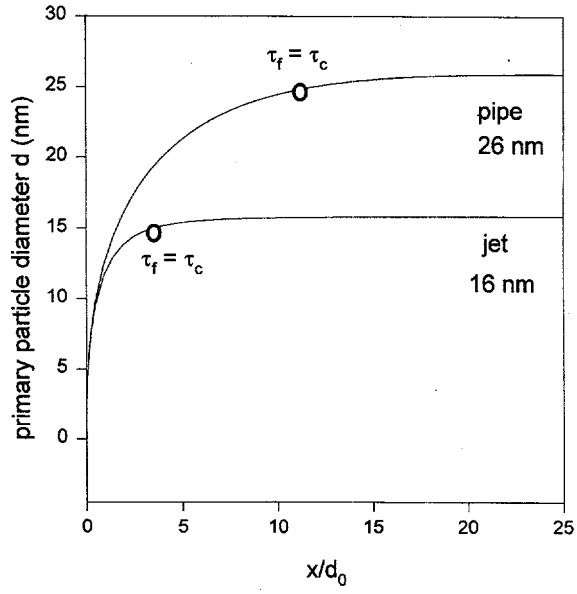

Fig. 3. Primary particle diameter d as a function of dimensionless axial distance x/d_0 with initial conditions: $d_0 = 1$ cm, $T_0 = 2000$ K, $T_a = 1000$ K, $u_0 = 100\,\mathrm{m\,s^{-1}}$ and $\phi_0 = 10^{-5}$. The points where the characteristic times τ_f and τ_c are equal, $x = 3.1d_0$ for the jet and $x = 11d_0$ for the pipe, are indicated with circles. The final primary particle size for the jet is 16 nm and for the pipe 26 nm.

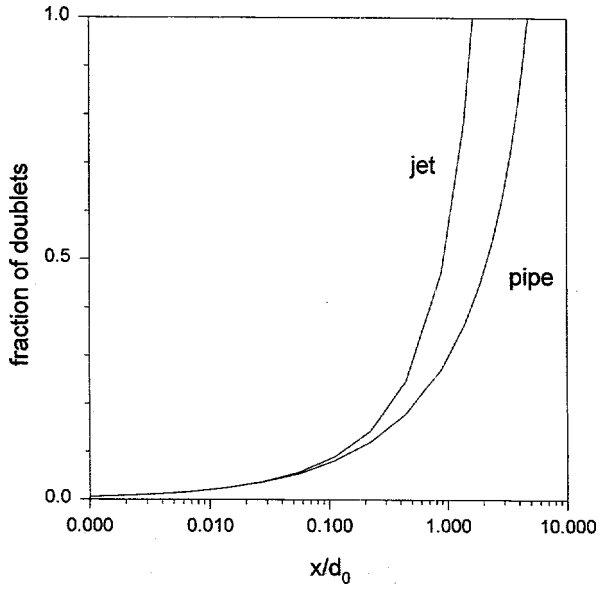

Fig. 4. Fraction of doublets as a function of distance during the initial stages of particle formation with the following conditions: $d_0 = 1$ cm, $T_0 = 2000$ K, $T_a = 1000$ K, $u_0 = 100\,\mathrm{m\,s^{-1}}$ and $\phi_0 = 10^{-5}$. It is assumed that all particles are either single spheres or doublets consisting of two primary particles.

3.3. *Effect of process conditions*

A numerical parametric study was made of the effect of the process parameters (initial velocity u_0, initial volume fraction of material ϕ_0, initial temperature T_0, and wall temperature (for the pipe)/temperature at infinity (for the jet) T_a on primary particle size. The numerical results are shown in Fig. 5a–d. Decreasing velocity or increasing volume loading or temperature increase the primary particle size for both pipe and jet flows.

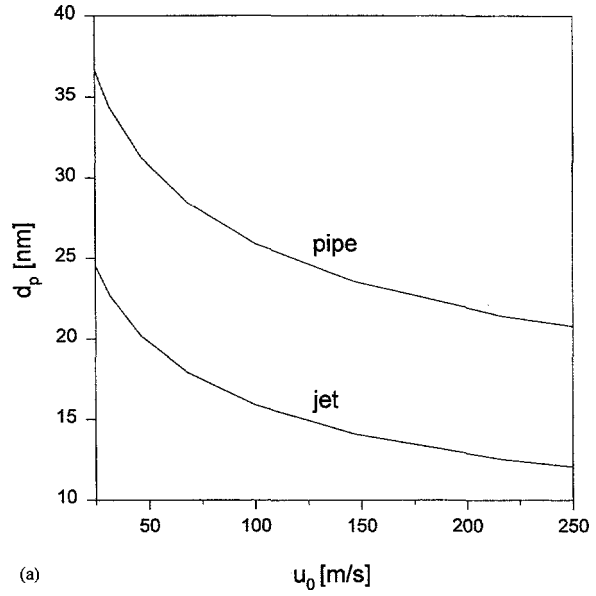

(a)

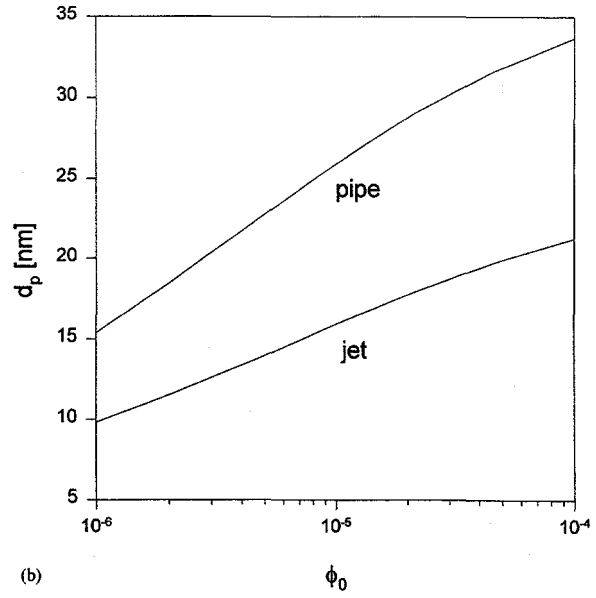

(b)

Fig. 5(a) and (b)—*caption overleaf.*

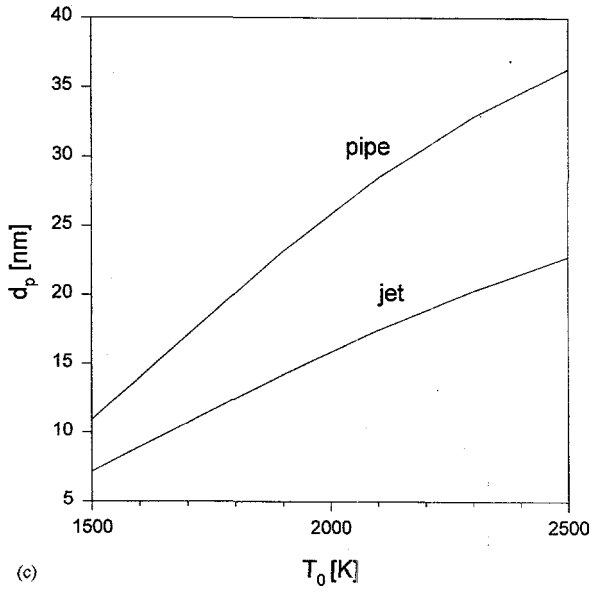

(c)

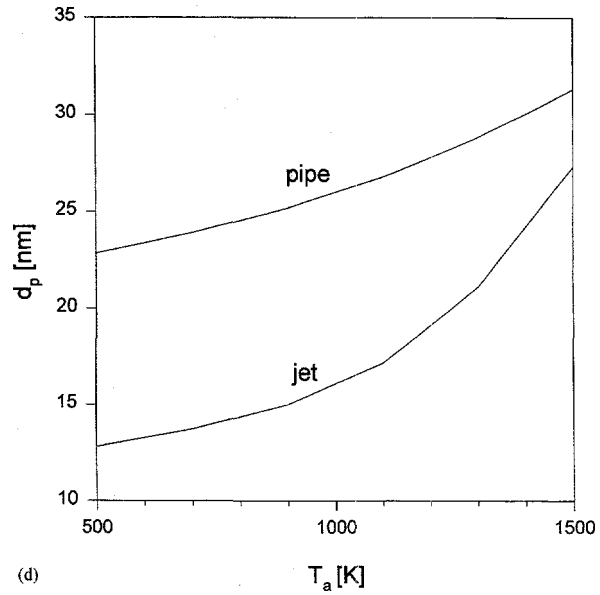

(d)

Fig. 5. Final primary particle diameter as a function of (a) initial velocity u_0, (*b*) initial volume loading ϕ_0, (c) initial temperature T_0, (d) wall (for the pipe) or ambient (for the jet) temperature T_a. The process parameters are varied one at a time around the following set of values: $T_0 = 2000$ K, $T_a = 1000$ K, $u_0 = 100\ \mathrm{m\,s^{-1}}$ and $\phi_0 = 10^{-5}$.

Increasing the volume fraction increases the coagulation rate and thus also primary particle size. For TiO_2-particles of diameter 10–30 nm, there is significant solid state diffusion in temperatures above about 1600 K. The length of this region can be varied by changing the initial temperature T_0 or wall temperature (pipe)/temperature at infinity (jet) T_a. Increasing

either temperature results in an increase of the length of the high temperature region and thus a larger primary particle size. Decreasing the velocity results in a longer residence time and thus larger particles. The results of these parametric studies are in qualitative agreement with the experimental results of Akhtar *et al.* (1991), who studied the effect of temperature, volume loading and residence time on TiO_2 particle size in an aerosol reactor experimentally.

In industrial processes, much of the primary particle growth may occur after the onset of dendrite formation, within the agglomerates (Willcox, 1957). This takes place at high volume loadings and longer residence times. The analysis in this paper covers the initial stages of these systems, up to the point where dendrites start to form. The behaviour of a system following dendrite formation is beyond the scope of this analysis.

3.4. *Variation of the melting temperature*

Very small particles melt at temperatures less than the bulk melting point. The melting point for spherical TiO_2 particles was calculated (Fig. 6) using data from Samsonov (1982) and the following equation (Peppiatt and Sambles, 1975):

$$T_b - T_p = \frac{4T_b}{L\rho_s d_p}\left(\sigma_s - \left(\frac{\rho_s}{\rho_l}\right)^{2/3}\sigma_l\right), \tag{36}$$

where T_p is the melting temperature of a particle of diameter d_p, T_b the bulk melting temperature, L the latent heat of fusion, ρ_s and ρ_l the solid and liquid densities and σ_s and σ_l the solid and liquid surface energies, respectively. The reduction in melting temperature affects the theoretical analysis during the earliest stages of particle formation but is less important for particles larger than about 5 nm. The melting point reduction means that in the earliest stages, the characteristic coalescence time has been overestimated in these calculations. This however has little effect on the results, since at these early stages even solid state diffusion is fast enough for complete coalescence of two particles before further collisions.

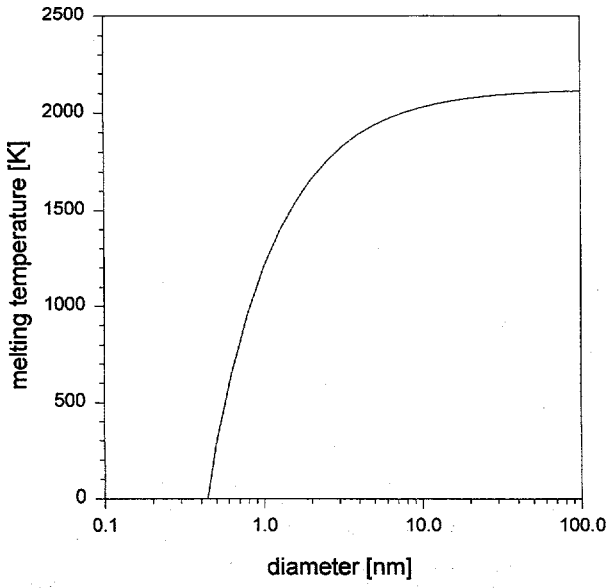

Fig. 6. Reduction of TiO_2 melting temperature as a function of particle diameter.

4. SUMMARY AND CONCLUSIONS

Primary particle growth of a system, where particles are growing as a result of collisions and coalesce is determined by the difference of the collision and coalescence frequencies. When the temperature is high enough, this difference is negative and agglomerates coalesce to form spheres before recolliding. In a cooling system, as the difference turns positive, collisions occur before complete fusion and thus dendritic structures begin to form. This behaviour is clearly demonstrated in our sample calculations. The point where the characteristic frequencies are equal represents a dramatic change in the particle dynamics—this is about where the dendritic structures start to form and the primary particle size stops growing.

The resulting primary particle size can be controlled by changing the process parameters: time–temperature history, initial volume loading and velocity. An increase in temperature or volume loading increases primary particle size, an increase in velocity decreases primary particle size. To double the primary particle diameter requires, roughly, a two order of magnitude increase in initial volume loading or one order of magnitude decrease in initial velocity. The sensitivity on temperature is not as simple, but stronger because of the Arrhenius-form temperature dependence of the solid state diffusion coefficient.

Acknowledgements—We wish to thank the VTT Exchange Program, IVO Research Foundation, Leo and Regina Wainstein Foundation and U.S. National Science Foundation, Grant CTS-9218222 for support of this research.

REFERENCES

Abramovich, G. N. (1963) *The Theory of Turbulent Jets*. M.I.T. Press, Boston.
Akhtar, M. K., Xiong, Y. and Pratsinis, S. E. (1991) Vapor synthesis of titania powder by titanium tetrachloride oxidation. *A.I.Ch.E. J.* **37,** 1561–1570.
Colbeck, I., Hardman, E. J. and Harrison, R. M. (1989) Optical and dynamical properties of fractal clusters of carbonaceous smoke. *J. Aerosol Sci.* **7,** 765–774.
Flagan, R. C. and Friedlander, S. K. (1978) Particle formation in pulverized coal combustion—A review. In *Recent Developments in Aerosol Science* (Edited by Shaw, D. T.), pp. 25–59. Wiley, New York.
Fotou, G. P., Pratsinis, S. E. and Baron, P. A. (1994) Coating of silica fibers by ultrafine particles in a flame reactor. *Chem. Eng. Sci.* **49,** 1651–1662.
Friedlander, S. K. (1977) *Smoke, Dust and Haze*. Wiley, New York.
Friedlander, S. K. and Wu, M. K. (1994) Linear rate law for the decay of the excess surface area of a coalescing solid particle. *Phys. Rev. B* **49,** 3622–3624.
Kingery, W. D., Bowen, H. K. and Uhlmann, D. R. (1976) *Introduction in Ceramics*. Wiley, New York.
Kobata, A., Kusakabe, K. and Shigeharu, M. (1991) Growth and transformation of TiO_2 crystallites in aerosol reactor. *A.I.Ch.E. J.* **37,** 347–359.
Koch, W. and Friedlander, S. K. (1990) The effect of particle coalescence on the surface area of a coagulating aerosol. *J. Colloid Inter. Sci.* **140,** 419–427.
Koch, W. and Friedlander, S. K. (1991) Particle growth by coalescence and agglomeration. *Part Part. Syst. Charact.* **8,** 86–89.
Kruis, F. E., Kusters, K. A., Pratsinis, S. E. and Scarlett, B. (1993) A simple model for the evolution of the characteristics of aggregate particles undergoing coagulation and sintering. *Aerosol Sci. Technol.* **19,** 514–526.
Kruse, W. E. (1996) Titanium dioxide from titanium tetrachloride and oxygen. U.S. Patent 3284159.
Lai, F. S., Friedlander, S. K., Pich, J. and Hidy, G. M. (1972) The self-preserving particle size distribution for Brownian coagulation in the free-molecular regime. *J. Colloid. Inter. Sci.* **39,** 395–405.
Megaridis, C. M. and Dobbins, R. A. (1990) Morphological description of flame-generated materials. *Combust. Sci. Technol.* **71,** 95–109.
Peppiatt, S. J. and Sambles, J. R. (1975) The melting of small particles. *Proc. R. Soc. Lond. A* **345,** 387–349.
Samsonov, G. V. (1982) *The Oxide Handbook*. IFI/Plenum, New York.
Siegel, R. W. (1994) *Nanophase Materials: Synthesis, Structure and Properties*. Springer Series in Material Sciences, Vol. 27 (Edited by Fujita, F. E.), pp. 65–105. Springer, Berlin.
Ulrich, G. D. and Subramanian, N. S. (1977) Particle growth in flames 3: Coalescence as a rate-controlling process. *Combustion Sci. Technol.* **17,** 119–126.
Welty, J. R., Wicks, C. E. and Wilson, R. E. (1984) *Fundamentals of Momentum, Heat and Mass Transfer*. Wiley, New York.
Willcox, O. B. (1957) Method and means for commingling and reacting fluid substances. U.S. Patent 2791490.
Windeler, R. (1994) Production of nanometer sized metal oxide particles in a coflow nonisothermal free jet. Ph.D. Prospectus, UCLA Department of Chemical Engineering.
Wu, M. K., Windeler, R. S., Steiner, C. K. R., Bors, T. and Friedlander, S. K. (1993) Controlled synthesis of nanosized particles by aerosol processes. *Aerosol Sci. Technol.* **19,** 527–548.
Xiong, Y. and Pratsinis, S. E. (1993) Formation of irregular particles by coagulation and sintering. *J. Aerosol Sci.* **24,** 283–300.

Reprinted with permission from the publisher.
In: Journal of Colloid and Interface Science 1996. Vol. 182, pp. 606 - 608.

PAPER E

NOTE

A Note on the Growth of Primary Particles in Agglomerate Structures by Coalescence

Aerosol particles at high concentrations grow by collisions and coalescence. If coalescence is faster, particles remain individual and spherical, and primary particle growth is determined by the collision rate. When collisions are faster, dendritic agglomerates consisting of a large number of primary particles form. Primary particle growth is then determined by the coalescence rate. In this Note a model is given for predicting primary particle growth based on the linear decay law for the surface area of a coalescing structure. In the collision-limited primary particle growth regime, the linear decay law is applied to the coalescing pairs of particles. In the coalescence-limited regime large agglomerates are present, and the linear decay law is applied to subregions of the agglomerates.

Key Words: coalescence; agglomeration; primary particle.

1. INTRODUCTION

Aerosol particles are often irregular clusters of fine spheroidal primary particles of approximately uniform diameter. The behavior of these clusters, usually called agglomerates, can differ significantly from spheres of the same mass. Aerosol agglomerates can be characterized by a power law exponent, which can be related to a fractal dimension. Agglomerates with low fractal dimension have larger collision cross sections but lower mobilities than agglomerates of the same volume but higher fractal dimension, thus affecting basically all dynamical properties of the aerosol (1, 2).

The ability to predict and control primary particle and agglomerate growth is important in the production of powdered materials, because the properties of materials formed from nanosized particles depend strongly on particle size, polydispersity, morphology, crystal structure, and chemical composition (3). The size of the particles is mainly determined by the rates of collision and coalescence (4). When temperatures are high, coalescence occurs almost on contact, resulting in agglomerates of large spherical particles. At low temperatures, when collision is faster than coalescence, fractal-like structures consisting of small primary particles and thus very large surface area are formed. Most of the recent models for describing simultaneous collision and coalescence are based on the linear decay law assumption of Koch and Friedlander (5) for the surface area of coalescing particles. This assumption is exact for the final stages of coalescence by viscous flow (6) and solid state diffusion (7). The analysis is however strictly applicable only to cooling systems, in which particle growth occurs through collisions and quick coalescence (collision limited growth) up to the onset of dendrite formation, where the primary particle size is determined (8).

In some practical applications much of the primary particle growth may occur within large agglomerates. An example is the free jet metal oxide particle generator (4), in which a jet of N_2/aerosol precursor vapor is introduced into the center of a coflow laminar flame jet, surrounded by ambient air. The precursor reacts quickly with oxygen forming a high concentration of very small metal oxide particles. The metal oxide stream is first heated by the flame, while further down the jet axis it is cooled by the entrained ambient air. In the region where particles first form, collisions are frequent because of the high particle concentration. Since the gases are still relatively cool, dendritic structures form. At higher temperatures further down the jet axis, the primary particles in the agglomerates coalesce (coalescence limited growth), until ambient air cooling freezes the primary particle size. In this paper, a model for predicting agglomerate and primary particle size is derived, applicable to both collision and coalescence limited growth regimes. In a forthcoming paper, this model will be applied to the free jet system.

Ulrich and Subramanian (9) described coalescence limited growth of particles in large agglomerates by defining a coalescence time (by the viscous flow mechanism) in which a predefined number of primary particles (chosen to be the average number of neighbors plus one) coalesce completely. This model has been applied recently to predict sintering in silver agglomerates in a heated flow (10).

For a system in which there are both collision and coalescence limited growth regions, earlier approaches, which are limited to either regime only, are not satisfactory. In this paper, we present a model which combines elements of (2), (5), and (9). Agglomerate size is predicted by using the self-preserving theory for fractal-like structures (2). In the collision limited growth region, the approach of Koch and Friedlander (5) is used to predict primary particle size. When the average number of primary particles is above a predefined limit, a method similar to Ulrich and Subramanian (9) is utilized. The linear decay law for the surface area (5) is used to describe coalescence in smaller domains of the agglomerate instead of the complete coalescence assumption within one characteristic coalescence time of (9). This way a model is obtained, which basically matches the collision–coalescence theory of Koch and Friedlander (5) to the large agglomerate coalescence model of Ulrich and Subramanian (9) at a predefined average number of primary particles per agglomerate. The effect of choice of this number to the growth rate of primary particles is also investigated.

2. THEORY

A uniform system with properties changing in time or a one-dimensional steady flow is assumed. An example of the former is the "batch" reactor, and of the latter a plug flow or the centerline of a jet. The mechanisms affecting agglomerate dynamics are assumed to be Brownian agglomeration, coalescence (or fusion), and dilution. Dilution may result from turbulent mixing, for example. The purpose of this Note is to develop a method for estimating the average agglomerate volume v_a and average primary particle volume v_p of the aerosol particles:

$$\frac{dv_a}{dt} = \left(\frac{dv_a}{dt}\right)_{agg} + \cancel{\left(\frac{dv_a}{dt}\right)_{coal}}^{\,0} + \cancel{\left(\frac{dv_a}{dt}\right)_{dil}}^{\,0} \qquad [1]$$

$$\frac{dv_p}{dt} = \cancel{\left(\frac{dv_p}{dt}\right)_{agg}}^{\,0} + \left(\frac{dv_p}{dt}\right)_{coal} + \cancel{\left(\frac{dv_p}{dt}\right)_{dil}}^{\,0} \qquad [2]$$

Cluster/cluster collisions bring separate agglomerates together, increasing v_a without affecting v_p. Coalescence refers to the transport of molecules within the agglomerates, increasing v_p but not causing any change in v_a. Dilution only changes the positions of the agglomerates in the gas and thus does not appear in equations for the average size variables. To determine

0021-9797/96 $18.00

the growth rate for v_a, only the effect of agglomeration needs to be evaluated. The growth rate for v_p is calculated from the coalescence rate.

To simplify the calculations, it is further assumed that at time t the agglomerate size distribution is (nearly) self-preserving (free-molecular regime), with average volume v_a, and that each agglomerate consists of spherical primary particles of volume v_p.

Growth of Agglomerates by Collisions

Fractal-like structures with a low fractal dimension grow much more rapidly than spherical particles of the same volume in the free molecular regime (2, 11–13). Both experiments and cluster–cluster agglomeration simulations (14) have shown that Brownian movement dominated agglomeration processes tend to produce agglomerates with fairly low fractal dimension ($1.6 < D_f < 2.2$). It is necessary to take the enhanced growth rate into account in describing the aerosol dynamics of such systems. Assuming a constant fractal dimension D_f throughout the growth process leads to the following differential equation for v_a (2):

$$\frac{dv_a}{dt} = \frac{1}{2}\alpha\sqrt{\frac{6kT}{\rho}}\left(\frac{3}{4\pi}\right)^{2/D_f-1/2} r_p^{2-6/D_f}\phi \cdot v_a^{2/D_f-1/2}$$

$$= \frac{1}{2}\alpha\sqrt{\frac{6kT}{\rho}}\left(\frac{3v_a}{4\pi}\right)^{1/6}\phi n^{2/D_f-2/3}. \quad [3]$$

Here k is Boltzmann's constant, T temperature, ρ density of particulate matter, r_p radius of primary particle, ϕ volume fraction of particulate matter (volume of particles/volume of gas), n average number of primary particles in an agglomerate, and α a constant, which depends on D_f approximately by the equation

$$\alpha = \int_0^\infty \int_0^\infty (\eta_1^{-1} + \eta_2^{-1})^{1/2}(\eta_1^{1/D_F} + \eta_2^{1/D_F})^2\psi(\eta_1)\psi(\eta_2)d\eta_1 d\eta_2$$

$$\approx 6.548 + 112.1 \cdot D_f^{-7.883}. \quad [4]$$

Equation [4] was obtained by solving the self-preserving distribution $\psi(\eta)$ numerically for different values of D_f, and then integrating and curve-fitting. It gives values for α within 0.4% compared with the results by Wu and Friedlander (13) and within 1.7% compared with α values obtained by using the self-preserving distributions calculated by Vemury and Pratsinis (12).

The enhanced agglomeration rate compared with an aerosol consisting of spherical particles is evident from Eq. [3]: For example, if $D_f = 2$ and $n = 100$, the growth rate of v_a is about 5 times higher than for $n = 1$.

The assumption that the fractal dimension D_f stays constant during coalescence is reasonable, if the primary particles are not able to rearrange within the agglomerate into a more dense packing. Of course, the assumption breaks down as $n \to 1$. The correct behavior in the limit $n \to 1$ is, however, accounted for in Eq. [3], since it reduces to the $D_f = 3$ case, when $n = 1$.

Growth of Primary Particles by Coalescence

To determine the growth rate of the average primary particle volume v_p, consider one such agglomerate with n spherical primary particles of diameter v_p. Friedlander and Wu (7) derived an equation for the final stages of coalescence by solid state diffusion of a slightly nonspherical particle:

$$\frac{da}{dt} = -\frac{1}{\tau_f}(a - a_s). \quad [5]$$

Here a is the surface area of the particle, a_s the surface area of a spherical particle of same volume (the surface area of the particle after complete coalescence), and τ_f the characteristic coalescence time:

$$\tau_f = \frac{3kTv}{64\pi D\sigma v_0}. \quad [6]$$

Here σ is the surface tension (assumed constant), v_0 is the molecular volume for diffusion, and D is the solid state diffusion coefficient.

The fusion law [5], which is derived for nearly spherical objects, presumably does not work well for dendritic structures. Therefore, it is assumed that the coalescence law holds for groups of m primary particles, not the whole agglomerate. A similar assumption was made by Ulrich and Subramanian (9) for viscous flow coalescence. They assumed that τ_f is the time needed for a group of m particles to coalesce completely, where $m - 1$ is the average coordination number of a primary particle. In the analysis which follows, m is left undetermined; the effect of the value selected is studied later.

For an agglomerate of n primary particles, there are n/m groups of m particles. The coalescence law holds for each of the n/m groups, so, instead of Eq. [5], the following equation for the total area a of the agglomerate is assumed:

$$\frac{da}{dt} = \frac{n}{m}\left[-\frac{1}{\tau_{fm}}(a_m - a_{sm})\right]. \quad [7]$$

Here a_m is the surface area of the group of m primary particles and a_{sm} is the surface area of a sphere of equal volume. The characteristic coalescence time τ_{fm} for a group of m primary particles is

$$\tau_{fm} = \frac{3kTmv_p}{64\pi D\sigma v_0}. \quad [8]$$

Changing variables in Eq. [7] to primary particle volume v_p,

$$a_m = m(36\pi)^{1/3}v_p^{2/3}, \quad [9]$$

$$a_{sm} = (36\pi)^{1/3}(mv_p)^{2/3} \quad [10]$$

$$a = n(36\pi)^{1/3}v_p^{2/3} = v_a(36\pi)^{1/3}v_p^{-1/3}, \quad [11]$$

gives the following differential equation for v_p:

$$\frac{dv_p}{dt} = \frac{3v_p}{\tau_{fm}}(1 - m^{-1/3}). \quad [12]$$

In analyzing coalescence for groups of m particles, it is necessary that $n > m$. If $n < m$, Eq. [5] can be used for the whole agglomerate, resulting in Eq. [12] with m replaced by n. Therefore for regions in which $n < m$, the model is equivalent to the theory of Koch and Friedlander (5).

Summarizing and including Eq. [8] for the characteristic coalescence time, two ordinary differential equations must be solved simultaneously, the first for the growth of the agglomerates and the second for the coalescence within the agglomerates:

$$\frac{dv_a}{dt} = \frac{1}{2}\alpha\sqrt{\frac{6kT}{\rho}}\left(\frac{3v_a}{4\pi}\right)^{1/6}\phi n^{2/D_f-2/3} \quad [13]$$

$$\frac{dv_p}{dt} = \begin{cases} \dfrac{64\pi D\sigma v_0}{kT}(m^{-1} - m^{-4/3}) & n = \dfrac{v_a}{v_p} > m \\ \dfrac{64\pi D\sigma v_0}{kT}(n^{-1} - n^{-4/3}) & n = \dfrac{v_a}{v_p} \leqslant m. \end{cases} \quad [14]$$

Equations [13] and [14] are coupled through $n = v_p/v_a$, the value of which also determines which right-hand side is used Eq. [14]. To solve these equations, the following information is needed:

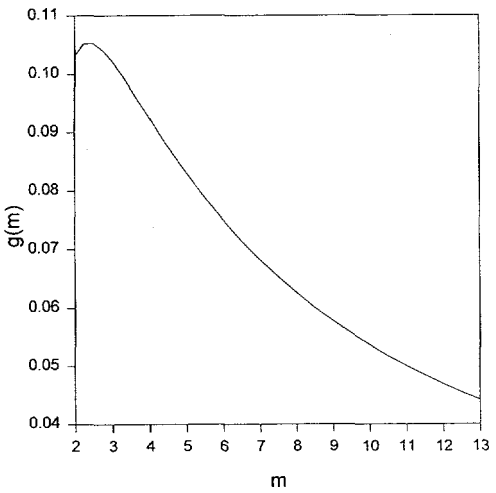

FIG. 1. Effect of the choice of m on the primary particle growth rate [14].

- the initial values for average agglomerate volume $v_a(0)$ and primary particle volume $v_p(0)$;
- system parameters: temperature $T(t)$ and volume fraction of particles as a function of time $\phi(t)$;
- material properties: density ρ, surface tension σ, solid state diffusion coefficient as a function of temperature $D(T)$, and molecular volume for diffusion v_m;
- fractal dimension of agglomerates D_f.

3. DISCUSSION

One remarkable aspect of Eqs. [13] and [14] is that in an isothermal system (constant solid state diffusion coefficient), where most of the primary particle growth happens within agglomerates (n large), the growth rate of the average primary particle volume is constant. Dilution does not affect the derivation of Eqs. [13] and [14]. Dilution will affect the dynamics of both v_a and v_p, through the volume fraction term ϕ in Eq. [13], but it does not affect the form of the equations.

The effect of the choice of m, which appears in Eq. [14] in the function

$$g(m) = m^{-1} - m^{-4/3}, \qquad [15]$$

is shown in Fig. 1. A larger value for m means that more particles are fused together in a group and the deviation from spherical shape is larger. This would result in an increased rate of primary particle growth. On the other hand, the characteristic coalescence time τ_f increases as the volume of the group of particles increases. This effect decreases the growth rate as m increases. In the region $m > 64/27$ (beyond the maximum in Fig. 1), the latter effect dominates and the primary particle growth rate decreases with increasing m. The value $m = 2$ corresponds to the case of pairwise coalescence of primary particles and 13 to the maximum possible coordination number (12) for spherical particles. Choosing $m = 2$ gives roughly a two times greater growth rate for the primary particle volume, or 1.3 times greater growth rate for the diameter, than choosing $m = 13$. In a typical dendritic aerosol agglomerate formed by Brownian agglomeration, the primary particles usually have 2 or 3 neighbors. Thus, following the approach of Ulrich and Subramanian (9) for choosing m, a choice of $m = 3$ or $m = 4$ seems reasonable.

Choosing a value for m is equivalent to setting a limit of applicability for the use of Eq. [5] (which is exact only for slightly nonspherical particles) to describe the coalescence of agglomerates. Koch and Friedlander (5) pointed out that Eq. [5] is a reasonable approximation for describing the whole coalescence process of (initially) two distinct spheres. When the number of primary particles n in an agglomerate increases, Eq. [5] becomes more inaccurate. Also, using Eq. [5] for coalescence of large agglomerates results in a dependence of the primary particle growth rate on the agglomerate size which is unlikely on physical grounds.

The model given in this paper, using Eq. [5] for domains of the agglomerates when $n > m$, is not intended to be a complete theory of coalescence, but to extend, in a simple way, the applicability of the Koch and Friedlander formalism to dendritic structures. The assumption that the aerosol consists of monodisperse primary particles is artificial but permits a simple way to describe agglomerate dynamics. Predicting coalescence in an initially dendritic structure rigorously is a much more complex problem that would require solving integro-differential equations which is beyond the scope of this paper.

ACKNOWLEDGMENTS

We thank the VTT Exchange Program, IVO Research Foundation, Leo and Regina Wainstein Foundation, and U.S. National Science Foundation, Grant CTS-9218222, for support of this research.

REFERENCES

1. Schmidt-Ott, A., *J. Aerosol Sci.* **19,** 553 (1988).
2. Matsoukas, T., and Friedlander, S. K., *J. Colloid Interface Sci.* **146,** 495 (1991).
3. Siegel, R. W., *in* "Nanophase Materials: Synthesis, Structure and Properties" (F. E. Fujita, Ed.), Springer Series in Material Sciences 27. Springer-Verlag, Berlin, 1994.
4. Windeler, R., Ph.D. Thesis, UCLA Dept. Chem. Eng., 1995.
5. Koch, W., and Friedlander, S. K., *J. Colloid Interface Sci.* **140,** 419 (1990).
6. Frenkel, J., *J. Phys.* **9,** 385 (1945).
7. Friedlander, S. K., and Wu, M. K., *Phys. Rev. B* **49,** 3622 (1994).
8. Lehtinen, K. E. J., Windeler, R. S., and Friedlander, S. K., *J. Aerosol Sci.*, in press (1996).
9. Ulrich, G. D., and Subramanian, N. S., *Combustion Sci. Tech.* **17,** 119 (1977).
10. Shimada, M., Seto, T., and Okuyama, K., *J. Chem. Eng. Japan* **27,** 795 (1994).
11. Gutsch, A., Pratsinis, S. E., and Loffler, F., *J. Aerosol Sci.* **26,** 187 (1995).
12. Vemury, S., and Pratsinis, S. E., *J. Aerosol Sci.* **26,** 175 (1995).
13. Wu, M. K., and Friedlander, S. K., *J. Aerosol Sci.* **24,** 273 (1993).
14. Wu, M. K., and Friedlander, S. K., *J. Colloid Interface Sci.* **159,** (1993).

KARI E. J. LEHTINEN[1]
ROBERT S. WINDELER
SHELDON K. FRIEDLANDER

Air Quality And Aerosol Technology Laboratory
Chemical Engineering Department
University of California
Los Angeles, California 90024

Received August 24, 1995; accepted March 28, 1996

[1] On leave (8/94–8/95) from VTT Energy, P.O. Box 1401, 02044 VTT, Finland. To whom correspondence should be addressed.

Reprinted with permission from the publisher.
Accepted for publication in Aerosol Science and Technology.

Production of Nanometer-Sized Metal Oxide Particles by Gas Phase Reaction in a Free Jet I: Experimental System and Results

Robert S. Windeler, Sheldon K. Friedlander and Kari E. J. Lehtinen*
Department of Chemical Engineering , Air Quality and Aerosol Technology Laboratory
University of California, Los Angeles, CA 90024
*VTT Energy, Aerosol Technology Group, P.O.Box 1401, 02044 VTT, Finland

Abstract

In a study of the effect of process conditions and material properties on aerosol characteristics, nanosized metal oxide particles were produced by injecting precursors as a free jet into a methane/air flame. Primary particle size increased with volume loading, solid state diffusion coefficient and maximum temperature. Larger particles were also obtained by decreasing the jet velocity. The number of particles per agglomerate increased with volume loading and decreased with solid state diffusion coefficient and maximum temperature. Metal oxides with diffusion coefficients ranging over several orders of magnitude produced different sized particles under the same process conditions (temperature profile and aerosol volume loading). Niobium oxide (largest diffusion coefficient) formed the largest particles with geometric volume mean diameters between 5.7 and 33.7 nm. Titania (mid-range diffusion coefficient) and alumina (lowest diffusion coefficient) formed particles with geometric volume mean diameters ranging from 3.8 to 21.3 nm and 2.8 to 10.7 nm, respectively. The geometric standard deviation for the metal oxide particles was about 1.2. The properties of the primary particles and agglomerates depend on the characteristic collision and coalescence times. The collision time was controlled by varying the aerosol volume loading from 10^{-7} to 10^{-6}. The coalescence time depends strongly on the solid state diffusion coefficient which ranged over several orders of magnitude as the jet temperature changed. Maximum jet temperatures from 1050 to 1920 K were obtained by adjusting the precursor jet and flame gas exit velocities from 4.8 to 53.2 m/sec and 0.14 to 0.51 m/sec, respectively. The mass production rate ranged from 0.05 to 1.0 g/hr for a jet orifice of 1.2 mm.

Introduction

Applications of Nanoparticles

Nanoparticles are loosely defined as particles in the size range between 1 and 100 nanometers. Because of their unique chemical and physical properties, nanosized metal oxide particles can be used in applications such as composite materials, insulation, adhesives, thickeners, and catalysts. The smallest particles, commonly called primary particles, are typically spheroidal and have unusual properties as a consequence of their high surface area (~300 m^2/g) (Siegel, 1994). After formation in the gas phase, the primary particles are usually attached to one another in the form of clusters or agglomerates whose bond strength may vary from weak van der Waals forces to significant necking between the primary particles (Weber and Friedlander, 1994).

Weak bonds between the primary particles facilitate the manufacture of advanced high strength ceramics, glasses, and composites (Siegel, 1994). The powder is shaped, pressed, and sintered into dense solid materials with little void space. Advanced composite materials, with properties quite different from those which currently exist, can be obtained from particles in the nanometer-size range (Andres et al., 1989).

Primary particles held together by strong necks can be used as insulating material, catalyst substrates, filters, and aerogels. These open structures, typically comprised of over 90 percent void space, form superior insulating material because of their low thermal conductivity. Large surface to volume ratios make agglomerates of nanoparticles attractive substrates for catalysts.

Nanosized particles offer the advantage of reduced production costs in manufacturing secondary objects because particles sinter at a lower temperature (Barringer and Bowen, 1982; Siegel, et al., 1988). Materials of high purity can be made by aerosol processes because the initial materials and production process are cleaner. Using relatively low temperatures, metal oxide films obtained from nanoparticles can be deposited on materials which cannot withstand high temperatures (Sakka, 1982).

Part I of this paper describes the results of an experimental study of the factors which control nanosized primary particle characteristics (size, crystal phase and shape) and agglomerate characteristics (number of primary particles and extent of necking). In Part II (Windeler et al., 1995), the results of an approximate theoretical method of predicting aerosol characteristics are compared with the experimental measurements.

Mechanisms of Particle Formation

Nanosized metal oxide aerosol particles were produced by injecting aerosol precursor vapors, volatile compounds of various metals, as a free jet into a methane/air flame. Formation of particles by mixing reacting gas streams is a common method of commercial production. In addition, the jet temperature, velocity, and concentration profiles can be predicted by modifying well-known theoretical results for certain ideal cases (Windeler, 1995).

Process conditions, including the precursor concentration and the gas temperature profile were systematically varied. Three different aerosol precursors were used to study the effect of material properties, especially the solid state diffusion coefficient. For each aerosol material, the volumetric concentration ranges were the same. The details of the experimental program can be set in perspective by considering the following mechanisms which are believed to control nanoparticle formation in this system.

High supersaturation ratios occur when precursor vapor molecules react to form metal oxides with very low vapor pressures. Calculations indicate that at these high supersaturation ratios, single metal oxide molecules can serve as stable condensation nuclei (Ulrich, 1971; Ulrich and Riehl, 1982; Bolsaitis, et al., 1987). The molecules collide to form particles which grow by a collision-coalescence mechanism (Ulrich, 1971; Bolsaitis, et al., 1987; Helble and Sarofim, 1989; Koch and Friedlander, 1990). Collisions take place as a result of the particle Brownian motion while coalescence is driven by the surface free energy excess of attached particles. The effects of the initial conditions, including chemical reaction (Xiong and Pratsinis, 1991) and nucleation, are unimportant to the final particle characteristics as long as the reaction/nucleation processes are fast compared with the collision/coalescence processes.

As shown in Part II, particle and agglomerate properties can be predicted from an analysis based on their characteristic collision and coalescence times. The characteristic collision time is defined as the time for the average volume of an agglomerate to double, and is given by (Matsoukas and Friedlander, 1991):

$$\tau_c = 2v^{3/2-2/D_f}\left(\frac{6kT}{\rho}\right)^{-1/2}\left(\frac{3}{4\pi}\right)^{1/2-2/D_f}\left(\frac{d_p}{2}\right)^{6/D_f-2}(\alpha\phi)^{-1} \quad (1)$$

where D_f and v are the fractal dimension and average volume of the agglomerate, k is the Boltzmann constant, ρ is the density of the particle, T is the temperature, d_p is the average particle diameter, α is a constant which depends on D_f (Lehtinen et al., 1996), and ϕ is the volume loading of the metal oxide (volume of particles/volume of carrier gas). This equation holds for agglomerates with a self-preserving size distribution in the free molecular regime. For completely coalescing particles, D_f equals 3 and Equation 1 reduces to the classical theory for spherical particles (Lai et al., 1972).

In this study, the collision time was varied, without significantly affecting the coalescence time, by changing the aerosol volume loading. As the volume loading is increased, particles collide more frequently, leading to a decrease in the collision time. Turbulence created by the jet flow does not affect the collision time for nanometer-sized agglomerates, since they are much smaller than Kolmogorov microscale eddies, which represent the smallest scale of turbulent fluctuations (Batchelor, 1953).

Particle coalescence is driven by the excess in the agglomerate surface free energy compared with that of an equilibrium (spherical) surface. Friedlander and Wu (1994) derived an equation for the reduction of surface area, A, during the final stages of solid state sintering:

$$\tau_f = \frac{9kT}{64\pi v_0 D\sigma}v \quad (2)$$

where v_0 is the volume of the diffusing vacancy, D is the solid state diffusion coefficient of the slowest moving ion, σ is the surface tension, and A_S is the surface area after complete sintering. Equation 2 can be extended to approximate the entire sintering process beginning with initial neck formation (Koch and Friedlander, 1990). Then t_f can be considered as a characteristic time for the sintering process, describing the time needed for coalescence of two initially distinct spherical particles.

The coalescence time was varied, independently of the collision time, by changing the solid state diffusion coefficient. The diffusion coefficient is strongly dependent on temperature and follows an Arrhenius expression (Kingery et al., 1976). The diffusion coefficient was varied by modifying the flame conditions, precursor jet velocity, and metal oxide. Three different metal oxides with markedly different values of the diffusion coefficient were chosen for study: niobium oxide, titania and alumina.

Metal Oxide Particle Morphology

The morphology of the material provides insight on the growth mechanism of the particles. Metal oxide particles can form crystalline, polycrystalline, or amorphous (glassy) structures depending on their material properties and formation temperature. At the atomic level, the

particles are comprised of polyhedra which consist of a central metal ion surrounded by 3 to 6 oxygen ions. The phase of the material can typically be determined by the coordination number of the polyhedra. Polyhedra that have a coordination number of 3 or 4 form glasses because they only share corners, creating an open random structure. Polyhedra which have a coordination number of 5 or 6 form crystals because they share edges and faces, resulting in an ordered structure (Zachariasen, 1932).

During aerosol generation, individual polyhedral structures probably form in the gas and collide on a molecular level at random orientations. If the temperature is too low, the polyhedra cannot orient themselves to decrease their free energy and the structure remains amorphous. Particles become crystalline when the polyhedra can rearrange sufficiently rapidly. As the temperature increases, the material forms more stable crystalline phases. For example, the commonly reported transformation order for alumina with increasing temperature is:

amorphous -> gamma (γ) -> theta (θ) + delta (δ) -> alpha(α)

where these phases are arranged in order of decreasing free energy (Chou, et al., 1991; Chou and Nieh, 1992). This change in phase is discussed in the results section to help explain the particle growth mechanism for alumina.

Experimental

Aerosol Generator

A schematic diagram of the aerosol generator and particle collection apparatus is shown in Figure 1. A nitrogen stream (99.999%, Matheson Ultra High Purity) was saturated with precursor vapor by flowing through a bubbler (Windeler, 1995). The precursor/nitrogen stream was then diluted with a second nitrogen stream. By adjusting the two flow rates, volume loading and jet exit velocity could be controlled independently. To minimize stray particle formation and concentration gradients, the precursor/nitrogen stream passed through a filter (Nupro "F" Series Inline Filter) and a motionless mixer, consisting of a quarter inch stainless steel tube packed with glass fibers. The particle-free stream then flowed through a 1/8" stainless steel tube inserted flush with the top of the flame arrestor, forming a 0.12 cm diameter jet orifice. A flame, operated under stoichiometric conditions, was generated from a premixed stream of air and methane (99.97%, Matheson Ultra High Purity). The flame burned evenly on a 3.7 cm diameter flame arrestor which was installed to prevent backflashing. By adjusting the flame gas flow rate, the precursor jet temperature could be controlled.

The particles formed in a system of three concentric streams: a precursor jet introduced into the center of a coflow laminar flame stream which is surrounded by ambient air. These streams mixed at different axial distances resulting in a complicated temperature profile (Figure 2). The jet was heated by the flame gases for the first 3 to 10 cm and then cooled by entrained ambient air.

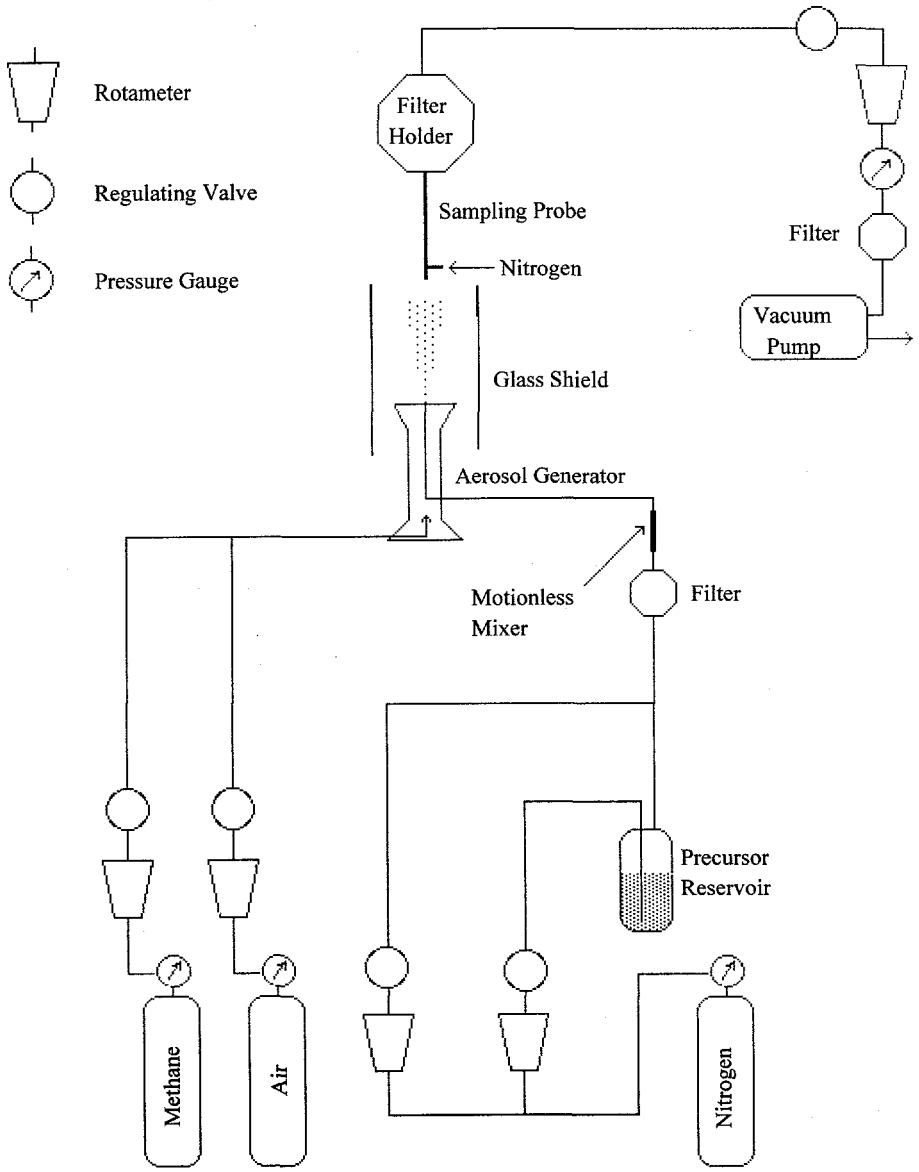

Figure 1. Schematic diagram of apparatus for generating aerosol

Fig. 1: Schematic diagram of experimental system

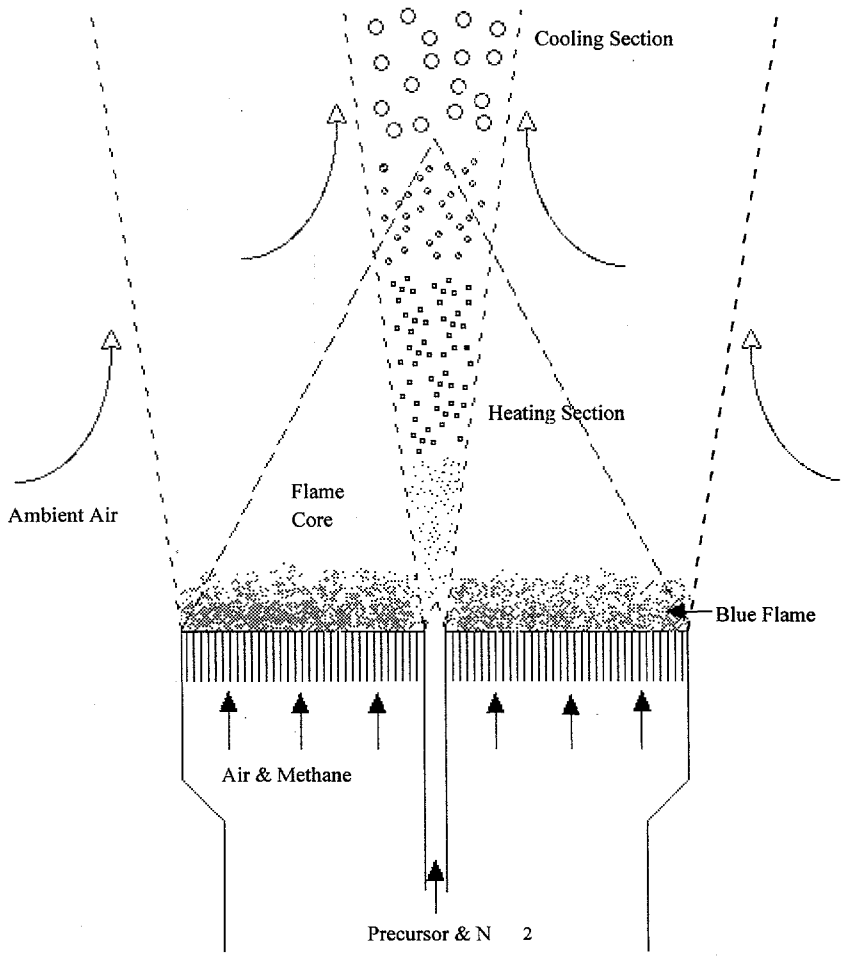

Fig 2: The jet generator is comprised of three concentric streams. Particles grow along the jet axis until coalescence is quenched by ambient air.

Aerosol Precursors

Introducing aerosol precursors as vapors into the flame avoids the residual particles which may be present when solid aerosol precursors are used (Helble and Morency, 1989; Steiner, 1991). Gaseous precursors are also used in the most common processes for commercial production of fine particles. High particle concentrations were obtained by choosing precursors with high vapor pressures ($\geq$10 mm Hg) at reasonably low temperatures. The particle volume loadings were estimated assuming that the nitrogen stream from the bubbler was saturated with precursor vapor. The mass balance of the system was determined to be closed by collecting all the metal oxide particles formed in the jet and comparing their mass flux to the precursor vapor flux. These precursors reacted rapidly to form amorphous and gamma alumina (Al_2O_3), anatase titania (TiO_2), and crystalline niobium oxide (Nb_2O_5).

Alumina particles were formed from trimethyl aluminum vapor (TMA) (97%, Aldrich Chemical Company). The TMA bubbler was operated at room temperature (21°C), corresponding to a calculated vapor pressure of 10.0 mm Hg (Bamford, et al., 1946). Raman spectrum measurements indicate oxide formation times of 0.037 msec for a TMA-O_2 flame under stoichiometric conditions at 4.1 mm Hg and an adiabatic flame temperature of 2600 K (Vanpee and Seamans, 1967). This implies that the precursor forms alumina in the initial region of the jet. Titania particles were produced from titanium tetrachloride vapor (99.995%, Aldrich Chemical Company). The bubbler was operated at room temperature, corresponding to a calculated vapor pressure of 10.0 mm Hg (Sax and Lewis, 1987). Niobium oxide particles were formed from niobium pentafluoride vapor (98%, Aldrich Chemical Company). The precursor was heated to 115°C in the bubbler to obtain a vapor pressure of 14.5 mm Hg (Fairbrother and Frith, 1951). To prevent the precursor from condensing, the tubes which connect the bubbler to the generator were kept at 200°C with heating tape.

Particle Sampling and Characterization

A glass shield, 30 cm long and 10.5 cm in diameter, reduced the effect of external disturbances on the precursor jet profiles. Metal oxide particles were collected from the jet centerline with a sampling probe. Primary particle and agglomerate growth was quenched at the probe entrance by diluting and cooling the aerosol with room temperature nitrogen. Particles were collected on a copper grid (Ted Pella Inc., carbon coated, 300 mesh Tab, Type A) which was attached to a quartz fiber filter (47 mm Whatman QM-A) for examination with a transmission electron microscope (TEM, JEOL-JEM 100CX). Typical collection and dilution flow rates for the sampling probe were 1.5 and 5.5 l/min, respectively. For most experiments, the probe height was 20 cm above the burner, but was varied to change the residence time. The residence time is defined as the time between the formation of metal oxide particles and their collection by the sampling probe.

Electron diffraction (JEOL-JEM 100CX) and Energy Dispersive Spectroscopy (EDS) with a windowless detector (KEVEX System 8000 with a DEC LSI 11/73 computer) were used to determine particle composition and phase. The average size, geometric standard deviation and shape of the particles were obtained from TEM photographs. An estimate of the number of particles per agglomerate, extent of neck formation, and coordination number were also determined from the photographs. Oblong particles were measured along their narrowest length to obtain the diameter of the last completely coalesced particle. Using this technique, the average primary particle diameter might be slightly underestimated. Typically between 50 and 100 particles were measured to obtain geometric volume mean particle diameters and geometric standard deviations. Some particles in dense agglomerates could not be measured because individual shapes were difficult to distinguish.

Flow Characteristics

Process conditions (temperature, volume loading and velocity) and material properties (solid state diffusion) were varied to determine their effect on particle and agglomerate characteristics. The precursor jet was operated with flow rates of 0.33, 1.02, 1.88, and 3.61 l/min at 21°C, corresponding to exit velocities of 4.8, 15.0, 27.8, and 53.2 m/sec, respectively. The mass production rate ranged from 0.05 to 1.0 g/hr, and the Reynolds number ranged from 330 to 3600 based on ambient exit conditions.

For free jets, the transition from laminar to turbulent flow occurs over a Reynolds number range which is sensitive to experimental conditions. This is reflected in the wide spread of values for the transition in the literature. Revill (1992) noted that jet flows with Reynolds numbers below 100 are laminar and those with Reynolds numbers above 1000-2000 are turbulent. Simpson (1975) found turbulent flows are not sustained below a Reynolds number of 1000, while Tatterson (1991) and Lane and Rice (1981) state that jet flows change from laminar to turbulent at a Reynolds number of approximately 2000.

The jet flow was turbulent at the highest exit velocity (Re [a]3600), while the other exit velocities (Re [a] 330, 1020 and 1880) corresponded to jet flows in the laminar or transition regime. For the highest exit velocity, the metal oxide particles spread with distance from the orifice, decreasing the volume loading. For the lower three exit velocities, a thin jet formed with a constant width from the orifice to the sampling tube, indicating little dilution. These observations correspond well to the range of transition in literature.

Temperature Distribution

The flame was operated under stoichiometric conditions with flow rates of 8.8 and 33 l/min at 21^{o}C, corresponding to exit velocities of 0.14 and 0.51 m/sec, respectively. As the methane/air flow rate increased, the flame became hotter, causing an increase in the precursor jet temperature along the length of the jet.

The temperature was measured along the jet axis with a subminiature R type thermocouple and corrected for radiation losses (Bradley and Matthews, 1968). The maximum temperature decreased with an increase in jet velocity, except for the highest velocity with a flame gas flow rate of 33 l/min (Figures 3a and 3b). Under this condition, the maximum temperature was higher than expected because the jet flow became turbulent and mixed quickly with the flame gases before diluting with ambient air.

The melting points of the metal oxides used in this study were compared to the jet temperature to determine whether coalescence occurred, at least partially, by a viscous flow mechanism. The melting point decreases with particle diameter for nanometer-sized particles (Peppiatt and Sambles, 1975). During a short period of time, the maximum jet temperature was higher than the melting point for small particle diameters and for niobium oxide with a flame gas flow rate of 33 l/min. In the absence of supercooling, these particles are expected to grow by solid state diffusion over most of the time period of interest. Final particle characteristics should not be affected by viscous flow even for particles that melt at the high jet temperatures.

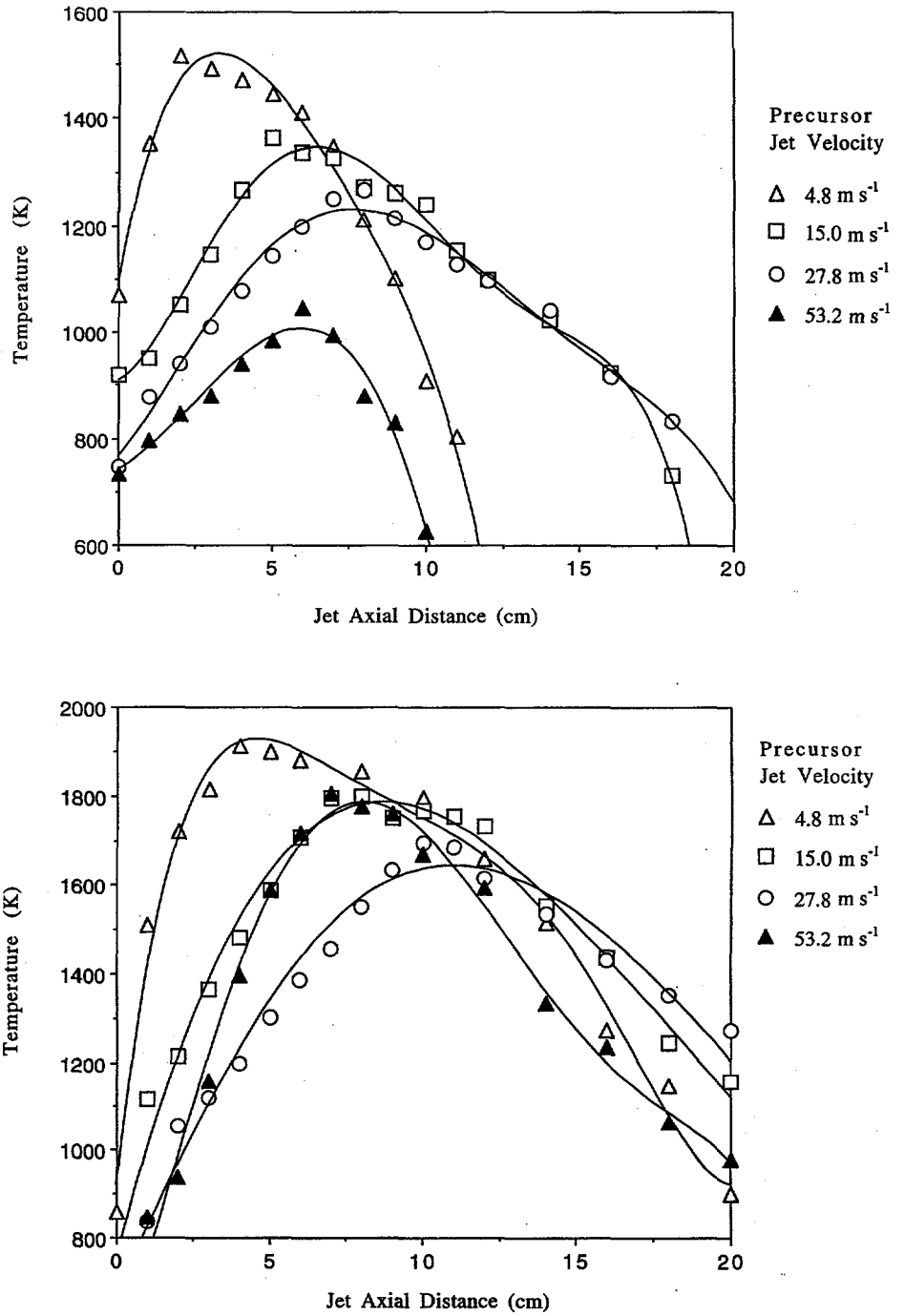

Fig. 3: Temperature profiles for the precursor jet exit velocities with a flame gas flow rate of a) 8.8 l/min and b) 33 l/min. The temperature was measured along the jet axis with a subminiature R type thermocouple. The jet was heated by flame gases in the initial region, and then cooled with ambient air.

Results

Parameters Controlling Primary Particle and Agglomerate Sizes

The solid state diffusion coefficient of the ion which moves most slowly through the metal oxide lattice controls the coalescence time (Kingery et al., 1976). Three metal oxides were chosen for study because their diffusion coefficients range over several orders of magnitude (Figure 4). The coalescence time increases with a decrease in diffusion coefficient. As a result, under similar process conditions, the largest particles were obtained for niobium oxide followed by titania and alumina (Figures 5a, 5b and 5c). This effect is also shown in Figures 6, 7 and 9.

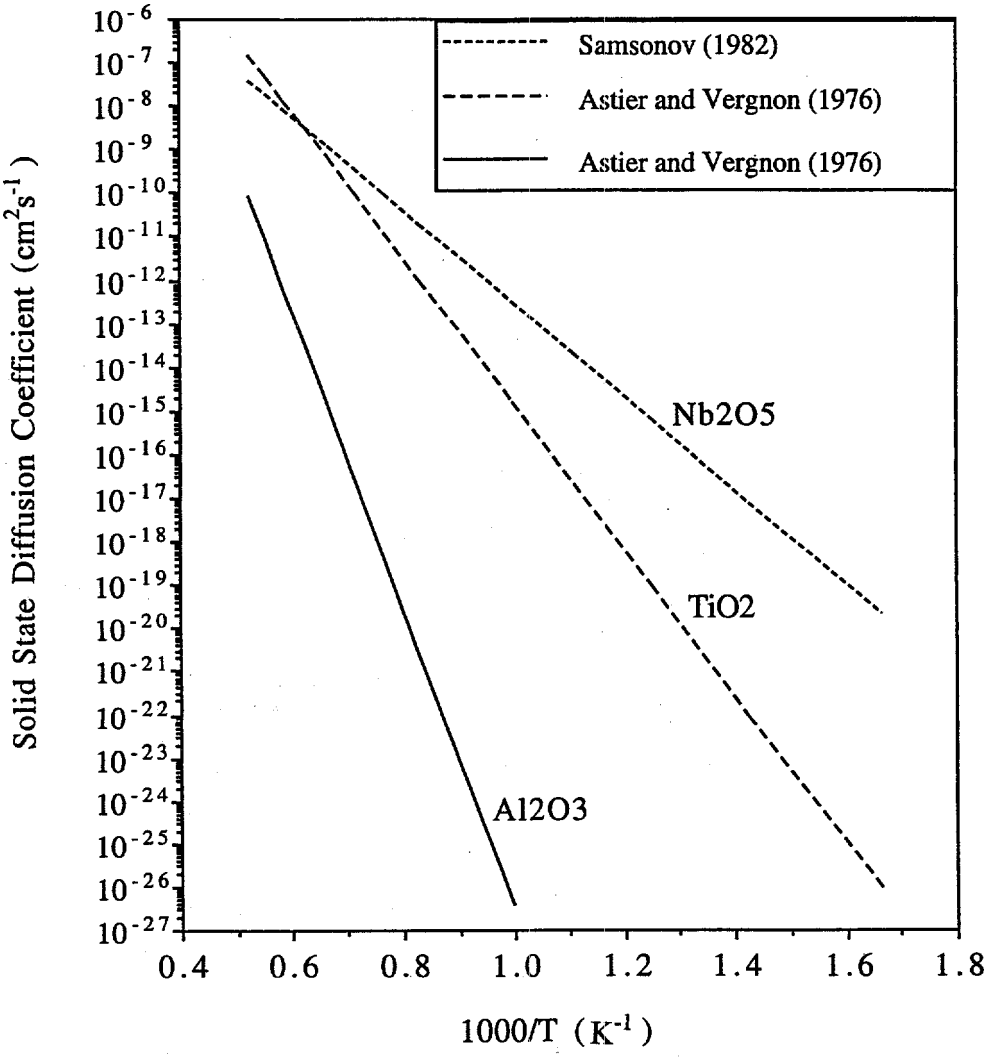

Fig. 4: Solid state diffusion coefficients depend strongly on temperature and follow an Arrhenius expression. Under similar process conditions, the metal oxide with the largest diffusion coefficient formed the largest particles.

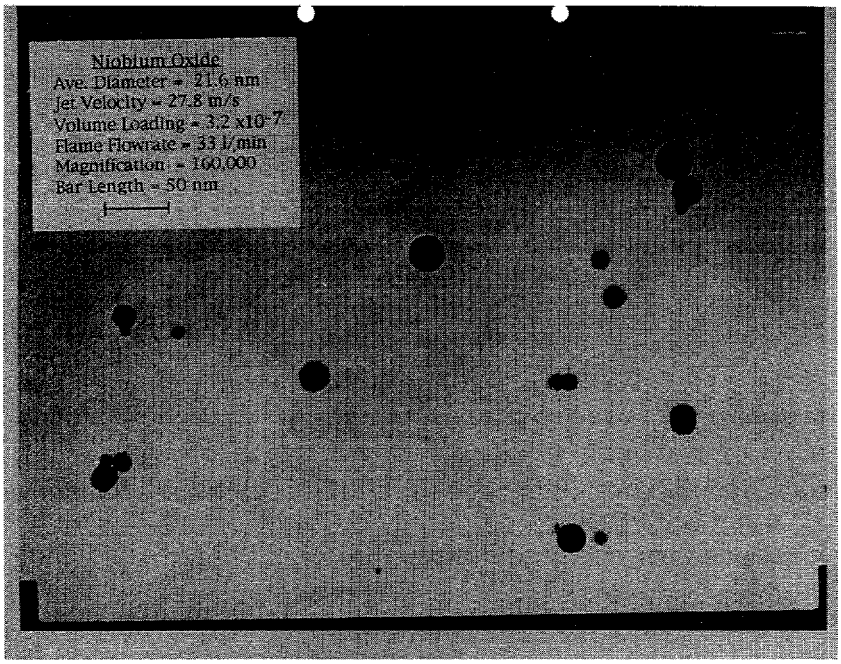

Fig. 5a: TEM photograph of niobium oxide. The particles are nearly spherical and showed no evidence of agglomeration because growth is collision limited. Particles do not neck when they agglomerate on the filter because growth has been quenched.

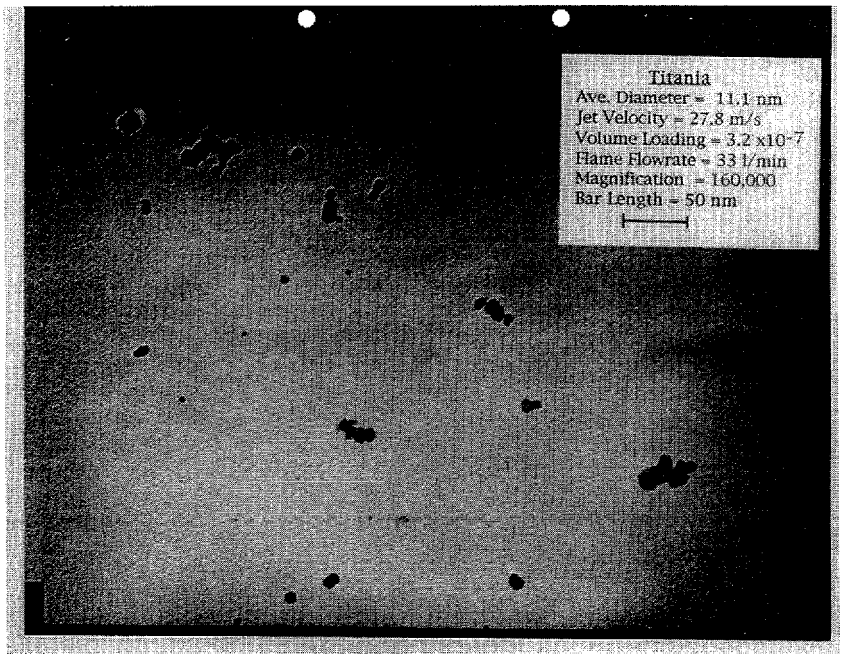

Fig. 5b: TEM photograph of titania. Some particles have facets indicating a crystalline material.

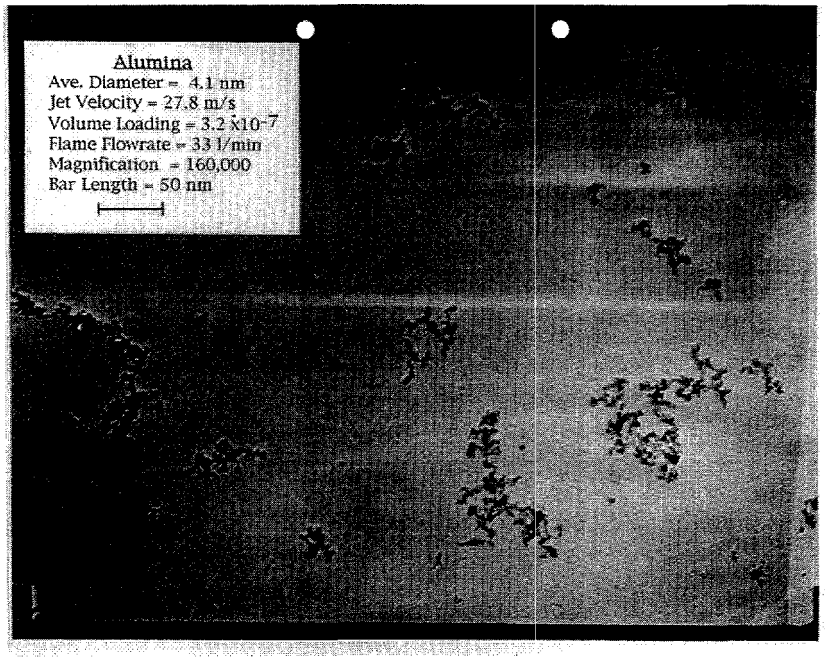

Fig. 5c: TEM photograph of alumina. Large agglomerates comprise of small, necked particles, because growth is coalescence limited.

Variations in the precursor velocity and flame gas flow rate affect the primary particle size and number of particles per agglomerate through the coalescence time. Particles grow as long as the temperature is high enough for coalescence to occur. As the precursor jet exit velocity decreased, particles were subject to higher temperatures for longer periods of time. This resulted in larger particles (Figure 6). Larger particles were also generated with a higher flame gas flow rate because the jet temperature increased along the jet axis. Formenti, et al. (1972), Ulrich and Riehl (1982) and Bolsaitis, et al. (1987) observed similar results.

Particle size can be controlled through the collision time by varying the metal oxide volume loading. The number of collisions per time increases with volume loading, and as long as the system is not coalescence limited, particles grow larger. Experiments were performed with the three metal oxides at volume loadings of $1.0x10^{-7}$, $3.2x10^{-7}$ and $1.0x10^{-8}$ (Figure 7). The effect of volume loading on particle size was most apparent for the high temperature experiments because particle growth occurred closer to the collision limited regime. Volume loading had no effect on alumina because particle growth was always coalescence limited.

Higher volume loadings also lead to larger agglomerates when collisions occur faster than the particles coalesce (Figure 8). TEM photographs provide only a rough estimate of the actual number of particles per agglomerate, but the trends can be seen. The number of particles per agglomerate increased more dramatically at lower temperatures because growth occurred closer to the coalescence limited regime. Volume loading had no effect on niobium oxide at high temperatures because particle growth was collision limited, resulting in agglomerate sizes of unity.

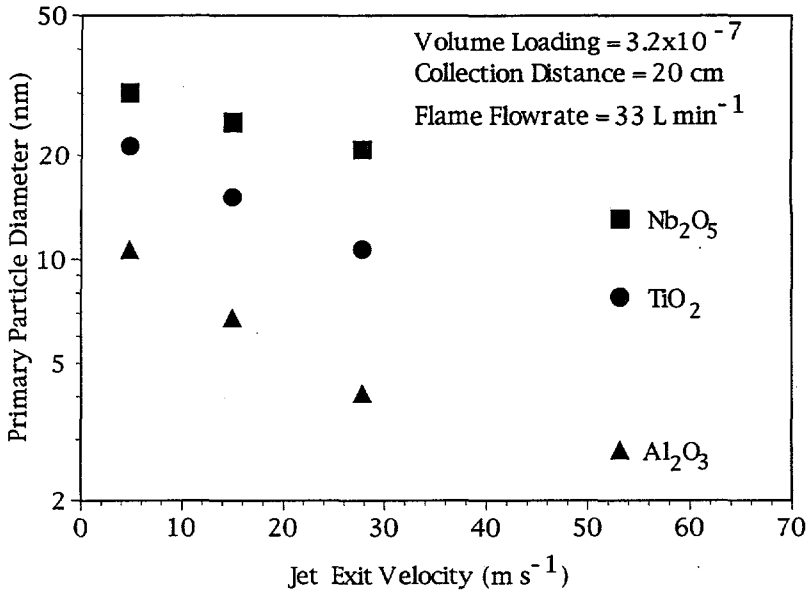

Fig. 6: Increasing the exit velocity decreased the jet temperature for laminar jet flows, resulting in smaller primary particles. The temperature affects the coalescence time through the diffusion coefficient.

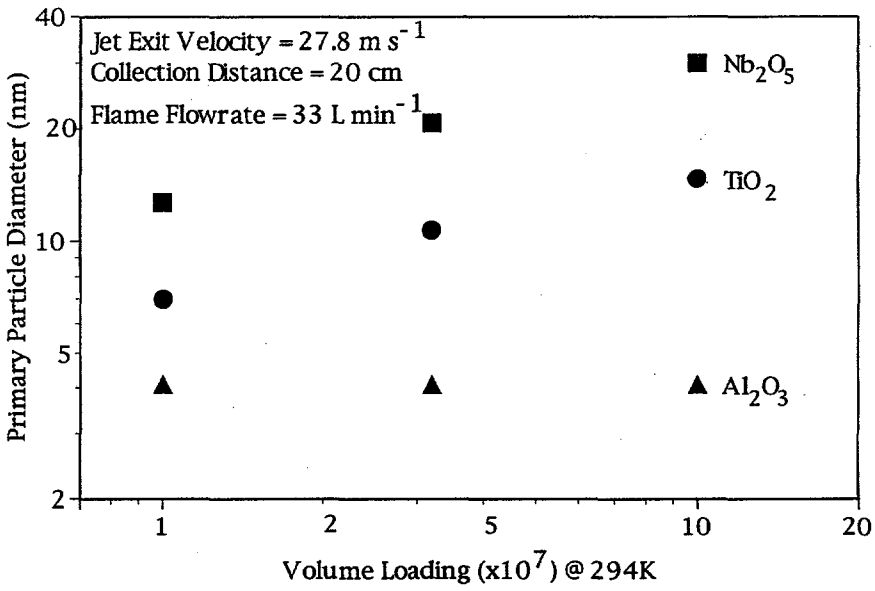

Fig. 7: Primary particle size increased with volume loading except for alumina, whose growth was coalescence limited.

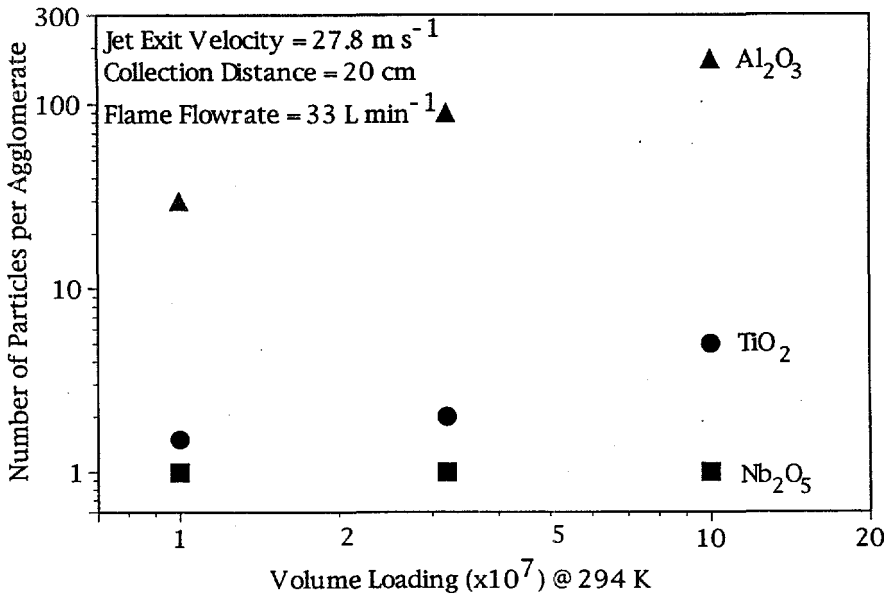

Fig. 8: The number of particles par agglomerate increased with volume loading except for niobium oxide at high temperatures because growth was collision limited.

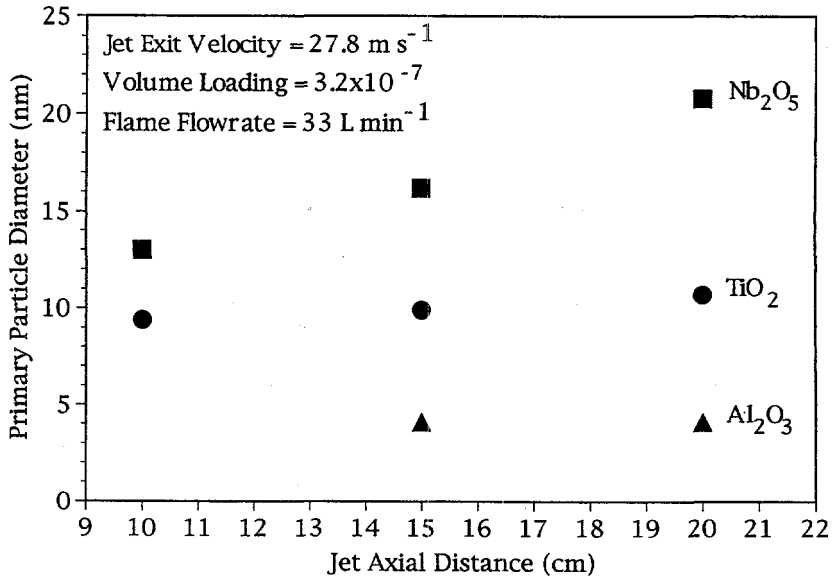

Fig. 9: Particle growth as a function of distance along the jet axis. Metal oxides with large diffusion coefficients continued to grow in the cooler regions of the jet.

Particle growth along the jet axis is shown in Figure 9. A change in particle size indicates coalescence was still occurring in that region of the jet. As expected, metal oxides with high diffusion coefficients continued to grow in the cooler jet sections. The alumina particles (lowest diffusion coefficient) did not increase in size along the second half of the jet; they grew only in the initial region where the temperature was highest.

Characteristics of the Three Metal Oxides

Niobium Oxide

EDS and electron diffraction patterns indicate that niobium pentafluoride oxidized to form crystalline niobium oxide (Nb_2O_5). Under similar process conditions, niobium oxide formed the largest primary particles for the metal oxides studied (geometric volume mean diameters ranged from 5.8 to 30.1 nm) because it has the largest diffusion coefficient. Table 1 summarizes the geometric volume mean diameters and the estimates of the number of particles per agglomerate under operating conditions.

Table 1. Primary Particle Diameters and Number of Particles per Agglomerate of Niobium Oxide under Various Jet Conditions

Flame Flowrate (L/min)	Exit Velocity (m/s) @ 294 K	Volume Loading ($x10^7$) @ 294 K	Sampling Point (cm)	Geometric Volume Mean Diameter (nm)	Geometric Standard Deviation	Particles per Agglomerate
8.8	4.8	3.2	20	16.9	1.2	45
8.8	15.0	3.2	20	11.0	1.2	40
8.8	27.8	3.2	20	7.4	1.2	50
8.8	53.2	3.2	20	5.7	1.2	60
8.8	27.8	10.0	20	8.1	1.2	60
8.8	27.8	1.0	20	5.6	1.1	10
8.8	27.8	3.2	15	6.3	1.1	25
8.8	27.8	3.2	10	6.0	1.1	25
33	4.8	3.2	20	33.7	1.3	1
33	15.0	3.2	20	26.8	1.2	1
33	27.8	3.2	20	21.6	1.2	1
33	53.2	3.2	20	13.6	1.2	1.5
33	27.8	10.0	20	32.5	1.3	1
33	27.8	1.0	20	13.2	1.2	1
33	27.8	3.2	15	16.6	1.1	1
33	27.8	3.2	10	13.5	1.2	1

At high temperatures (flame gas flow rate = 33 l/min) non-agglomerated, nearly spherical particles were observed which indicates that growth was collision limited (Figure 5a). For long sampling times, agglomeration occurred on the TEM grid. These particles touched at a single point with little or no necking. At low temperatures, agglomerates formed in the jet by the time particle growth was quenched, resulting in oblong particles necked together. The highest jet temperatures rise above the melting point of niobium oxide (1790 K). At these temperatures, sintering occurs very rapidly through the viscous flow mechanism. However, primary particle size predictions using Equations 1 and 2, which are based on solid state diffusion, will be the same as predictions based on the viscous flow mechanism since growth is collision limited for either model at these temperatures.

Titania

Electron diffraction patterns indicate that the titania produced by oxidizing titanium tetrachloride was in the anatase form. Under similar operating conditions, titania (mid-range diffusion coefficient) formed particle sizes between that of alumina and niobium oxide. Geometric volume mean particle diameters ranged from 3.8 to 21.3 nm with a geometric standard deviation of about 1.2. Table 2 summarizes the geometric volume mean diameters and the estimates of the number of particles per agglomerate under operating conditions.

Table 2. Primary Particle Diameters and Number of Particles per Agglomerate of Titania under Various Jet Conditions

Flame Flowrate (L/min)	Exit Velocity (m/s) @ 294 K	Volume Loading ($x10^7$) @ 294 K	Sampling Point (cm)	Geometric Volume Mean Diameter (nm)	Geometric Standard Deviation	Particles per Agglomerate
8.8	4.8	3.2	20	12.4	1.2	25
8.8	15.0	3.2	20	7.4	1.2	50
8.8	27.8	3.2	20	4.9	1.1	60
8.8	53.2	3.2	20	4.0	1.1	50
8.8	27.8	10.0	20	6.4	1.1	80
8.8	27.8	1.0	20	3.9	1.1	25
8.8	27.8	3.2	15	4.6	1.1	60
8.8	27.8	3.2	10	4.4	1.2	60
33	4.8	3.2	20	24.2	1.3	1
33	15.0	3.2	20	16.1	1.2	2
33	27.8	3.2	20	11.1	1.2	2
33	53.2	3.2	20	8.0	1.2	2
33	27.8	10.0	20	15.8	1.2	5
33	27.8	1.0	20	7.3	1.2	1.5
33	27.8	3.2	15	10.4	1.2	1.5
33	27.8	3.2	10	9.7	1.2	1

Some large titania particles have flat faces indicating a crystalline material (Figure 5b), while smaller particles are typically smooth and oblong. Particles generated at high temperatures appear to be weakly held together because there is little necking. At low temperatures, particles form necks in agglomerates similar to the niobium oxide particles produced at low temperatures. Titania particle size may depend on water vapor concentration. This system, as with any system with a flame, has a high water vapor concentration, and particles were probably covered by hydroxyl groups. The effect of water vapor could not be determined in this study since the water concentration was similar for each experiment.

Alumina

EDS and electron diffraction patterns indicate that TMA oxidized to form gamma and amorphous alumina at high and low temperatures, respectively. Alumina (lowest diffusion coefficient) formed the smallest particles of the three metal oxides. Geometric volume mean particle sizes ranged from 2.8 to 10.7 nm with a geometric standard deviation of about 1.2. Table 3 summarizes the geometric volume mean diameters and the estimates of the number of particles per agglomerate under operating conditions. Particle size increased with temperature, but not volume loading, indicating growth was coalescence limited. The particles are oblong and attached by thick necks in large open agglomerates (Figure 5c). Under some operating conditions, alumina particles were not formed, instead, cloudy indistinct shapes where observed in the TEM photographs.

Table 3. Primary Particle Diameters and Number of Particles per Agglomerate of Alumina under Various Jet Conditions

Flame Flowrate (L/min)	Exit Velocity (m/s) @ 294 K	Volume Loading ($x10^7$) @ 294 K	Sampling Point (cm)	Geometric Volume Mean Diameter (nm)	Geometric Standard Deviation	Particles per Agglomerate
8.8	4.8	3.2	20	4.9	1.2	250
8.8	15.0	3.2	20	3.6	1.1	200
8.8	27.8	3.2	20	3.0	1.1	70
8.8	53.2	3.2	20	*		
8.8	27.8	10.0	20	3.0	1.1	150
8.8	27.8	1.0	20	3.0	1.1	25
8.8	27.8	3.2	15	3.0	1.1	40
8.8	27.8	3.2	10	3.0	1.1	20
33	4.8	3.2	20	11.1	1.2	45
33	15.0	3.2	20	7.1	1.2	60
33	27.8	3.2	20	4.1	1.1	90
33	53.2	3.2	20	2.9	1.2	20
33	27.8	10.0	20	4.1	1.1	175
33	27.8	1.0	20	4.1	1.1	30
33	27.8	3.2	15	4.1	1.1	40
33	27.8	3.2	10	*		

* Experimental conditions produced cloudy indistinct particles.

Although unusual, amorphous alumina has been produced by other investigators (Formenti, et al., 1972; Ulrich 1984; Okuyama, et al., 1986; Windeler, 1992). Alumina crystallizes at about one third its melting point (Mackenzie, 1988) because it consists of AlO_6 octahedra which share edges and faces. Amorphous alumina is probably formed by polyhedra that collide and do not have enough energy to rearrange into an ordered array. This disordered structure is similar to glass.

The formation of amorphous alumina indicates that alumina particles may not sinter by the solid state lattice diffusion mechanism at low temperatures. If the particles could coalesce, they should also be able to rearrange into a crystalline structure. At higher temperatures, particles are expected to grow by the collision-coalescence mechanism because the alumina particles are crystalline.

Conclusions

Nanosized particles were produced by injecting metal compound vapors as a free jet into a methane/air flame. Primary particle characteristics (size, crystal phase and shape) and agglomerate characteristics (number of particles and extent of necking) were determined by the aerosol collision and coalescence times. These times were controlled by changing process conditions and material properties.

The solid state diffusion coefficient strongly affected the primary particle size through the coalescence time. Holding process conditions constant, particle size increased with the diffusion coefficient. Niobium oxide, which has the largest diffusion coefficient, formed the largest particles (geometric volume mean diameters ranged from 5.7 to 33.7 nm). Titania (mid-range diffusion coefficient) and alumina (smallest diffusion coefficient) formed particles with geometric volume mean diameters ranging from 3.8 to 21.3 nm and 2.8 to 10.7 nm, respectively. Particle size also increased with maximum temperature and volume loading. Number of particles

per agglomerate increased with volume loading and decreased with the diffusion coefficient and maximum temperature.

Acknowledgment

The authors wish to thank the National Science Foundation, Grant CTS-9218222, and the Northrop Corporation for financial support.

References

Andres, R.P., Averback, R.S., Brown, W.L., Brus, L.E., Goddard, W.A., Kaldor, A., Louie, S.G., Moscovits, M., Peercy, P.S., Riley, S.J., Siegel, R.W., Spaepen, F., and Wang, Y. (1989) Research Opportunities on Clusters and Cluster-Assembled Materials - a Department of Energy, Council on Materials Science Panel Report, *J. Mater. Res.* 4:704.

Astier, M., and Vergnon, P. (1976) Determination of the Diffusion Coefficients from Sintering Data of Ultrafine Oxide Particles, *J. Solid State Chem.* 19:67.

Bamford, C.H., Levi, D.L., and Newitt, D.M. (1946) Physical and Chemical Properties of Organo-metallic Compounds. Part I. The Vapour Pressures and Freezing Points of Simple Metal Alkyls of Groups II, III and V. *J. Chem. Soc.* 40:468-471.

Barringer, E.A., and Bowen, H.K. (1982) Formation, Packing, and Sintering of Monodisperse TiO_2 Powders, *J. Amer. Ceram. Soc.* 65:c-199.

Batchelor, Y.K. (1953) *The Theory of Homogeneous Turbulence*, Cambride University Press, London.

Bolsaitis, P.P., McCarthy, J.F., and Mohiuddin, G. (1987) Formation of Metal Oxide Aerosols for Conditions of High Supersaturation, *Aerosol Sci. Technol.*, 6:225.

Bradley, D., and Matthews, K.J. (1968) Measurement of High Gas Temperatures with Fine Wire Thermocouples, *J. Mech. Eng. Sci.* 10, 4:299.

Chou, T.C., and Nieh, T.G. (1992) Interface-Controlled Phase Transformation and Abnormal Grain Growth of a-Al_2O_3 in Thin g-Alumina Films,*Thin Solid Films* 221:89-97.

Chou, T.C., Nieh, T.G., McAdams, S.D., and Pharr, G.M. (1991) Microstructures and Mechanical Properties of Thin Films of Aluminum Oxide, *Scr. Metall.* 25:2203.

Fairbrother, F., and Frith, W.C. (1951) The Halides of Niobium and Tantalum. Part III. The Vapour Pressures of Niobium and Tantalum Pentafluorides, *J. Chem. Soc.* 3051-3056.

Formenti, M., Juillet, F., Meriaudeau, P., Teichner, S.J., and Vergnon, P. (1972) Preparation in a Hydrogen-Oxygen Flame of Ultrafine Metal Oxide Particles, *J. Colloid Interface Sci.* 39:79.

Friedlander, S.K., and Wu, M.K. (1994) Linear Rate Law for the Decay of the Excess Surface Area of a Coalescing Solid Particle, *Phys. Rev. B* 49, 5:3622.

Helble, J.J., and Morency, J.R. (1989) *PSI Technology Report 2081/TR-966.*

Helble, J.J., and Sarofim, A.F. (1989) Factors Determining the Primary Particle Size of Flame-Generated Inorganic Aerosols, *J. Colloid Interface Sci.* 128:348.

Kingery, W.D., Bowen, H.K., and Uhlmann, D.R. (1976) *Introduction to Ceramics*, John Wiley & Sons, New York.

Koch W., and Friedlander, S.K. (1990) The Effect of Particle Coalescence on the Surface Area of a Coagulating Aerosol, *J. Colloid Interface Sci.* 140:419.

Kuczynski, G.C., Abernethy, L., and Allen, J. (1959) *Kinetics of High-Temperature Processes*, John Wiley and Sons Inc., New York.

Lai, F.S., Friedlander, S.K., Pich. J., and Hidy, G.M. (1972) The Self-Preserving Particle Size Distribution for Brownian Coagulation in the Free-Molecule Regime, *J. Colloid Interface Sci.* 39:395.

Lane, A.G.C., and Rice, P. (1981) An Experimental Investigation of Liquid Jet Mixing Employing a Vertical Submerged Jet, *IChemE Symposium Series No. 64.*

Lehtinen, K.E.J., Windeler, R.S., and Friedlander, S.K. (1996) A Note on the Growth of Primary Particles in Agglomerate Structures by Coalescence, Accepted for publication in *J. Colloid Interface Sci.* .

Mackenzie, J.D. (1988). *Ultrastructure Processing of Advanced Ceramics*, Mackenzie, J.D., Ulrich, D.R. eds., Wiley-Interscience, New York.

Matsoukas, T., and Friedlander, S.K. (1991) Dynamics of Aerosol Agglomerate Formation, *J. Colloid Interface Sci.* 146, 2:495.

Okuyama, K., Kousaka, Y., Tohge, N., and Yamamoto, S. (1986) Production of Ultrafine Metal Oxide Aerosol Particles by Thermal Decomposition of Metal Alkoxide Vapors, *AIChE Journal*, 32:2010.

Peppiatt, S.J., and Sambles, J.R. (1975) The Melting of Small Particles. I. Lead, *Proc. R. Soc. London*, 345:387.

Revill, B.K. (1992) *Mixing in the Process Industries 2nd Ed.*, Edwards, N.H. ed., Butterworth-Heinemann, Oxford.

Sakka, S. (1982) *Treatise on Materials Science and Tech.*, Tomozawa, M., and Doremus, R., eds., Academic Press, New York.

Samsonov, G.V. (1982) *The Oxide Book*, Translated from Russian by Johnston, R.K., IFI/Plenum, New York.

Sax, N.I., and Lewis, R.J. (1987) *Hazardous Chemicals Desk Reference*, Van Nostrand Reinhold Company, New York.

Siegel, R.W. (1994) Nanophase Materials: Synthesis, Structure and Properties, (Fujita, F.E. ed.) Springer Series in Material Sciences 27:65-105.

Siegel, R.W., Ramasamy, S., Hahn, H., Zonguan, L., Ting, L., and Gronsky, R. (1988) Synthesis, Characterization, and Properties of Nanometer TiO_2, *J. Mater. Res.* 3:1367.

Simpson, L.L. (1975) *Turbulence in Mixing Operations*, Brodkey, R.S. ed., Academic Press, New York.

Steiner, C.K. (1991) *Metal Oxide Aerosol Formation in High Temperature Processes*, Masters Thesis in Chemical Engineering, University of California, Los Angeles.

Tatterson, G.B. (1991) *Fluid Mixing and Gas Dispersion in Agitated Tanks*, McGraw-Hill, New York.

Ulrich, G.D. (1971) Theory of Particle Formation and Growth in Oxide Synthesis Flames, *Combustion Sci. Technol.* 4:47.

Ulrich, G.D., and Riehl, J.W. (1982) Aggregation and Growth of Submicron Oxide Particles in Flames, *J. Colloid Interface Sci.* 87:257.

Ulrich, G.D. (1984) Flame Synthesis of Fine Particles, *C and EN Special Report*.

Vanpee, M., and Seamans, T.F. (1967) Spectrophotometic Study of Premixed Trimethylaluminum-Oxygen Flames, *Eleventh Symposium (International) on Combustion*, 931.

Weber, A.P., and Friedlander, S.K. (1994) Determination of the Bond Strength between Nanosized Particles, *Mater Res. Soc. Symp. Proc.* 351:331.

Windeler, R.S. (1995) *Production of Nanometer-Sized Metal Oxide Particles by Gas Phase Reaction in a Free Jet,* Ph.D. Thesis in Chemical Engineering, University of California, Los Angeles.

Windeler, R.S., (1992) *Production of Nanometer Sized Alumina Particles from a Turbulent Free Jet*, M.S. Thesis in Chemical Engineering, University of California, Los Angeles.

Windeler, R.S., Lehtinen, K.E.J., and Friedlander, S.K. (1995) Production of Nanometer-Sized Metal Oxide Particles by Gas Phase Reaction in a Free Jet II: Particle Size and Neck Formation - Comparison with Theory, Accepted for publication in *J. Colloid Interface Sci.*

Xiong, Y., and Pratsinis, S.E. (1991) Gas Phase Production of Particles in Reactive Turbulent Flows, *J. Aerosol Sci.* 22, 5:637.

Zachariasen, W.H. (1932) The Atomic Arrangement in Glass, *J. Am. Chem. Soc.* 54:3841.

Reprinted with permission from the publisher.
Accepted for publication in Aerosol Science and Technology.

PAPER G

Production of Nanometer-Sized Metal Oxide Particles by Gas Phase Reaction in a Free Jet II: Particle Size and Neck Formation - Comparison with Theory

Robert S. Windeler, Kari E. J. Lehtinen* and Sheldon K. Friedlander
Department of Chemical Engineering , Air Quality and Aerosol Technology Laboratory
University of California, Los Angeles, CA 90024
*VTT Energy, Aerosol Technology Group, P.O.Box 1401, 02044 VTT, Finland

Abstract

Experimental measurements of nanosized primary particle diameters were compared with calculated values based on a collision-coalescence model. The method of analysis permits calculation of the primary particle size when growth is collision limited (individual particles colliding), coalescence limited (primary particles coalescing in agglomerates), or in a transition regime (particles coalesce about as fast as they collide). Calculated particle sizes compared well with experimental measurements. Particle characteristics were studied along the jet axis for the following conditions: exit velocity = 27.8 m/s, volume loading = 3.2×10^{-7}, flame gas flow rate = 33 l/min. The growth of niobium oxide particles (largest diffusion coefficient) was collision limited, yielding particles that are large and non-agglomerated. The growth of titania particles (mid-range diffusion coefficient) occurred in the collision limited and coalescence limited regimes to form mid-sized particles in agglomerates. The growth of alumina particles (lowest diffusion coefficient) was coalescence limited forming small, oblong particles necked together in large agglomerates. The extent of necking between particles can be estimated from the collision and coalescence times along the jet axis. When the coalescence time rapidly exceeds the collision time, subsequent collisions form agglomerates which are loosely held together. When the coalescence time slowly becomes longer than the collision time, strong necks form between the particles.

Introduction

Part I summarized the results of an experimental study of the effect of operating conditions (temperature, volume loading, velocity) and material properties (solid state diffusion coefficient) on nanoparticle characteristics. Nanosized metal oxide particles were generated by injecting a vapor phase aerosol precursor in the form of a jet into a methane/air flame. Particle size, number of particles per agglomerate, and extent of necking were examined.

The collision-coalescence model, described in earlier work, (Lehtinen, et al., 1996a) is used in this paper to estimate primary particle and agglomerate characteristics formed by the jet generator. Calculated values were compared to data for three metal oxides. To calculate primary particle growth in agglomerates, the theory of Koch and Friedlander (1990a, b) was extended to the coalescence limited regime by dividing the agglomerates into domains in which coalescence occurs. This enables the particle growth to be calculated in the low temperature regions of the jet.

Particle Formation and Growth

The precursor reacts rapidly to produce metal oxide molecules. The supersaturation ratio is very high, so individual molecules probably serve as stable nuclei (Ulrich, 1971; Bolsaitis, et al., 1987) for particles which grow by a collision-coalescence mechanism. When the particles consist of a small number of molecules, the details of the coalescence mechanism are obscure. The particles are too small for molecular transport by conventional solid state volume diffusion. Macroscopic diffusion cannot occur until the particle diameter is sufficiently large compared to the elementary lattice unit (Vergnon, et al., 1970). Ulrich and Subramanian (1977) noted that, at short residence times, the measured particle growth rate exceeded the calculated growth rate. To explain their results they assumed coalescence occurred almost instantaneously until the particles became large enough (more than 1000 molecules) to exhibit macroscopic properties. Simulations of silicon particle growth, using a constant energy molecular dynamic method, indicate that particles are amorphous until they grow to 2000 atoms before becoming crystalline (Zachariah et al., 1996). Particles in our study were assumed to coalesce rapidly (coalescence time shorter than the collision time) until they grew to 1000 molecules. Below this size, at least half the molecules reside on the surface and the particles do not behave as if they have bulk properties (Windeler, 1995).

Many mechanisms have been proposed for particle coalescence, including evaporation-condensation, viscous flow, solid state diffusion, and plastic deformation (Ulrich, 1971; Ulrich and Riehl, 1982; Bolsaitis, et al., 1987). For modeling purposes, it is important to identify the mechanism with the fastest rate, which will control the particle coalescence time (Ashby, 1974). For the metal oxides studied (alumina, titania, niobium oxide), solid state diffusion becomes the dominant coalescence mechanism as particle size increases.

There are several solid state diffusion mechanisms (volume, grain boundary and surface) which occur simultaneously and which are usually incorporated into an apparent diffusion coefficient (Astier and Vergnon, 1976). The diffusion coefficient is strongly dependent on temperature through an Arrhenius expression:

$$D = D_0 \exp\left(\frac{-E_a}{kT}\right) \tag{1}$$

where D_o is the pre-exponential constant, E_a is the activation energy, k is the Boltzmann constant and T is the temperature. The coalescence time is controlled by the apparent diffusion coefficient of the slowest moving ion through the metal oxide. Reported diffusion coefficients for the same material may differ from one another by orders of magnitude because they depend on parameters whose values are unknown or not adequately controlled. These include temperature, impurity concentration, volume fraction of grain boundaries and phase of the material. The effect of particle diameter on diffusion coefficient is not well understood for nanosized particles. The above mentioned uncertainties in the diffusion coefficients, in addition to the complicating effects of halogen precursors (Seto et al., 1995), make it difficult to obtain accurate ab initio simulations of coalescence. In our analysis, diffusion coefficients from the literature were selected which gave the best agreement of our theoretical predictions with measured particle sizes over a wide range of conditions, including gas velocity, aerosol volume loading and temperature distributions.

Earlier Collision-Coalescence Theories

In this section, several collision-coalescence theories, which have been used to predict particle growth in the free molecular regime, are briefly described. In those studies the initial growth mechanism and particle size are not known, but as the particles grow, the collision-coalescence mechanism dominates growth. The effects of the initial conditions, including chemical reaction and nucleation, are not important sufficiently far downstream.

Ulrich (1971) derived an expression for particle growth in a precursor/flame jet cooled by cocurrent air flow. Particles in Brownian motion grow as a result of collisions, and coalesce almost instantaneously until the temperature falls to 80% of their melting point. At this point, it is assumed that coalescence stops, the primary particle size is determined, and further collisions lead only to agglomerate growth.

Ulrich and Subramanian (1977) expanded the previous theory by considering both collision and coalescence rates. Agglomerates form when the collision rate is faster than the coalescence rate. Coalescence occurs with neighboring particles in sintering cells consisting of ξ+1 particles. The value for ξ was about four based on the particle coordination number determined from TEM photographs.

Koch and Friedlander (1990a, b) extended the general dynamic equation for aerosol dynamics (Friedlander, 1977) to include particle coalescence and sintering processes in addition to the classical collision and nucleation phenomena. They applied the extended theory, making certain approximations to predict primary particle size in the case of a linear cooling rate. Particle coalescence is driven by the excess surface free energy above the equilibrium state. In the final stages of coalescence, the change in surface area is given by (Koch and Friedlander, 1990b; Friedlander and Wu, 1994):

$$\frac{dA}{dt} = -\frac{1}{\tau_f}(A - A_s) \tag{2}$$

where τ_f is the characteristic coalescence time, A is the surface area of the two particles, and A_s is the resulting minimum surface area after complete coalescence. Friedlander and Wu (1994) derived a coalescence time based on the slowest sintering step (the final stage as a spheroid approaches a spherical particle):

$$\tau_f = \frac{3kT}{64\pi v_0 D\sigma} v \tag{3}$$

where v is the volume of the coalescing particles, v_o is the volume of the diffusing vacancy, D is the solid state diffusion coefficient, and σ is the surface tension. Equation 2 has been widely used to model the entire coalescence process from sphere contact to complete coalescence. The validity of this assumption is discussed by Koch and Friedlander (19990a) who point out that the final stage is the rate controlling step in the approach to sphericity because the early stages of coalescence after collision are very rapid.

Method of Calculating Particle Growth

Components of the above models have been incorporated in an improved method for the calculation of the primary particle size. This method (Lehtinen, et al., 1996a) can be used to predict aerosol characteristics for real systems since it is not limited to idealized temperature, velocity or volume loading profiles. Particle and agglomerate growth can be calculated in the collision limited regime (individual particles colliding), coalescence limited regime (primary particles coalescing in agglomerates), and transition regime (collision and coalescence times are comparable).

The primary particle and agglomerate characteristics are explained in terms of the collision and coalescence times and their rates of change (Windeler and Friedlander, 1995, Flagan and Lunden, 1995, Lehtinen et al., 1996b). The characteristic collision time is defined as the time for the average volume of an agglomerate to double. The collision time can be varied, without significantly affecting the coalescence time, by changing the volume loading. An increase in volume loading, increases the number of collisions per unit time and shortens the collision time.

The coalescence time, τ_f, in Equation 2 characterizes the time for two initially distinct spheres to coalesce. The coalescence time can be varied, without significantly affecting the collision time, by changing D. The diffusion coefficient depends strongly on temperature through an Arrhenius expression, and an increase in temperature reduces the coalescence time. By using metal oxides with diffusion coefficients that vary over several orders of magnitude, the coalescence time can be changed for given flow and temperature profiles.

The model is used to calculate the change in average agglomerate volume (collision time) and average primary particle volume (coalescence time) along the jet axis. Assuming a self-preserving size distribution for fractal agglomerates, the change in agglomerate volume is given by (Matsoukas and Friedlander, 1991):

$$\frac{dv_a}{dt} = \frac{1}{2}\alpha\sqrt{\frac{6kT}{\rho}}\left(\frac{3v_a}{4\pi}\right)^{1/6}\phi n^{2/D_f - 2/3} \tag{4}$$

where v_a is the average volume of an agglomerate, ρ is the particle density, n is the average number of particles in an agglomerate, ϕ is the aerosol volume loading, and α is a constant that depends on the fractal dimension, D_f (Lehtinen, et al., 1996a,b).

The change in primary particle volume is obtained by modifying Equation 2 to apply to growth in the coalescence limited regime. Equation 2, which was derived for the final stages of coalescence of a slightly nonspherical particle, can be applied to coalescence of particles in large agglomerates by dividing agglomerates into small domains in which coalescence occurs. The size of the domain (number of particles per domain) was found to have only a small effect on particle growth (Lehtinen, et al., 1996a). A domain size equal to the average coordination number plus one (center particle) was chosen.

The change in the primary particle volume, v_p, is obtained by applying Equation 2 to domains in which coalescence occurs, and writing the area, A, in terms of the average primary particle volume (Lehtinen, et al., 1996a):

$$\frac{dv_p}{dt} = \begin{cases} \frac{64\pi D\sigma v_0}{kT}\left(m^{-1} - m^{-4/3}\right) & n = \frac{v_a}{v_p} > m \\ \frac{64\pi D\sigma v_0}{kT}\left(n^{-1} - n^{-4/3}\right) & n = \frac{v_a}{v_p} \le m \end{cases} \quad (5)$$

where n and m are the number of particles in an agglomerate and domain, respectively. When the number of primary particles per agglomerate, n, exceeds m, the upper equation is used, otherwise the lower equation. From TEM photographs, the average coordination number was about four, corresponding to a domain size m = 5.

Temperature, Velocity and Concentration Distributions in the Jet

The distributions of the temperature, velocity, and volume loading along the jet axis are complex because the aerosol generator includes three concentric streams. The innermost stream, a high velocity precursor jet, is centered in a laminar methane flame stream which in turn is surrounded by stationary ambient air. Four exit velocities were studied allowing examination of the precursor jet flow in turbulent and laminar regimes.

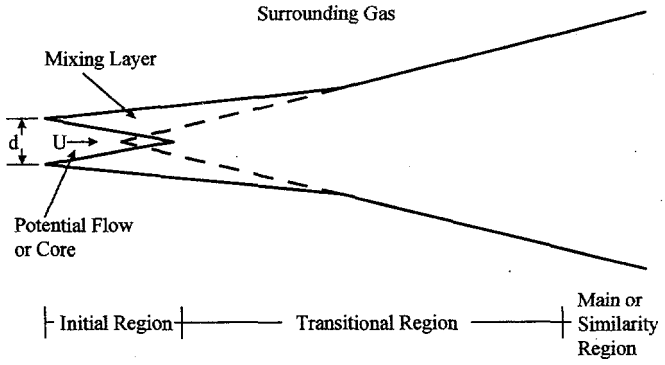

Fig. 1: The turbulent jet is divided into three regions: initial region, transitional region, and main or similarity region.

The precursor jet can be approximated as a free jet issuing into stagnant gas because the flame gas velocity was typically at least an order of magnitude lower than the precursor jet velocity (Abramovich, 1963). A free jet can be divided into three regions: initial, transitional, and main (Figure 1). The initial region (first six orifice diameters down the jet axis, $x/d \le 6$) consists of a shear layer and potential core. The potential core is a cone-shaped region, unaffected by the surroundings, with the same temperature, velocity, and concentrations as the exiting gas. The shear layer is the region between the potential core and the undisturbed surrounding gas. Within the shear layer, the gas from the potential core and surroundings mix, causing the temperature, velocity, and concentrations to change. The precursor gas molecules react and form particles in this region. Because the jet profiles in the transition region are not well known, the jet profiles in the main flow are assumed to apply after the initial region. In the main region, the temperature, velocity and volume loading profiles each fall on a single curve, regardless of axial distance, when plotted with dimensionless parameters (Abramovich, 1963).

The temperature of the gas leaving the jet orifice is relatively low. The jet increases in temperature as it is heated by the flame stream, and then cools by mixing with ambient air further downstream. For each exit velocity, the temperature was measured along the jet axis with a subminiature R type thermocouple and corrected for radiation losses (Windeler and Friedlander, 1995).

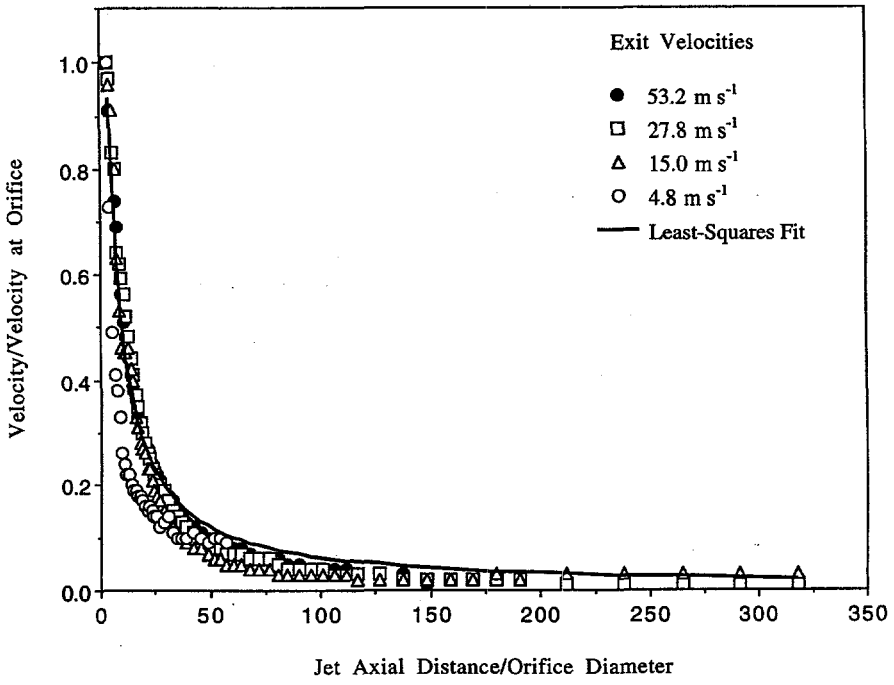

Fig.2: Velocity profiles were measured along the jet axis using a constant temperature hot wire anemometer.

The velocity was measured along the jet axis in a series of isothermal experiments using a constant temperature hot wire anemometer (TSI model 1053B, probe model 1276-10A). The anemometer measurements for all exit velocities fall on a single curve when plotted in dimensionless form (Figure 2). The velocity distribution was fit to a least squares equation and corrected for temperature (Hinze, 1975; Simpson, 1975):

$$\frac{U}{U_0} = \frac{6.27}{\frac{x}{d}\left(\frac{T}{T_0}\right)^{1/2} + 2.5} \qquad (6)$$

where U and T are the velocity and temperature at a distance x from the orifice, U_o and T_o are the velocity and temperature at the orifice, and d is the orifice diameter.

The volume loading or ratio of metal oxide volume to carrier gas volume was calculated from correlations obtained from the literature. The Reynolds number at the highest jet exit velocity was 3600, corresponding to a turbulent flow. Experiments performed at the lower three exit velocities (Re = 330, 1020, 1880) formed laminar or transitional flows (Simpson, 1975; Lane and Rice, 1981; Tatterson, 1991; Revill, 1992). At the highest exit velocity, the jet spread after leaving the orifice and mixed with the outside gases. At the lower three exit velocities, the width of the jet remained fairly constant from the orifice to the sampling tube, indicating that little dilution occurred. The volume loading along the jet axis in the main region of a turbulent jet is approximately (Abramovich, 1963):

$$\frac{\phi}{\phi_0} = \frac{4.6}{\frac{x}{d} + 1.9} \frac{T_0}{T} \tag{7}$$

where the volume loading is corrected for temperature using the ideal gas law. ϕ and ϕ_o are the volume loadings at x and the orifice, respectively. The volume loading for an isothermal laminar jet does not change substantially with axial distance (Simpson, 1975). When corrected for temperature, the volume loading is given by:

$$\frac{\phi}{\phi_0} = \frac{T_0}{T} \tag{8}$$

Particle Growth and Neck Characteristics

The characteristics of the particles formed in the jet depend on the relative values of the local collision and coalescence times along the axis (Figure 3). In Figure 3, the coalescence time, τ_f, is calculated from Equation 3, which is based on diffusion in a bulk material. The value for τ_f is not accurate during the first several centimeters of the jet where the primary particle size is very small, so an assumption of instantaneous coalescence up to 1000 molecules was used. This avoids the assumption of agglomerates containing primary particles of molecular size.

When the coalescence time is less than the collision time, the aerosol consists of individual particles which completely coalesce after each collision (collision limited). This occurs when the temperature in the jet is high or the volume loading is low. Particle size is determined by the number of collisions. Growth is coalescence limited when the coalescence time is greater than the collision time. In this case, particles grow by coalescing with their neighbors in the agglomerates. Particle size is determined by the diffusion coefficient of the slowest moving ion through the metal oxide. When collision and coalescence times are comparable, both times are used in determining the particle size.

In the initial region of the jet, the temperature is low and the coalescence time can be greater than the collision time after the particles have grown to a size of several nanometers. Agglomerates of very fine primary particles form in this region. As the temperature increases down the jet axis, the coalescence time becomes less than the collision time. In this region, the aerosol typically coalesces completely to form non-agglomerated particles. These particles continue to grow by a collision-coalescence mechanism until the temperature decreases again and quenches particle growth.

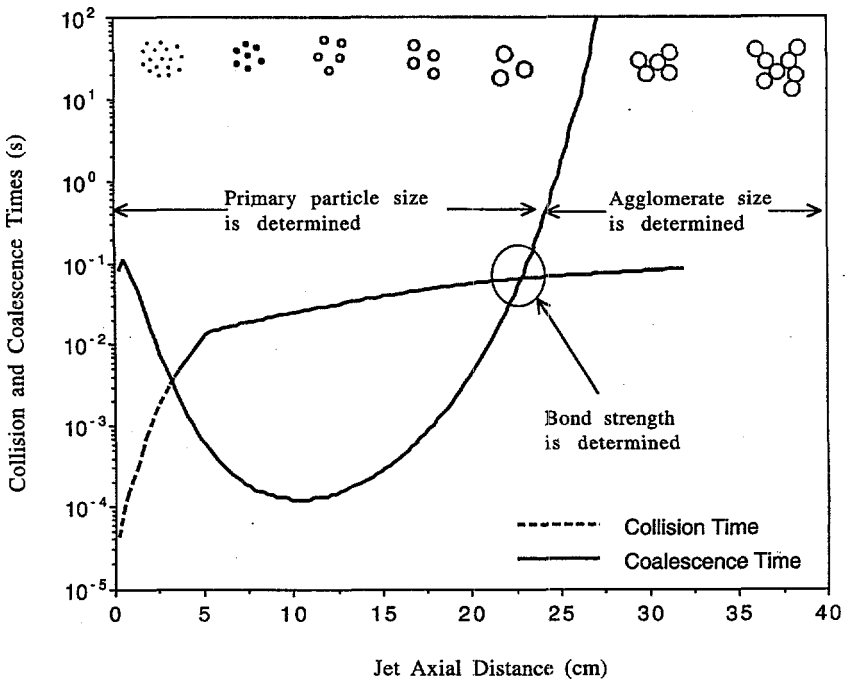

Fig. 3: The collision and coalescence times are used to determine the particle size and shape, number of particles per agglomerate and bond strength. The schematic diagram shows the behaviour of the niobium oxide and titania systems.

Based on our experimental observations, we believe that particle shape and extent of necking are determined by the rate at which the coalescence time exceeds the collision time. Spheres form when the coalescence time quickly exceeds the collision time, that is when $d\tau_f/dt >> d\tau_c/dt$ in the region where $\tau_f = \tau_c$ (Figure 4a). In this case, particles coalesce completely before their growth is quenched. Subsequent collisions form agglomerates composed of particles held together by weak van der Waals forces.

Oblong particles form when the coalescence time slowly becomes longer than the collision time ($d\tau_f/dt \approx d\tau_c/dt$ in the region where $\tau_f = \tau_c$) (Figure 4b). These particles, which are typically found in agglomerates, only partially coalesce before being quenched and are held strongly together by necks.

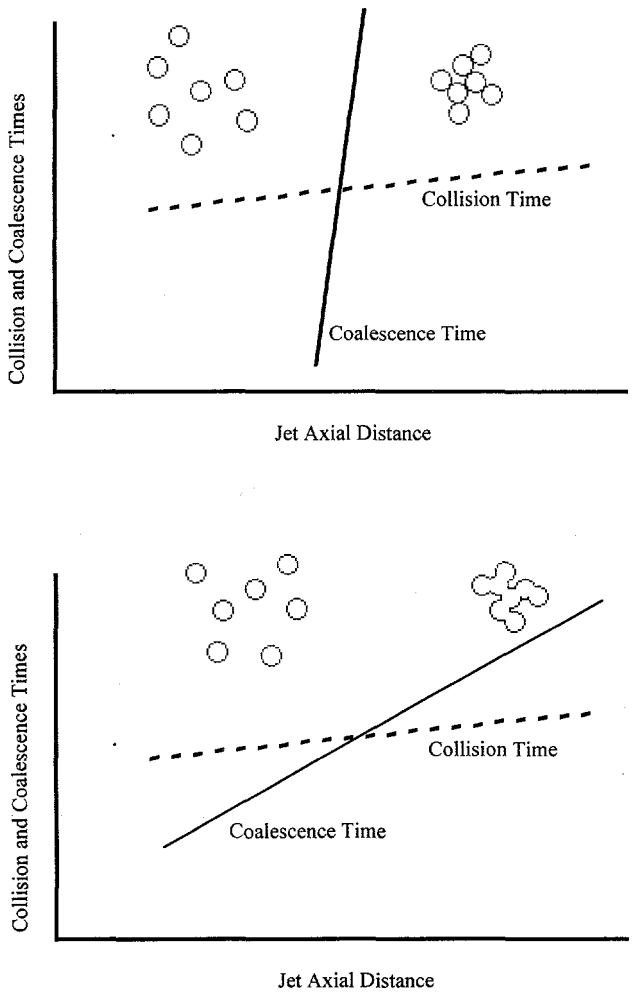

Fig. 4: a) Particles are held together by weak van der Waals forces when the coalescence time quickly passes the collision time. b) Particles form necks with strong ionic bonds when the coalescence time slowly passes the collision time

Comparison of Calculated and Measured Particle Sizes

Particles were produced in the three growth regimes (collision limited, coalescence limited, and transition) using metal oxides with diffusion coefficients that vary over several orders of magnitude. Aerosol characteristics were studied for the different materials while holding constant the jet fluid mechanics and temperature profile. The collision and coalescence times for the metal oxides were calculated along the jet axis for the following experimental conditions: exit velocity = 27.8 m/s, volume loading = 3.2 $x10^{-7}$, flame gas flow rate = 33 l/min, fractal dimension = 2.0, and the material properties given in Table 1.

Table 1. Metal Oxide Properties

Refer to Equations 1 and 3

Property	Niobium Oxide	Ref.	Titania	Ref.	Alumina	Ref.
Diffusion Pre-exponential, D_o (cm^2/s)	1.72×10^{-2}	a	7.2×10^{-2}	e	2.5×10^{4}	g
Diffusion Activation Energy, E_a (kJ/mole)	206	a	286	e	565	g
Surface Tension, σ (dynes/cm)	750	b	600	f	905	h
Vacancy Volume, v_o ($Å^3$)	20	c	17	c	21	c
Density, ρ (g/cm^3)	3.96	d	3.84	d	4.47	d

a) Samsonov, 1982
b) Nicholas, 1988
c) Calculated
d) CRC Handbook, 1989
e) Astier and Vergnon, 1976
f) Bruse , 1965
g) Kuczynski, et al., 1959
h) Kingery, et al., 1976

The collision times fall approximately on a single curve (Figure 5) because the volume loading profiles were the same for each material. The coalescence times depend on the jet temperature and have complicated profiles. The coalescence times were long near the orifice, reached a minimum, and then increased again. Particles were collected 20 cm down the jet axis and examined with a transmission electron microscope. Particles retained their characteristics once they entered the probe because nitrogen was added at the probe tip to dilute and cool the aerosol, suppressing collisions and coalescence.

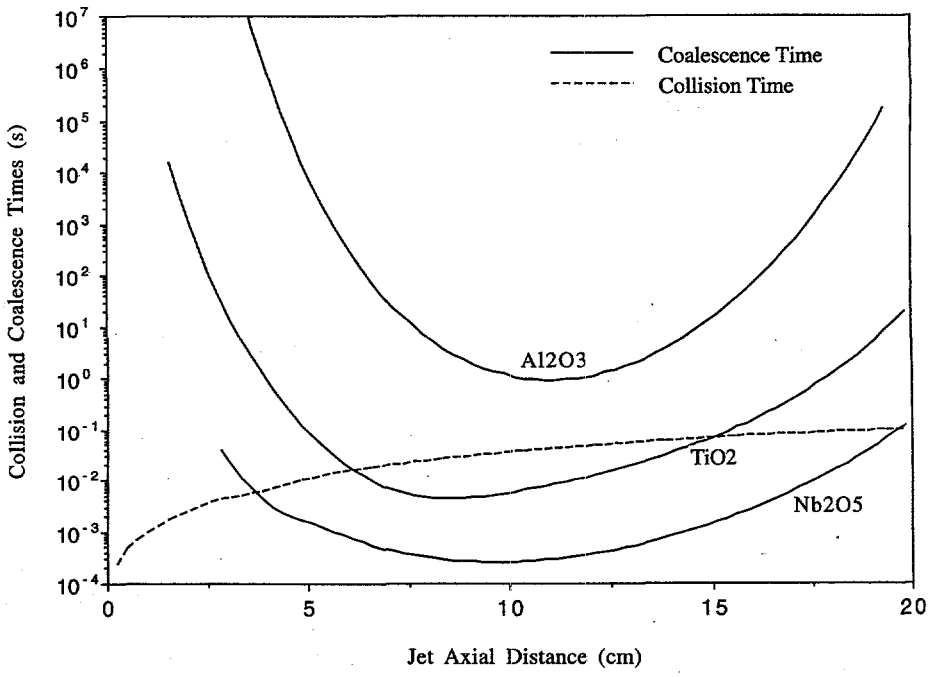

Fig. 5: The effects of the collision and coalescence times on aerosol characteristics were studied using three metal oxides with diffusion coefficients that varied over several orders of magnitude.

Niobium oxide has the largest diffusion coefficient (shortest coalescence time) and formed the largest particles (Windeler and Friedlander, 1995). When a small number of particles was sampled from the gas, the particles were nearly spherical and showed no evidence of agglomeration. When a large number of particles was sampled, agglomerates formed because the particles collided with one another as they were collected on the TEM grid. When agglomerated, the particles appeared to touch at a single point and were probably held together by Van der Waals forces.

Titania particles (mid-range diffusion coefficient) also grew by the collision limited mechanism over much of the jet. Particles collected 10 cm from the orifice, where the coalescence time was shorter than the collision time, showed no evidence of agglomeration. At about 15 cm from the orifice, the coalescence time became longer than the collision time and agglomerates began to form. Particles collected 20 cm from the orifice formed small agglomerates with diameters between that of niobium oxide and alumina. Alumina particles (lowest diffusion coefficient) always grew by a coalescence limited mechanism. Alumina formed large agglomerates of small, oblong primary particles which were strongly necked together.

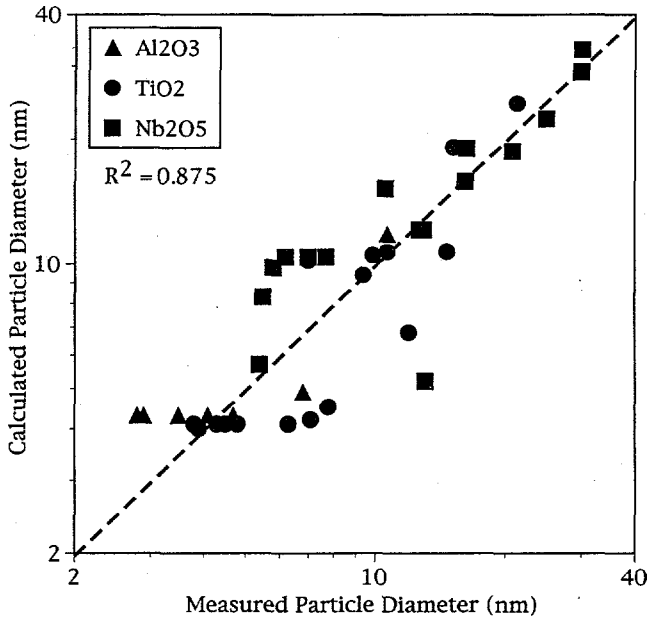

Fig 6: Calculated particle sizes compared well with measured diameters. Calculations were closer to measured results for larger particles probably because the material properties approached the bulk values used in calculations.

Calculated particle sizes were compared with measured volume mean diameters (Figure 6). Calculated values for niobium oxide fall closest to measured results (Table 2). This is expected because particles were large and growth was predominantly collision limited. As nanosized particles increase in diameter, their properties approach the values of bulk material used for calculations. Estimates of the collision time have smaller errors than the coalescence time

because the latter depends on the value of diffusion coefficient which may not be precisely known.

Table 2. Measured and Calculated Primary Particle Diameters of Niobium Oxide under Various Jet Conditions

Flame Flowrate (L/min)	Exit Velocity (m/s) @ 294 K	Volume Loading ($x10^7$) @ 294 K	Sampling Point (cm)	Measured Volume Mean Diameter (nm)	Calculated Volume Mean Diameter (nm)	Percent Deviation (%)
8.8	4.8	3.2	20	16.3	19.4	19
8.8	15.0	3.2	20	10.6	15.6	47
8.8	27.8	3.2	20	7.0	10.5	50
8.8	53.2	3.2	20	5.4	5.7	6
8.8	27.8	10.0	20	7.7	10	30
8.8	27.8	1.0	20	5.5	8.5	55
8.8	27.8	3.2	15	6.2	10.5	69
8.8	27.8	3.2	10	5.8	9.9	71
33	4.8	3.2	20	30.1	33.6	12
33	15.0	3.2	20	24.9	22.9	-8
33	27.8	3.2	20	20.8	19	-9
33	53.2	3.2	20	13.1	5.3	-60
33	27.8	10.0	20	30.0	29.8	-1
33	27.8	1.0	20	12.7	12.4	-2
33	27.8	3.2	15	16.2	16.2	0
33	27.8	3.2	10	13.0	12.4	-5

Table 3. Measured and Calculated Primary Particle Diameters of Titania under Various Jet Conditions

Flame Flowrate (L/min)	Exit Velocity (m/s) @ 294 K	Volume Loading ($x10^7$) @ 294 K	Sampling Point (cm)	Measured Volume Mean Diameter (nm)	Calculated Volume Mean Diameter (nm)	Percent Deviation (%)
8.8	4.8	3.2	20	12.0	6.9	-43
8.8	15.0	3.2	20	7.1	4.2	-41
8.8	27.8	3.2	20	4.8	4.1	-15
8.8	53.2	3.2	20	3.9	4	3
8.8	27.8	10.0	20	6.3	4.1	-35
8.8	27.8	1.0	20	3.8	4.1	8
8.8	27.8	3.2	15	4.5	4.1	-9
8.8	27.8	3.2	10	4.3	4.1	-5
33	4.8	3.2	20	21.3	24.9	17
33	15.0	3.2	20	15.2	19.6	29
33	27.8	3.2	20	10.7	10.9	2
33	53.2	3.2	20	7.8	4.6	-41
33	27.8	10.0	20	14.7	10.9	-26
33	27.8	1.0	20	7.0	10.5	50
33	27.8	3.2	15	9.9	10.7	8
33	27.8	3.2	10	9.4	7.1	-24

In the high temperature runs (flame gas flow rate = 33 l/min), calculated titania particle sizes compare well with experimental measurements (Table 3). For low temperatures, calculated particle sizes follow the measured trends but are smaller than the measured values. This is probably because particles are not large enough for bulk properties to apply, or the literature value for the solid state diffusion coefficient is low. Although alumina calculations compare reasonably well with measurements (Table 4), the method of analysis applies only when particles grow larger than the arbitrarily set 1000 molecules (4.3 nm). The small alumina particles

probably grow by a mechanism other than conventional solid state diffusion because only a small percentage of molecules are in the particle core.

Table 4. Measured and Calculated Primary Particle Diameters of Alumina under Various Jet Conditions

Flame Flowrate (L/min)	Exit Velocity (m/s) @ 294 K	Volume Loading ($x10^7$) @ 294 K	Sampling Point (cm)	Measured Volume Mean Diameter (nm)	Calculated Volume Mean Diameter (nm)	Percent Deviation (%)
8.8	4.8	3.2	20	4.7	4.3	-9
8.8	15.0	3.2	20	3.5	4.3	23
8.8	27.8	3.2	20	2.9	4.3	48
8.8	53.2	3.2	20	*	4.3	N.A.
8.8	27.8	10.0	20	2.9	4.3	48
8.8	27.8	1.0	20	2.9	4.3	48
8.8	27.8	3.2	15	2.9	4.3	48
8.8	27.8	3.2	10	2.9	4.3	48
33	4.8	3.2	20	10.7	12	12
33	15.0	3.2	20	6.8	4.9	-28
33	27.8	3.2	20	4.1	4.3	5
33	53.2	3.2	20	2.8	4.3	54
33	27.8	10.0	20	4.1	4.3	5
33	27.8	1.0	20	4.1	4.3	5
33	27.8	3.2	15	4.1	4.3	5
33	27.8	3.2	10	*	4.3	N.A.

* Experimental conditions produced cloudy indistinct particles.

Calculated and measured particle sizes for the experimental jet exit velocities are compared in Figure 7. Values are calculated at three separate jet exit velocities in the laminar regime, and a line has been drawn between these calculated values. For these three exit velocities, the calculated particle sizes compare well with measured diameters. However, for the highest exit velocity (jet flow was turbulent) the calculated particle sizes follow the trends of the measured diameters but were usually smaller. The large discrepancy between calculated and measured particle sizes may result from assumptions concerning the volume loading. Calculations in this study were performed assuming an average aerosol volume loading for a given axial distance (Equation 7). However, in the turbulent regime, the aerosol is transported by eddies which are much larger than the particles. Since the diffusion of nanosized particles is relatively slow, the eddies form pockets or regions with high volume loadings. In these high concentration regions, particles grow faster than predicted from the calculations which are based on an average volume loading.

Figure 8 shows calculated and measured particle sizes as a function of volume loading. Values were calculated for the three volume loadings and a linear interpolation is made between each pair of calculated values. The calculations compare well to measured values for each metal oxide except for titania. Calculated particle sizes for titania do not increase as much with volume loading as the experimental values (i.e., the calculated vales are relatively invariant to volume loading). This indicates that the titania growth is closer to the collision limited regime than the calculations show.

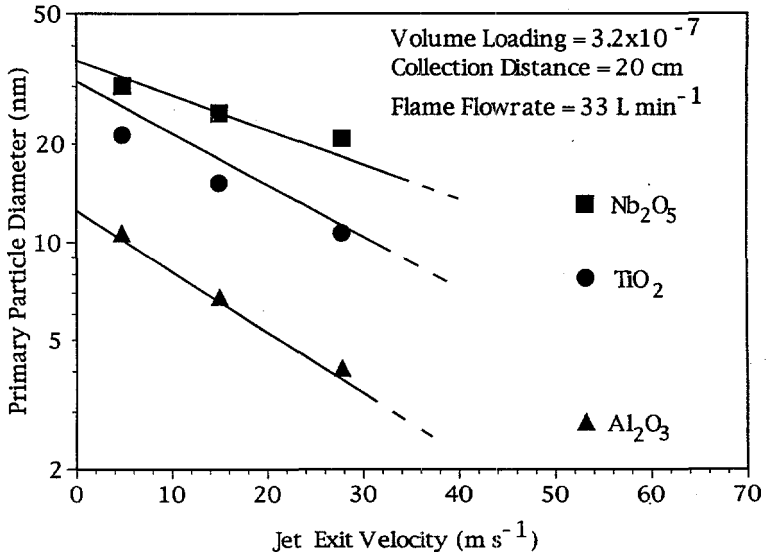

Fig. 7: In the laminar regime, calculated values (lines) compared well with measured results (symbols) for the three metal oxides. In the turbulent regime, calculated particle sizes differed significantly from measured diameters probably because of the values assumed for the volume loading distribution.

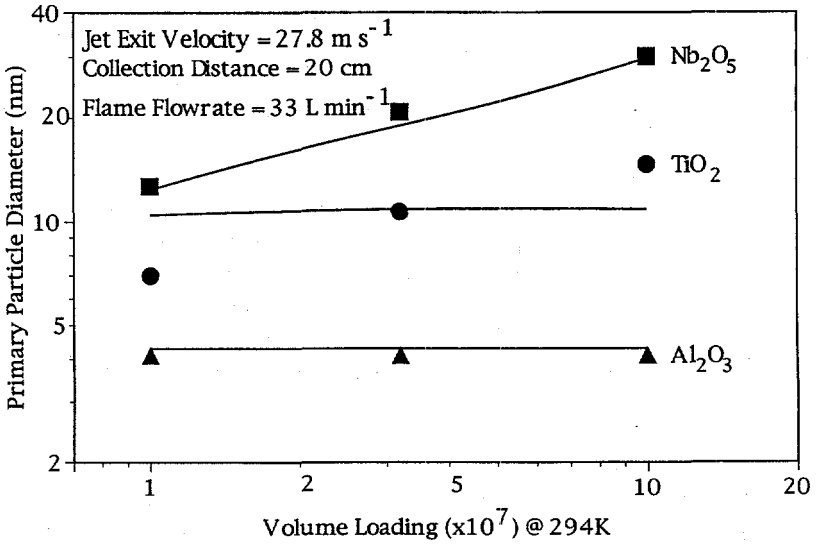

Fig 8: Niobium oxide particles increase in size with volume loading because growth is collision limited. Alumina is unaffected by volume loading because growth is coalescence limited. Calculated sizes (lines) compared well with measured diameters (symbols) for the three metal oxides.

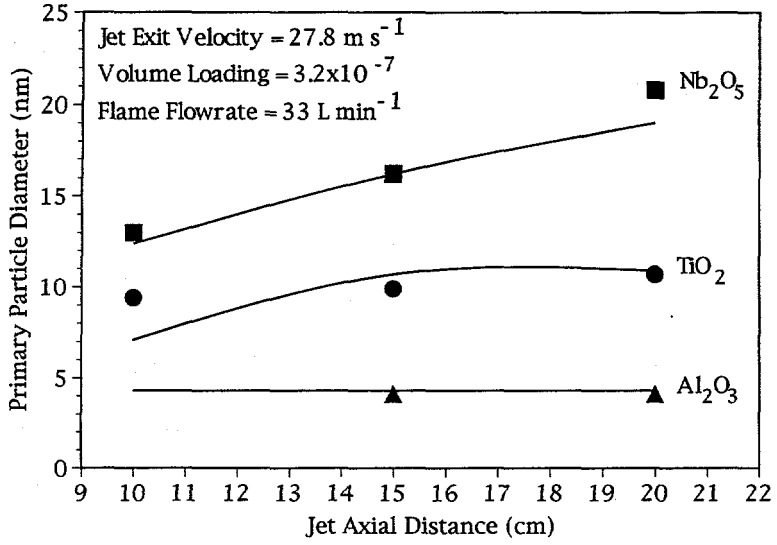

Fig. 9: Effect of residence time on particle size: calculated values (lines) compared well with measured results (symbols) for the three metal oxides.

Primary particle size along the jet axis is plotted in Figure 9, showing the effect of residence time. The calculated particles sizes, shown by the lines, compare well with measured particle diameters. Because of the low diffusion coefficient of alumina, particles only grow in the first half of the jet where the temperature is highest. Niobium, with its high diffusion coefficient, continues to grow along the axis, even in the lower temperature regions of the jet.

Conclusions

Calculated particle sizes compared well with measured diameters using a particle growth model derived in earlier work (Lehtinen, et al., 1996a). The analysis is based on a modification of the theory of Koch and Friedlander (1990a,b) and applies to the coalescence limited regime by dividing agglomerates into domains in which coalescence occurs. The calculations indicated that the growth mechanism changed from the collision to coalescence limited regimes, as the diffusion coefficient decreased. Calculated particle sizes followed the trends of the measured particle diameters as the jet exit velocity, volume loading, and residence time were varied for niobium oxide, titania and alumina.

The extent of necking between the particles can be predicted from the relative rate of change of the coalescence and collision times at the point where the times are equal. Particles held together by weak van der Waals forces form when the coalescence time rapidly exceeds the collision time. Particles form agglomerates with significant necking when the coalescence time slowly passes the collision time.

Acknowledgment

The authors wish to thank the National Science Foundation, Grant CTS-9218222, and the Northrop Corporation for financial support.

References

Abramovich, G.N. (1963) *The Theory of Turbulent Jets*, translation by scripta technica.

Ashby, M.F., (1974) A First Report on Sintering Diagrams. *Acta Metallurgica*, 22, 275-289.

Astier, M., and Vergnon, P. (1976) Determination of the Diffusion Coefficients from Sintering Data of Ultrafine Oxide Particles, *J. Solid State Chem.* 19:67.

Bolsaitis, P.P., McCarthy, J.F., and Mohiuddin, G. (1987) Formation of Metal Oxide Aerosols for Conditions of High Supersaturation, *Aerosol Sci. Technol.* 6:225.

Bruse, R.H. (1965) *Science of Ceramics Vol. 2*, Steward, G.H. ed., Academic Press, New York.

CRC Handbook of Chemistry and Physics (1989) Editor-in-Chief: Weast, R.C., CRC Press Inc., Florida.

Flagan, R.C., and Lunden, M.M. (1995) Particle Structure Control in Nanoparticle Synthesis from the Vapor Phase, *Materials Sci. Eng.* A204, 113-124.

Friedlander, S.K. (1977) *Smoke Dust and Haze*, Wiley-Interscience, New York.

Friedlander, S.K., and Wu, M.K. (1994) Linear Rate Law for the Decay of the Excess Surface Area of a Coalescing Solid Particle, *Phys. Rev. B*, 49, 5:3622.

Hinze, J.O. (1959) *Turbulence*, McGraw-Hill, New York.

Kingery, W.D., Bowen, H.K., and Uhlmann, D.R. (1976) *Introduction to Ceramics*, John Wiley & Sons, New York.

Koch, W., and Friedlander, S.K. (1990a) The Effect of Particle Coalescence on the Surface Area of a Coagulating Aerosol, *J. Colloid Interface Sci.* 140:419.

Koch W., and Friedlander, S.K. (1990b) Particle Growth by Coalescence and Agglomeration, *Aerosol Sci. Technol.* 21, Suppl. 1: S73.

Kuczynski, G.C., Abernethy, L., and Allen, J. (1959) *Kinetics of High-Temperature Processes*, John Wiley and Sons Inc., New York.

Lane, A.G.C., and Rice, P. (1981) An Experimental Investigation of Liquid Jet Mixing Employing a Vertical Submerged Jet, *IChemE Symposium Series No. 64.*

Lehtinen, K.E.J., Windeler, R.S., and Friedlander, S.K. (1996a) A Note on the Growth of Primary Particles in Agglomerate Structures by Coalescence, Accepted for publication in *J. Colloid Interface Sci.*

Lehtinen, K.E.J., Windeler, R.S., and Friedlander, S.K. (1996b) Prediction of Nanoparticle Size and the Onset of Dendrite Formation using the Method of Characteristic Times, Accepted for publication in *J. Aerosol Sci.*

Matsoukas, T., and Friedlander, S.K. (1991) Dynamics of Aerosol Agglomerate Formation, *J. Colloid Interface Sci.* 146, 2:495.

Nicholas, M.G. (1988) *Materials Science Form: External and Internal Surfaces in Metal Oxides*, (Dufour, L.C., and Nowotny, J. eds.) Trans Tech Publications, Switzerland.

Revill, B.K. (1992) *Mixing in the Process Industries 2nd Ed.*, (Edwards, N.H. ed.) Butterworth-Heinemann, Oxford.

Samsonov, G.V. (1982) *The Oxide Book*, Translated from Russian by Johnston, R.K. IFI/Plenum, New York.

Seto. T., Shimada, M., and Okuyama, K. (1995) Evaluation of Sintering of Nanometer-Sized Titania Using Aerosol Method, *Aerosol Sci. Technol.*, 23:183-200.

Simpson, L.L. (1975) *Turbulence in Mixing Operations*, Brodkey, R.S. ed., Academic Press, New York.

Tatterson, G.B. (1991) *Fluid Mixing and Gas Dispersion in Agitated Tanks*, McGraw-Hill, New York.

Ulrich, G.D. (1971) Theory of Particle Formation and Growth in Oxide Synthesis Flames, *Combustion Sci. Technol,* 4:47-57.

Ulrich, G.D., and Subramanian, N.S. (1977) Particle Growth in Flames III. Coalescence as a Rate-Controlling Process, *Combustion Sci. Technol.* 17:119-126.

Ulrich, G.D., and Riehl, J.W. (1982) Aggregation and Growth of Submicron Oxide Particles in Flames, *J. Colloid Interface Sci.* 87:257.

Vergnon, P.G., Juillet, F.E., Astier, M.P., and Teichner, S.J. (1970) *Science of Ceramics*, Brosset, C., and Knopp, E. eds., The Swedish Institute for Silica Research.

Windeler, R.S., and Friedlander, S.K. (1995) Production of Nanometer-Sized Metal Oxide Particles by Gas Phase Reaction in a Free Jet I: Experimental System and Results, Submitted to *Aerosol Sci. Technol.*

Windeler, R.S. (1995) *Production of Nanometer-Sized Metal Oxide Particles by Gas Phase Reaction in a Free Jet,* Ph.D. Thesis in Chemical Engineering, University of California, Los Angeles.

Zachariah, M.R., Carrier, M.J. and Blaisten-Barojas, E. (1996) Molecular Dynamics Calculation of the Properties of Silicon Nanoparticles, Accepted for publication in *J. Phys. Chem.*

Published by

VTT

Vuorimiehentie 5, P.O.Box 2000, FIN–02044 VTT, Finland
Phone internat. + 358 9 4561
Fax + 358 9 456 4374

Series title, number and report code of publication
VTT Publications 304 VTT–PUBS–304

Date
March 1997

Project number
N7SU00189

Author(s)

Lehtinen, Kari E. J.

Name of project

Commissioned by

Title

Theoretical studies on aerosol agglomeration processes

Abstract

In this thesis, theoretical modeling of certain aerosol systems has been presented. At first, the aerosol general dynamic equation is introduced, along with a discretization routine for its numerical solution. Of the various possible phenomena affecting aerosol behaviour, this work is mostly focused on aerosol agglomeration. The fundamentals of aerosol agglomeration theory are thus briefly reviewed. The two practical applications of agglomeration studied in this thesis are flue gas cleaning using an electrical agglomerator and nanomaterial synthesis with a free jet reactor.

In an electrical agglomerator the aerosol particles are charged and brought into an alternating electric field. The aim is to remove submicron particles from flue gases by collisions with larger particles before conventional gas cleaning devices that have a clear penetration window in the problematic 0.1–1 μm size range. A mathematical model was constructed to find out the effects of the different system parameters on the agglomerator's performance. A crucial part of this task was finding out the collision efficiencies of particles of varying size and charge. The original idea was to use unipolar charging of the particles, and a laboratory scale apparatus was constructed for this purpose. Both theory and experiments clearly show that significant removal of submicron particles can not be achieved by such an arrangement. The theoretical analysis further shows that if the submicron particles and the large collector particles were charged with opposite polarity, significant removal of the submicron particles could be obtained.

The second application of agglomeration considered in this thesis is predicting/controlling nanoparticle size in the gas-to-particle aerosol route to material synthesis. In a typical material reactor, a precursor vapor reacts to form molecules of the desired material. In a cooling environment, a particulate phase forms, the dynamics of which are determined by the rates of collisions and coalescence. In the thesis, it is first theoretically demonstrated how the onset of dendrite formation and primary particle size can be predicted by studying the characteristic time scales of collision and coalescence. Then it is shown how the linear rate law for coalescence can be approximately applied to agglomerate structures by dividing the agglomerates into sections. The developed models are then applied to a free jet material reactor. From the comparisons between theory and experiment it is obvious that such a model is able to capture the effects of the system parameters (temperature, velocity, volume loading of material and location of collection) on the primary particle size of the produced material.

Activity unit

VTT Energy, Energy Use, Biologinkuja 7, P.O.Box 1401, FIN–02044 VTT, Finland

Series title and ISSN numbers

VTT PUBLICATIONS

1235–0621 (soft back edition)
1455–0849 (URL: http://www.inf.vtt.fi/pdf/)

ISBN

951–38–5047–1 (soft back edition)
951–38–5048–X (URL: http://www.inf.vtt.fi/pdf/)

Language

English

Class (UDC)

541.182.2/.3

Keywords

aerosols, aerosol dynamics, electrical agglomeration, agglomerates, particle collisions, coalescence, nanomaterials

Sold by VTT Information Service
P.O. Box 2000, FIN–02044 VTT, Finland
Phone internat. + 358 9 456 4404
Fax + 358 9 456 4374

Pages

45 p. + app. 89 p.

Price group

C

VTT PUBLICATIONS

284 Pakanen, Jouko. Detecting and isolating faults of an air-handling unit using on-line diagnostic tests. 1996. 52 p.

285 Tuominen, Pasi. The synchronization of loosely coupled motion control systems. 1996. 139 p. + app. 16 p.

286 Mäkäräinen, Minna. Application management requirements for embedded software. 1996. 99 p.

287 Kurkela, Esa. Formation and removal of biomass-derived contaminants in fluidized-bed gasification processes. 1996. 47 p. + app. 87 p.

288 Manninen, Mikko, Taivassalo, Veikko & Kallio, Sirpa. On the mixture model for multiphase flow. 1996. 67 p.

289 Seppälä, Anssi. Load research and load estimation in electricity distribution. 1996. 118 p. + app. 19 p.

290 Kiviaho, Jari. Fischer-Tropsch synthesis catalysed by cobalt-rhodium and cobalt-ruthenium carbonyl clusters on silica. 1996. 36 p. + app. 84 p.

291 Kurkela, Esa, Laatikainen-Luntama, Jaana, Ståhlberg, Pekka & Moilanen, Antero. Pressurised fluidised-bed gasification experiments with biomass, peat and coal at VTT in 1991–1994. Part 3. Gasification of Danish wheat straw and coal. 1996. 41 p. + app. 5 p.

292 Syrjälä, Seppo. Numerical study of flow and heat transfer behaviour of power-law non-Newtonian fluids in rectangular channels. 1996. 30 p. + app. 87 p.

293 Karioja, Pentti. Integrated optics for instrumentation applications. 1996. 44 p. + app. 65 p.

294 Linder, Markus. Structure-function relationships in fungal cellulose-binding domains. 1996. 29 p. + app. 22 p.

295 Björkman, Jouni & Keski-Rahkonen, Olavi. Response of fire detectors to different smokes. 1997. 33 p.

296 Vares, Sirje, Sarvaranta, Leena & Lanu, Matti. Cellulose fibre concrete. 1997. 94 p. + app. 2 p.

297 Hattula, Tapani. Adenosine triphosphate breakdown products as a freshness indicator of some fish species and fish products. 1997. 48 p. + app. 31 p.

298 Ailisto, Heikki. CAD model-based planning and vision guidance for optical 3D co-ordinate measurement. 1997. 70 p. + app. 63 p.

299 Yli-Kauhaluoma, Jari. Antibody catalysis of some organic and biochemical reactions. 1997. 125 p. + app. 36 p.

300 Tuomisaari, Maarit. Visibility of exit signs and low-location lighting in smoky conditions. 1997. 32 p.

301 Hanhijärvi, Antti. Perpendicular-to-grain creep of Finnish softwoods in high temperature drying conditions. Experiments and modelling in temperature range 95–125 °C. 1997. 94 p. + app. 176 p.

302 Keski-Rahkonen, Olavi, Björkman, Jouni & Farin, Juho. Derating of cables at high temperatures. 1997. 57 p. + app. 2 p.

303 Nevalainen, Markku J. Fracture toughness comparison between a semielliptical surface crack in a 4PB plate and a through-thickness crack in a 3PB fracture toughness test specimen. 1997. 34 p.

304 Lehtinen, Kari E. J. Theoretical studies on aerosol agglomeration processes. 1997. 45 p. + app. 89 p.